UNIVERSITÁ DEGLI STUDI DI PADOVA

FACOLTÀ DI SCIENZE MM. FF. NN.
Dipartimento di Geoscienze

TESI DI LAUREA MAGISTRALE IN
GEOLOGIA E GEOLOGIA TECNICA

MARINE GEOLOGY OF CORE V28-179 AND PLIO-PLEISTOCENE CLIMATE IMPLICATIONS

GEOCHIMICA E NANNOFOSSILI CALCAREI DEL CORE V28-179: IMPLICAZIONI CLIMATICHE DURANTE IL PLIO-PLEISTOCENE

Relatore: *Prof.ssa Eliana FORNACIARI*
Correlatore: *Prof. Jan BACKMAN*

Laureando: Miriam PACCAGNELLA

ANNO ACCADEMICO 2012/2013

To my family,

who supported me psychologically and economically

in this adventure.

Alla mia famiglia,

Che mi ha sostenuto sia psicologicamente che economicamente

In questa avventura.

ACKNOWLEDGEMENT

TABLE OF CONTENTS

LIST OF TABLES

LIST OF FIGURES

ABSTRACT

The Central Pacific Ocean is an area of great interest for the oceanographers because the current high amount of nutrients and productivity provide an excellent study area for past environmental changes. A study was performed on a Plio-Pleistocene Core VEMA 28-179 (V28-179) positioned at 4° 37' N, 139° 36' W in the Pacific Ocean, 2081 cm in length and 4502 meters depth below the sea level in order to improve the paleoceanographic knowledges. The core is located along the equatorial zone which extends a range of high nutritional values.

Several studies are been performed on the Core V28-179 (Shackleton and Opdyke, 1977; Backman and Shackleton, 1983; Dunn, 1982) and integrated with sedimentation rates, carbonate contents, isotopic values and fossil contents in this thesis. It was possible to emphasize 2.7 to 3 million years ago a change of orbital and tectonic parameters, which would lead progressively to the North Hemisphere Glaciation.

Chapter 1 analyzes the visual description of the color, the carbonate content, particle size, the fossil content, sedimentary structures, the presence or absence of bioturbation and contacts that delimit net changes in the characteristics of the sediment. The high degree of compositional and structural changes indicate considerable variations in the carbonate content.

Chapter 2 analyzes the magnetic polarity reversals occurred in Core V28-179, based on Laurens et al. (2004). The sedimentation rate has not remained constant over the time. Different causes may have been variations of orbital parameters and variations of physical (particle transport and sedimentation) and chemical (diagenesis) parameters. In addition, the carbonate component from surface productivity involves almost all of the sediment composition in V28-179.

Chapter 3 analyzes the fossil content. In particular, we considered three species of calcareous nannofossils *Discoaster brouweri*, *Discoaster tamalis* and *Discoaster asymmetricus*. In particular we carried out the analysis of the abundance of species in the sediment from 1000 to 2065 cm, showing an effective predominance of the species *D. brouweri* than the other two species, up to about 700 individuals per mm-2 against approximately 110 and 75 respectively for *D. asymmetricus* and *D. tamalis*.

Chapter 4 is dedicated to the discussion about the processes involved in the carbon cycle (production, transport, deposition and post-depositional processes). V28-179 is positioned in an area of high surface productivity, driven by a high nutrients input, due to upwelling of cold deep waters in the east Pacific Ocean. This results in a high carbonate content. The $CaCO_3$ content analysis also showed a progressive increase from 4,085 Ma to the present time, probably caused by a nutrients increase, and an initial prominent cyclicity of ca. 400 000 years, that becomes indistinguishable in younger sediments. The migration northward of V28-179 position (plate tectonics movements), the migration of the high nutrient content area or its expansion can be the causes of variation in the calcium carbonate content.

Chapter 5 analyzes the isotopic values of oxygen (^{18}O / ^{16}O) and carbon (^{13}C / ^{12}C), both reconnected to the carbon cycle. From the carbon isotope at 2.1 Ma is evident a change in the mode of deposition. The comparison with the $CaCO_3$ content shows a stronger anti-phasing trend from 2.1 to 0 Ma. Oxygen isotope values shows an increase in $\delta^{18}O$ values, representing the transition from a warm climate to the formation of ice sheets in the northern hemisphere. Data were then compared with the isotopic values described by Shackleton and Opdyke (1977) and was summarized the isotopic antithetical diversity with the Atlantic Ocean.

In Chapter 6 was performed a research on temperature and orbital parameters variations, occurred during the Plio-Pleistocene. The closure of the Isthmus of Panama, the tibetan uplift and the closure of Indonesian Seaway are among the possible causes that has led to the glaciation of the northern

hemisphere, concomitant to changes in orbital parameters from cycles of 41 000 years to 100 000 years. The change in ocean circulation has led to strong variation in the heat distribution in oceanic waters and to the formation of upwelling zones, especially in the equatorial Pacific and along east coasts, where even today there is a seasonal atmospheric disturbance known as El Niño, the proof of the great changes that occurred in the past.

RIASSUNTO

L'Oceano Pacifico centrale è una zona di grande interesse per l'oceanografia perché l'attuale elevata quantità di nutrienti e la produttività organica forniscono un'ottima area per lo studio dei cambiamenti paleoambientali. Al fine di contribuire al miglioramento delle conoscenze paleoceanografiche dell'area, è stato eseguito uno studio sulla carota di età Plio-Pleistocenica VEMA 28-179 (V28-179). Questa carota, lunga 2081 cm e prelevata ad una profondità di 4502 m al di sotto del livello del mare, è stata recuperata nell'Oceano Pacifico equatoriale, a 4° 37' di latitudine N, e a 139° 36' di longitudine O, in una fascia caratterizzata attualmente da alti apporti di nutrienti.

Gli studi eseguiti in precedenza sul Core V28-179 (Shackleton e Opdyke, 1977; Backman e Shackleton, 1983; Dunn, 1982) sono stati integrati con quelli eseguiti durante questa tesi. Essi sono consistiti nell'analisi geochimica isotopica, paleontologica e nel calcolo delle velocità di sedimentazione della carota indagata. Su queste basi è stato possibile mettere in evidenza un cambiamento dei parametri orbitali e tettonici che portò 2.7-3 milioni di anni fa alla progressiva glaciazione dell'emisfero nord.

Nel Capitolo 1 è stata fatta una descrizione macroscopica della carota (colore, contenuto in carbonato, granulometria, contenuto fossilifero, strutture sedimentarie, presenza o meno di bioturbazione e/o contatti netti che delimitano cambiamenti nelle caratteristiche del sedimento). L'elevato grado di cambiamenti composizionali e strutturali indicano forti oscillazioni del tenore in $CaCO_3$.

Nel Capitolo 2 sono riportati i dati magnetostratigrafici ed il modello di età basati su Laurens et al. (2004). Questi dati indicano che il tasso di sedimentazione non è rimasto costante nel tempo. La causa può essere attribuita sia a variazioni dei parametri orbitali, sia a variazioni dei parametri fisici (e.g. sedimentazione) e chimici (e.g. diagenesi). Inoltre, la maggior parte del contributo carbonatico dei sedimenti analizzati deriva dalla produttività superficiale

Nel Capitolo 3 viene analizzato il contenuto in nannofossili calcarei del Core V28-179. In particolare, nell'intervallo tra 1000 cm e 2065 cm, sono prese in considerazione le abbondanze su mm^{-2} di tre specie di nannofossili calcarei: *Discoaster brouweri*, *Discoaster tamalis* e *Discoaster asymmetricus*. I risultati delle analisi indicano la predominanza della specie *D. brouweri* rispetto alle altre due (700 individui per mm^{-2} contro circa 110 e 75 rispettivamente per *D. asymmetricus* e *D. tamalis*).

Nel Capitolo 4 vengono affrontate le problematiche relative ai processi che intervengono nel ciclo del carbonio (produzione, trasporto, deposizione e processi post-deposizionali). La carota V28-179 è posizionata in un'area ad alta produttività superficiale a causa di upwelling di acque profonde e fredde nel Pacifico orientale. Questa ingente produttività determina l'elevato tenore in Carbonato di Calcio nei sedimenti. Le analisi del contenuto in $CaCO_3$ mostrano, inoltre, sia un progressivo aumento dello stesso a partire da 4.085 milioni di anni, presumibilmente generato da un aumento dei nutrienti, sia una evidente ciclicità di ca. 400 000 anni, che però diventa indistinguibile nei sedimenti più giovani. Cause della variazione nel contenuto in carbonato di calcio potrebbero essere: la migrazione verso nord della posizione del Core V28-179 provocata da movimenti tettonici, la migrazione della zona ad elevato contenuto in nutrienti o la sua espansione.

Nel Capitolo 5 vengono analizzati i dati delle curve degli isotopi stabili dell'ossigeno (^{18}O / ^{16}O) e del carbonio (^{13}C / ^{12}C) sul *bulk* prodotte durante questa tesi. I dati relativi all'andamento della curva degli isotopi stabili del carbonio evidenziano come a 2.1 milioni di anni sia avvenuto un cambiamento nella modalità di deposizione. Il confronto con la curva del $CaCO_3$ mostra un ben evidente andamento anti-fase da 2.1 a 0 milioni di anni. L'andamento della curva degli isotopi stabili dell'ossigeno mostra il passaggio da un clima caldo ad un clima caratterizzato da calotte di ghiaccio nell'emisfero nord. I dati prodotti durante la tesi sono stati poi confrontati con quelli di Shackleton e Opdyke (1977) basati sull'analisi isotopiche del foraminifero bentonico *Globocassidulina*

Subglobosa . Infine è stata sintetizzata la diversità dei valori isotopici che è antitetica rispetto l'Oceano Atlantico.

Nel Capitolo 6, è sono stati confrontati i dati delle curve geochimiche (CaCO3 isotopi stabile del C e dell'O) prodotte durante l'elaborato di tesi con quelle della temperature e dei parametri orbitali di Maslin e Ridgwell (2005) avvenute durante il Plio-Pleistocene.

La chiusura dell'Istmo di Panama, l'innalzamento dell'Altopiano del Tibet e la chiusura dello stretto indonesiano sono tra le possibili cause che hanno portato alla glaciazione dell'emisfero nord, assieme al cambiamento dei parametri orbitali da cicli di 40 000 anni a 100 000 anni. La variazione nella circolazione oceanica portò a sconvolgimenti delle temperature delle acque oceaniche e alla formazione di zone di upwelling, specialmente nel Pacifico equatoriale e lungo le coste orientali, dove ancora tutt'oggi è presente una perturbazione stagionale chiamata El Niño, la prova delle grandi variazioni avvenute nel passato.

CHAPTER 2

AGE MODEL

2.1   Magnetostratigraphy

The Magnetostratigraphy method is used to establish the magnetic field at the moment of the deposition of a stratum. Several oriented and not magnetically alterated samples are collected through a section and carried to the laboratory for the Remanent Magnetization analysis. This method use diamagnetic (for example organic matter, quartz, calcite) and paramagnetic (biotite, pyrite, ilmenite, siderite) materials to identify, through advisable corrections, the paleoposition of the taken samples to reconstruct the paleopole and the Earth's magnetic field at the sample deposition time.
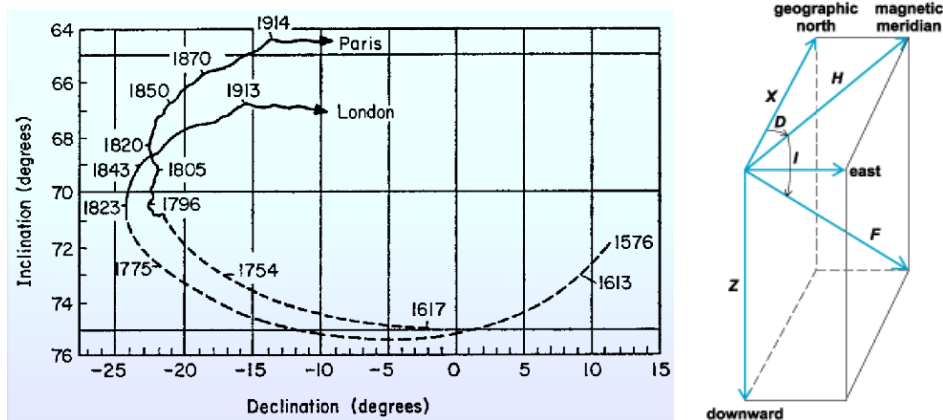
Figure 1 Paleopole position from 16th century. Inclination is referred to the angle between the magnetic meridian and the true magnetic field, the declination is referred to the angle between the geographic North and the magnetic meridian (web sites: http://geophysics.ou.edu/solid_earth/notes/mag_earth/earth.htm, http://www.answers.com/topic/geomagnetism-1).

A Geomagnetic Polarity Time Scale (GPTS) it was created using magnetic anomalies of samples measured on the ocean basins in order to compare these data with data on the land and to provide the best possible dating.

Several scales are been used in the past and a lot of changes are been applied in conjunction with technical evolutions and the research progress; in this thesis has been used the Lourens et al. (2004) time scale, which integrate magnetobiochrono stratigraphy with orbital parameters, in particular with first-order cycles, and link marine sediments with quaternary sediments . This timescale it is based on sea-floor spreading South Atlantic measurements. Black parts represent normal polarity and white parts represent inverse polarity.
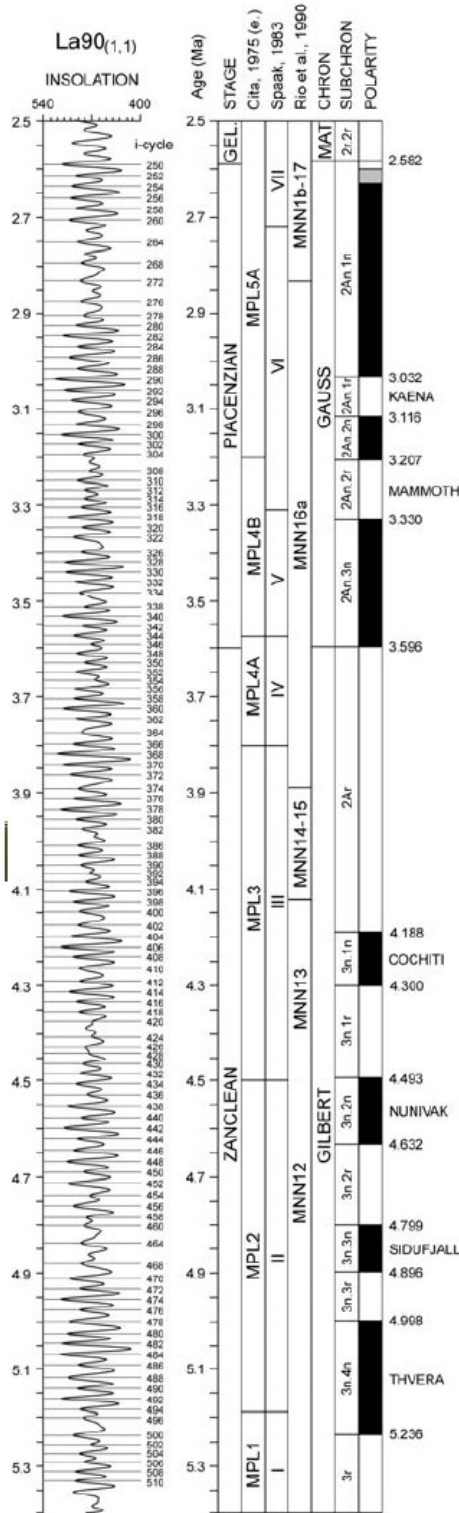
Figure 2 Lourens et al. (2004) Pliocene astronomical tuned time scale for the Cenozoic Era and the Geological Time Scale for the last 23 Ma (from International Stratigraphic chart, ICS 2008).

Figure 3 Correlation method

(website: http://www2.brevard.edu/reynoljh/vita/magnetostratigraphy.html).

The age data can be correlated with thicknesses of the same lithologic composition to found the sedimentation rates in marine environment and understand the processes at the base of the formation of the sediment.

2.2   Magnetic boundaries and sedimentation rate

In core V28-179 a magnetic record has been presented by Shackleton and Opdyke (1977) in order to correlate the depth in the core and the magnetic record using the paleomagnetic polarity scale.

They proposed the follow magnetic boundaries (with a depth error between 2.5 cm and 3 cm):

Table 1 Magnetic boundaries and correlation with the age (Lourens et al., 2004).

Core V28-179 boundaries	Depth (m) Shackleton and Opdyke, 1977	Age (m.y.) Lourens et al., 2004
Top	0,00	0
Brunhes/Matuyama	5,27	0,781
Matuyama/Jaramillo	6,57	0,988
Jaramillo/Mautyama	7,00	1,072
Matuyama/Olduvai	10,07	1,778
Olduvai/Matuyama	10,68	1,945
Matuyama/Gauss	13,58	2,581
Gauss/Kaena	14,88	3,032
Kaena/Gauss	15,17	3,116
Gauss/Mammoth	15,58	3,207
Mammoth/Gauss	16,22	3,330
Gauss/Gilbert	17,79	3,596

The magnetic measurements are made every 5 cm interval using a fluxgate magnetometer (Molyneaux, 1971), consist of a magnetically susceptible core surrounded by an electrical current passing through a wire and activated by a magnetic field.

Between reversal boundaries, sedimentation rates can be calculated for each level using the follow expression:

$$LSR = \frac{Depth\ 2 -\ Depth\ 1}{Age\ 2 - Age\ 1}$$

Were LSR is linear sedimentation rate and is expressed in m/m.y.

Table 2 Linear sedimentation rate.

Depth (m) Shackleton and Opdyke, 1977	Age (m.y.) Lourens et al., 2004	LSR (m/m.y.)
0,00	0	
5,27	0,781	6,75
6,57	0,988	6,28
7,00	1,072	5,12
10,07	1,778	4,35
10,68	1,945	3,65
13,58	2,581	4,56
14,88	3,032	2,88
15,17	3,116	3,45
15,58	3,207	4,51
16,22	3,330	5,20
17,79	3,596	5,90
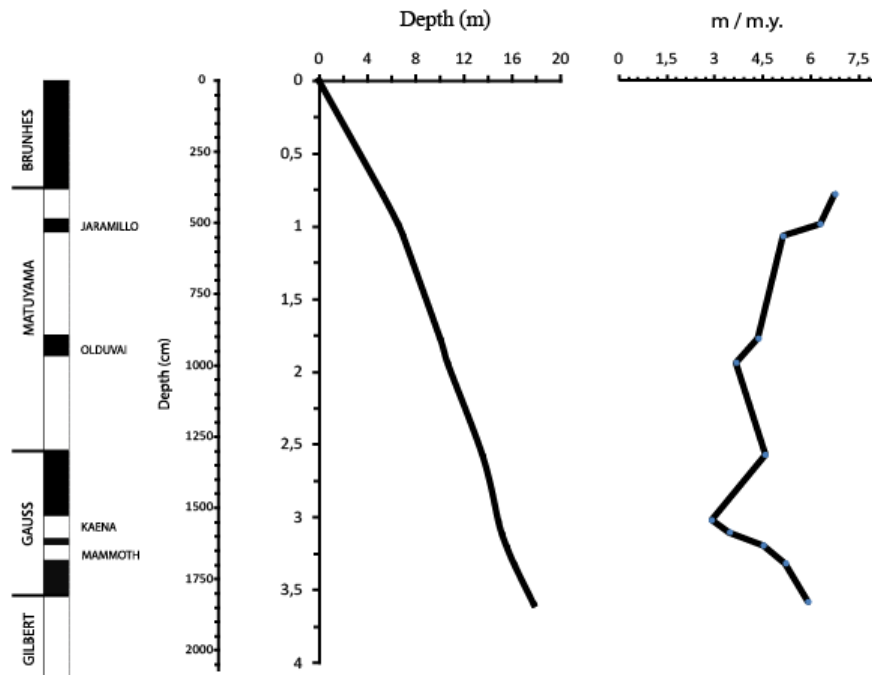
Figure 4 Age versus depth and sedimentation rate (m / m.y.) in hole V28-179.

This is an average based only on the magnetic boundaries but it is possible to observe that there are some slight variations in sedimentation rate (SR) between the different magnetic times: more the curve is leaning and more low is the SR, less the curve is leaning and more high is the SR.

In the upper 2,581 m the SR is more or less constant, with a light decrease between 0,988 m and 1,072 m and between 1,778 m and 1,945 m . At 2,581 m the SR decrease from 4,56 m/m.y. to 2,88 m/m.y. At 3,032 m the SR increase from 2,88 m/m.y. to 5,90 m/m.y. A change in litology occur in combination whit the change in SR.

The factors that can lead to a variation in sedimentation rate can subdivide by astronomical processes, physical processes and chemical processes and are connected to each other.

The first group enclose all that processes that involve changes in astronomical parameters like seasonal variations, variation of the Earth's orbit and obliquity (see Chapter 6).

The second group, physical processes, include all that processes that involve physical parameters like wind transport, deep circulation transport or gravity flow.

In the last group are involved those processes that are dominated by chemical reactions for example precipitation from hydrothermal solutions (in proximity of mid-ocean ridges; in the South Pacific near the East Pacific Rise), authigenic deposits. Connected to these factors are the ocean water parameters in which the reactions take place and the input material in the ocean; salinity, temperature and density of the water (connected with temperature) play together to modify the dissolution degree.

Input of biogenic material depend by a combination of all these processes (e.g. change in orbital parameters = change in oceanic circulation = increase of nutrients = increase in productivity = increase in the flow to the ocean floor = deepening of the total dissolution depth (e.g. calcite compensation depth CCD) = increase of SR).

So the sedimentation rate can be influenced by all these factors and is inversely proportional to the depth because at greater depth (depends by the ocean conditions) all the major biogenic, terrigenous or carbonate particles are dissolved and the sedimentation rate is very slow.

Nearshore sediments, turbidites	Up to km/my (kilometers/million years)
Hemipelagic deposits	Tens to hundreds of m/my
Drift deposits	40-400 m/my
Mid-latitude eolian deposits	3 to 10 m/my
Ice rafted material	10+ m/my
Carbonate oozes	Up to 50 m/my
Siliceous oozes	Up to 10 m/my
Hydrothermal deposits (off ridge axes)	About 0.5 m/my
Hydrogenous sediments	Rarely exceed 0.2 m/my
Ferromanganese nodules	0.0002 to 0.005 m/my (0.2 to 5 mm/my)

Figure 5 Typical sedimentation rates taken from different marine cores (website http://www2.ocean.washington.edu/oc540/lec01-16/).

In V28-179 the SR seesaw between about 7 m/m.y. and 3 m/m.y.; this rate is very low because the inputs from the continent doesn't reach long distances. The only inputs came from fine particles transported by the wind and biogenic input, the last more meaningful than the first.

Then it can be deducible that have been variations in surface productivity caused by variations in the oceanic conditions.
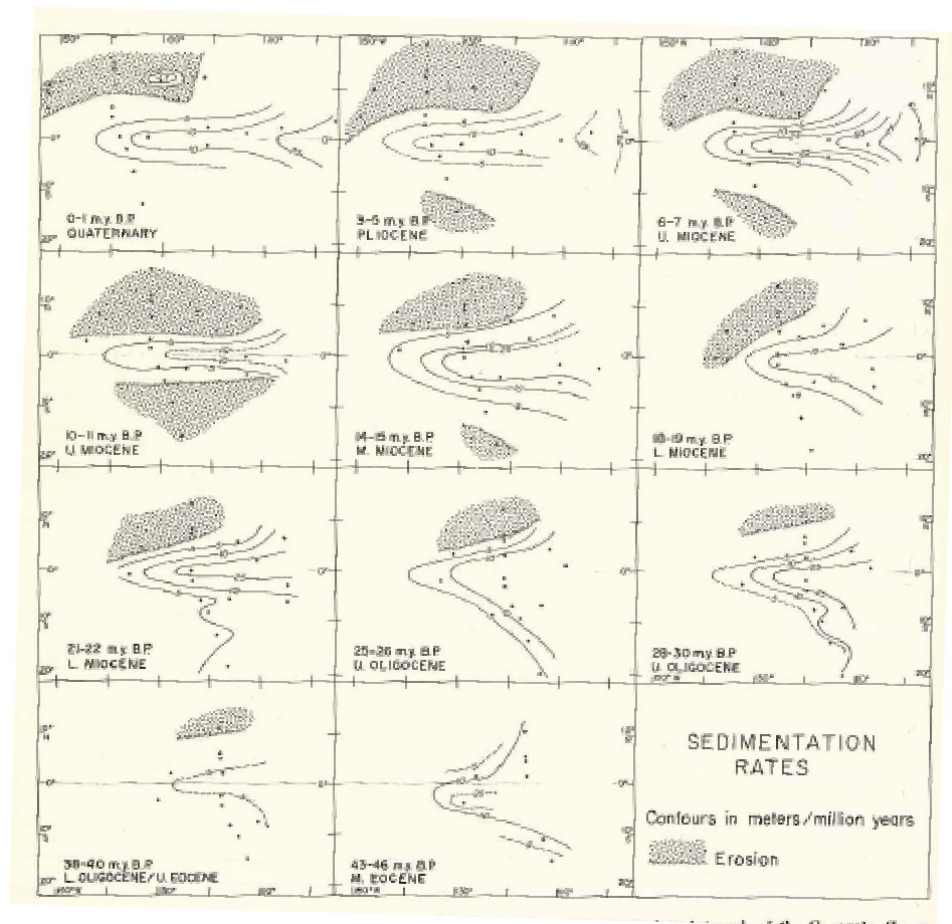
Figure 6 Isopleth maps of sedimentation rate during the Cenozoic
(Van Andel, 1975).

CHAPTER 3

NANNOFOSSILS IN V28-179

Calcareous nannofossils are useful for investigating biostratigraphic relationships in marine sediments. They may also be useful for paleoenvironmental analysis, for example, from stable isotope (δ^{18}O and δ^{13}C) measurements of their carbonate shells. These organisms may record the water paleoconditions of the oceans such as temperature and salinity and, through their abundance, can record nutrient supply.

Furthermore, the taxonomic composition change with latitude (temperature) showing decreasing diversification away from the Equator.

Countless studies have been performed in the Pacific Ocean by different authors. For example, Backman and Shackleton (1983) studied the Plio-Pleistocene calcareous nannofossils in the Pacific, Atlantic and Indian Ocean, and Bukry (1971) studied the Cenozoic calcareous nannofossils of the Pacific Ocean.

3.1   Nannofossils morphology and distribution

The morphology of the nannofossils skeletons allow us to classify living and fossil species. This classification, called taxonomy, is useful for correlating individual species in different parts of the world and provide a means to reconstruct paleoenvironments in the past. In addition, assuming that the processes that occur today follow the same laws as those that occurred in the past, it is possible to reconstruct past conditions by studying living forms, that currently populate our oceans.

Nannoplancton is subjected to the life-cycle, in which they record isotopes values, flow to the sea-bed and time in which organisms remain there, correlated to dissolution rate.

They are marine unicellular autotroph algae that during their life secretes carbonate to create the coccosphere. This is composed by several number of coccoliths (10 to 100 and dimensions 1-50 µm), disk-like plates, that after the death descend along the water column and deposits on the sea floor.

They represent the highest carbonate contributor to pelagic and hemipelagic sediments.

The majority of this type of skeletal remains of carbonate are called coccoliths and nannoliths.

The coccolithogenesis (the formation of the coccoliths) takes place in the cell. When they are formed, or almost formed, they migrate towards the membrane and forms the coccosphere.
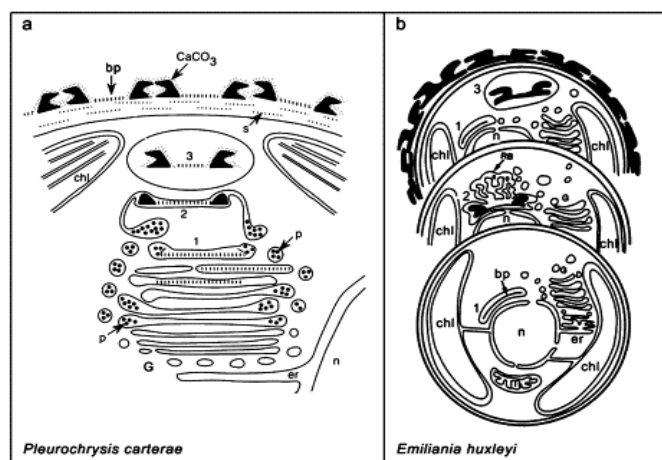
Figure 7 Formation of the coccosphere through the extrusion of coccoliths. In this case *Pleurochrysis carterae* and *Emiliania huxleyi* (Marsh, 2003).

The function of this shell is not yet known exactly but can serve to: protection from predators, metabolic barrier, flotation, light-protection or vice versa light-absorption or waste products

(Source: http://www.ucl.ac.uk/GeolSci/micropal/calcnanno.html).

3.2   Studies in V28-179

Calcareous nannofossils in Core V28-179 was performed by Backman and Shackleton (1983). Their abundance data have been used in this study for the following taxa: *Discoater brouweri* (Tan Sin Hok, 1927) , *Discoaster asymmetricus* (Gartner, 1969), and *Discoaster tamalis* (Kamptner, 1967).

These studies were based on the abundance of the species (specimens / mm^2) using a light microscope.

Backman and Shackleton (1983) suggested that their counting method is proportional to the absolute abundance of the individual taxa. After weighing the sediment and filtering on microfilters, a few micrograms were separated for counts of total number of nannofossils using a scanning electron microscope. This number is related to the number of microfossils per gram of the sediment.

Another method to count the abundance is to count the number of specimens of a species respect to all specimens of a same genus. This method can be rather time-consuming but it can be useful to compare different data types. Core V28-179 preserves sedimentological, biostratigraphical and magnetostratigraphical records for the past 3.8 million years. It shows how the composition of the sediment and the abundance of species vary during Plio-Pleistocene times.

The three *Discoaster* species have been analyzed from 10 mbsf (meters below sea floor) to the base of the core.

The Cenozoic calcareous nannoplankton zonation by Martini (1971; NN Zones) and the nannofossil biostratigraphic scheme of Okada and Bukry (1980; CN Zones) have been used. The three taxa discussed are presented below:

Table 3 *Discoaster brouweri* taxonomy. Online source:
http://nannotax.org/category/nanno-
taxonomy/nannoliths/discoasteraceae/discoaster/d-brouweri-group/discoaster-
brouweri.

Name:	*Discoaster brouweri*
Description :	Ray tips non-bifurcate and with marked proximal extensions giving it a distinctive concavo-convex form. The distal surface is usually rather smooth, proximal surface more sculpted with proximal boss often present. Probably evolved from *D. exilis* and first occurrence is very gradational.
Type level:	This species is one of the most abundant and widespread forms of the late Tertiary, occurring in nearly every. Miocene sample examined from both sides of the Atlantic, Mediterranean and Pacific Oceans. It also occurs, less abundantly in sediments of probable late Oligocene age, and extends up into the Pliocene.
Type locality:	Road cut at U.S. Agric. Field Station at Mafron, Haiti; Rotti, near Timor; Suva formation, Fiji.
Remarks:	---
Geological time periods:	NN9, NN18 (Martini, 1971).
Occurrence:	Very common NN11-18 (Martini, 1971).
Biblio Reference:	Young, JR, 1998. Neogene. Calcareous nannofossil biostratigraphy, pp: 225-265.
Morphology and SEM photos:	

Table 4 *Discoaster tamalis* taxonomy. Online source:
http://nannotax.org/category/nanno-
taxonomy/nannoliths/discoasteraceae/discoaster/d-brouweri-group/discoaster-
triradiatu.
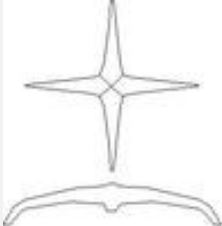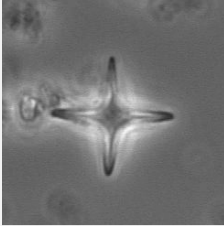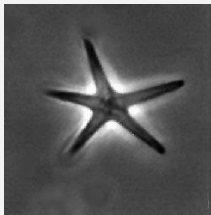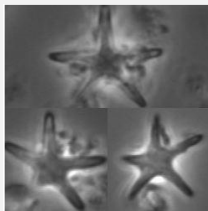
Name:	*Discoaster tamalis*
Description :	Variety of *D. brouweri* with four, symmetrically disposed rays.
Type level:	---
Type locality:	Station 388 Challenger Expedition, South Atlantic Ocean 21°15' S, 14°7' W.
Remarks:	Unlike *D. asymmetricus,* this form is very rare outside the mid Pliocene. It seems to have genuine first and last occurrences at, or very near to, the levels of the beginning and end of the *D. asymmetricus* acme. Within this range its abundance is closely related to that of *D. asymmetricus* (Bergen 1984, Backman 1986, Chapman & Chepstow-Lusty 1997). These two discoasters are also of similar size in any one sample.
Geological time periods:	NN16 , NN14 (Martini, 1971).
Occurrence:	Common in upper part of NN18 (typically occurring at 1/5 to 1/2 the abundance of D. brouweri), occasional specimens NN9-21 (but rarely occurring at more than a few percent of abundance of D. brouweri). (Martini, 1971).
Biblio Reference:	Young, JR, 1998. Neogene. Calcareous nannofossil biostratigraphy, pp: 225-265.
Morphology and SEM photos:	

Table 5 *Discoaster asymmetricus* taxonomy. Online source:
http://nannotax.org/category/nanno-
taxonomy/nannoliths/discoasteraceae/discoaster/d-brouweri-group/discoaster-
asymmetric.

Name:	***Discoaster asymmetricus***
Description :	Asymmetric 5-rayed variety of *D. brouweri*.
Type level:	Discoaster asymmetricus occurs from about the middle of the planktonic foraminifer zone N19 to middle of N21. Pliocene of Atlantic and Pacific.
Type locality:	DSDP 2 - 12C4; 19°41,76'N, 26°00,03'W; 4542 m; 32,6 m - 41,8 m beacath sea floor, 427 m recovered.
Remarks:	Most six rayed species produce asymmetric five rayed specimens, and *D. asymmetricus* can be found throughout the range of *D. brouweri*. However, they are notably more abundant, and more consistently present, in mid Pliocene sediments. It seems to be an intraspecific variety with a restricted stratigraphical acme. Both the beginning and the end of the acme can be used for biostratigraphy (cf. Bukry 1973a, Backman 1986).
Geological time periods:	NN18 , NN15 (Martini, 1971).
Occurrence:	Common NN15 to 16, occasional specimens NN9-18. (Martini, 1971)
Biblio Reference:	Young, JR. 1998. Neogene. Calcareous nannofossil biostratigraphy, pp: 225-265.
Morphology and SEM photos:	

Age (Ma)	GPTS	Epoch	Stage	CALCAREOUS NANNOFOSSIL ZONES				BIOHORIZON primary and additional
				Okada & Bukry 1980	Martini 1971	this study		
0.0	C1n	PLEISTOCENE (middle & late)		CN15	NN21	**CNPL11**	*C. cristatus* PRZ	Bc *Emiliania huxleyi*
				CN14b	NN20			B *Emiliania huxleyi* (0.29)
0.5		PLEISTOCENE (early)	Calabrian	CN14a	NN19	**CNPL10**	*Gephyrocapsa* (≥4µm) / *P. lacunosa* CRZ	T *Pseudoemiliania lacunosa* (0.43)
1.0	C1r							Tc *Reticulofenestra asanoi* (0.91) / Ta *Gephyrocapsa* (≥4 µm; 1.06)
				CN13b		**CNPL9**	Small *Gephyrocapsae* PRZ	Bc *Reticulofenestra asanoi* (1.14) / T *Helicosphaera sellii*
1.5						**CNPL8**	*Gephyrocapsa* (>5.5 µm) / *Gephyrocapsa* (≥4 µm) CRZ	T *Gephyrocapsa* (>5.5 µm; 1.25) / B *Gephyrocapsa* (>5.5 µm; 1.59) / T *Calcidiscus macintyrei* (1.60) / B *Gephyrocapsa* (≥4 µm; 1.71)
	C2n			CN13a		**CNPL7**	*C. macintyrei* PRZ	T *Discoaster brouweri* (1.93)
2.0	C2r	PLIOCENE (late)	Gelasian	CN12d	NN18	**CNPL6**	*D. brouweri* TZ	Bc *Discoaster triradiatus* (2.16)
2.5				CN12c	NN17	**CNPL5**	*D. pentaradiatus* TZ	T *Discoaster pentaradiatus* (2.39) / T *Discoaster surculus* (2.53)
		PLIOCENE (middle)	Piacenzian	CN12b				T *Discoaster tamalis* (2.76)
3.0	C2An			CN12a	NN16	**CNPL4**	*D. tamalis* TZ	
3.5								
								T *Sphenolithus* spp. (3.61)
4.0	C2Ar		Zanclean	CN11b	NN15 + NN14	**CNPL3**	*D. asymmetricus / R. pseudoumbilicus* CRZ	T *Reticulof. pseudoumbilicus* (3.82) / B *Pseudoemiliania lacunosa* / Bc *Discoaster asymmetricus* (4.04)
4.5	C3n	PLIOCENE (early)		CN11a	NN13	**CNPL2**	*S. neoabies* PRZ	T *Amaurolithus primus* (4.58) / B *Helicosphaera sellii*
				CN10c				
5.0				CN10b	NN12	**CNPL1**	*C. acutus* TRZ	T *Ceratolithus acutus* (5.04) / B *Ceratolithus rugosus* (5.08) / T *Triquetrorhabdulus rugosus* (5.23) / B *Ceratolithus larrymayeri* (5.33) / B *Ceratolithus acutus* (5.36)
5.5	C3r	MIO-CENE (late)	Mess-inian	CN10a		**CNM20**	*T. rugosus* PRZ	B *Ceratolithus atlanticus* (5.39) / T *Discoaster quinqueramus* (5.53)
				CN9b	NN11	**CNM19**	*D.quinqueramus* TZ	

Figure 8   Calcareous nannofossil biostratigraphic zonation of the past 5.7 Ma (Backman et al., submitted). Note base common of *D. asymmetricus* at 4.04 Ma, top *D. tamalis* at 2.76 Ma and top *D. brouweri* at 1.93 Ma.

39

3.2.1 Abundance and considerations

Core V28-179 from the middle Pacific Ocean, SW from the Hawaii islands, shows a low sedimentation rate (a mean of about 4.8 m/m.y.).

Below is a description of the abundance curves from 1005 cm to 2055 cm for the three studied species. Biohorizons are defined by using the concepts Base (B) and Top (T) (Backman et al., submitted), to avoid misunderstandings with the labels of FO / LO and HO / LO, which LO could refer both to Last Occurrence and Lowest Occurrence (Rio et al., 1984; Fornaciari et al., 2010). Furthermore, the common presence of a species is defined as Base common (Bc) and Top Common (Tc) (Raffi and Flores, 1995).

Discoaster brouweri is the most abundant species with respect to *D. tamalis* and *D. asymmetricus*, because its abundance exceed 650 specimens per mm^2 (Figure 9).

In the lower part of our core (20,65 m ±0,05) the *Discoaster* was present but in low quantity (about 40 specimens / mm^2); at about 19,45 m depth the number of specimens begins to grow to 16,70 m ±0,05 (~3.237 Ma) where the number of specimens exceed 600 specimens / mm^2. The ascent from the base of the core has a parabolic appearance. After this peak there is a sudden drop from 16,70 m ±0,05 to 16,10 m ±0,05, corresponding to a time interval of approximately 0.09 m.y. The subsequent recovery is much slower compared to the previous and is characterized by up and down cycles to the top at 12,55 m ±0,05 (~2.286 Ma) where the number of specimens is about 460 / mm^2. From this point start a new descent, slightly less abrupt than the last, leading to the extinction (T) at ~1.93 Ma (10,95 m ±0,05) as described by Backman and Shackleton (1983) (Figure 9).
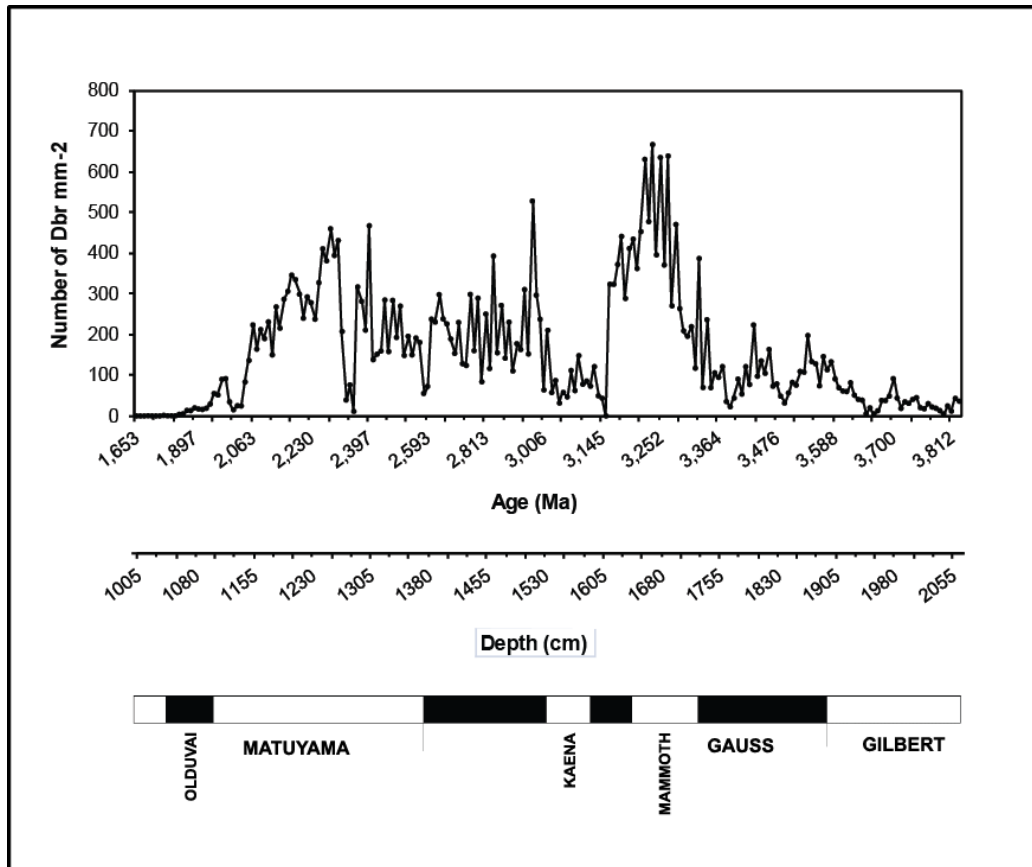
Figure 9   Abundance of *D. brouweri* in core V28-179
(number of specimens / mm^2).

Discoaster asymmetricus shows a similar trend but with substantial variations (Figure 10): the number of specimens at the bottom of the core is low (~0 to ~12 specimens per mm^2) to ~3.64 Ma (19,40 m ±0,05) when a slow and then rapid increase take place during a time interval of ~50.000 years. This "up and down" trend continues until ~3.305 Ma (17,15 m ±0,05). After this point there is a parabolic trend with upwards concavity and a minimum point between ~3.19 Ma and ~3.04 Ma. At 14,75 m ±0,05 (~2.872 Ma). This peak its only momentary because follow an unstoppable decline toward the top of the species included in a time interval between ~2.65 Ma and ~2.12 Ma. The uppermost occurrences were probably caused by reworked forms because the abundances are low after ~2.62 Ma (~1.4 specimens per mm^2).

41

Note the difference of the vertical scale compared to the scale of *D. brouweri*.
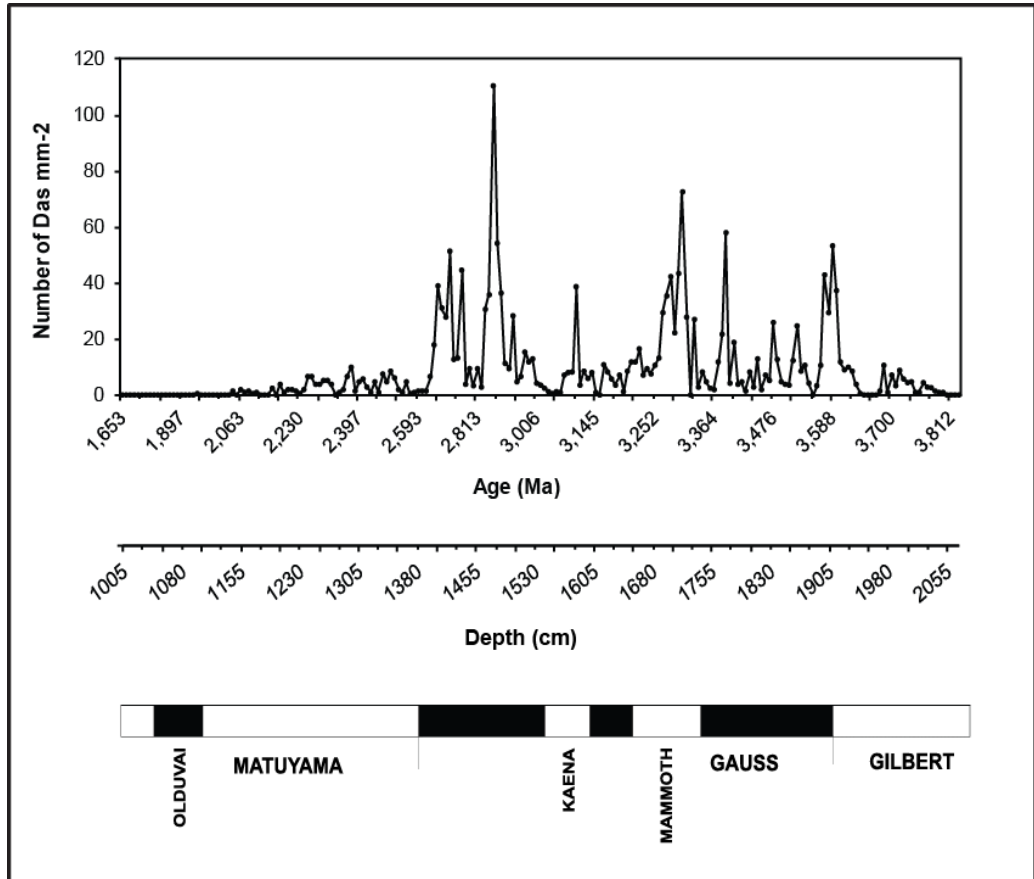
Figure 10 Abundance of *D. asymmetricus* in Core V28-179
(number of specimens / mm^2).

Discoaster tamalis shows an abundance pattern much more similar to *D. asymmetricus* than *D. brouweri* (Figure 11), but the number of specimens is even lower (the scale has been further reduced for the limited number of specimens). From the bottom of the core, *D. tamalis* remains absent to ~3.73 Ma (20 m ±0,05), marking the first appearance of the species. Until about 3,33 Ma the number of specimens varies between ~0 and ~21 (N / mm^2). At ~3.32 Ma the number increases abruptly to about 73, the most high number during the core interval.

This peak ends at ~3.25 Ma (16,80 m ±0,05). There is a new plateau (~0 to ~42 specimens) ending at ~2.92 Ma where there is a new peak that reaches 64 specimens, and finishes at ~2.83 Ma. There is a small recovery between ~2.77 Ma and ~2.64 Ma (1,395 m ±0,05) where there top of the range occurs.
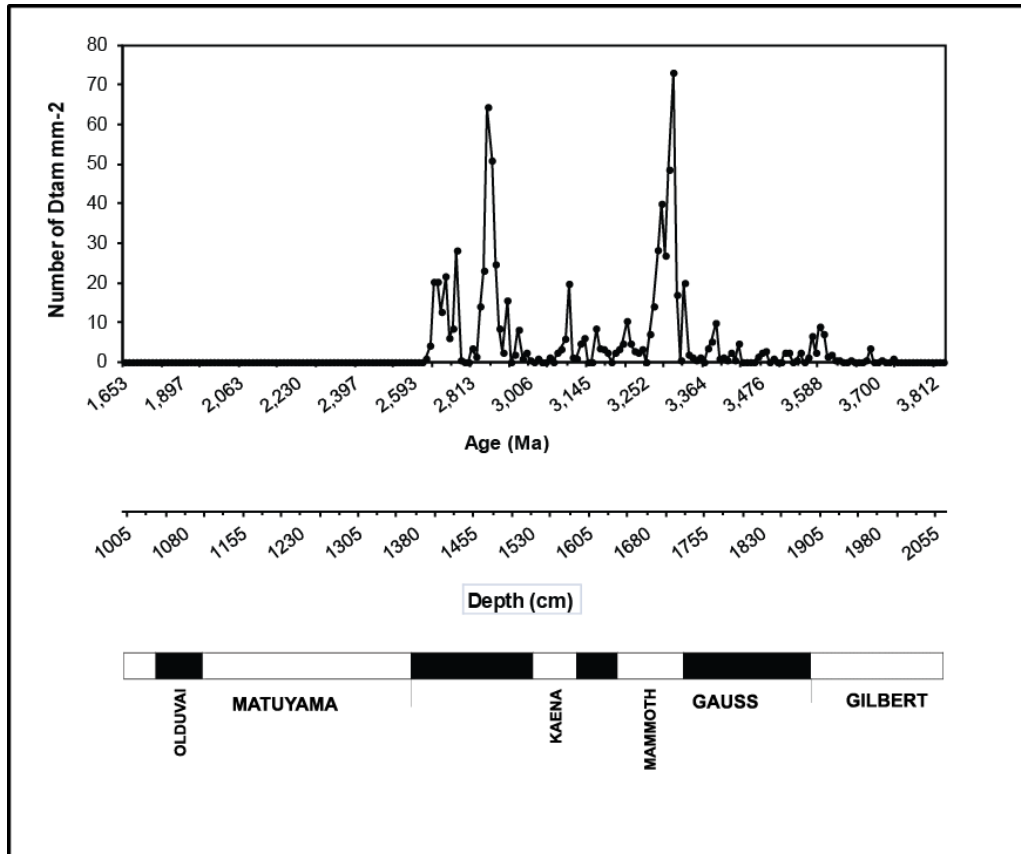
Figure 11 Abundance of *D. tamalis* in Core V28-179
(number of specimens / mm^2).

Table 6 Biohorizons for calcareous nannofossils (Backman et al., submitted)

from about 1.653 Ma to 3.828 Ma in core V28-179.

T = top, B=base, Tc = top common, Bc = base common.

Event	Species	Age (Ma)	Depth (cm)	LSR (m/m.y.)	GPTS (Lourens et al. 2004)
T	*D. brouweri*	1.93	1095	2,012	
T	*D. tamalis*	2.76	1437	2,764	
Bc	*D. asymmetricus*	4.04	----	----	
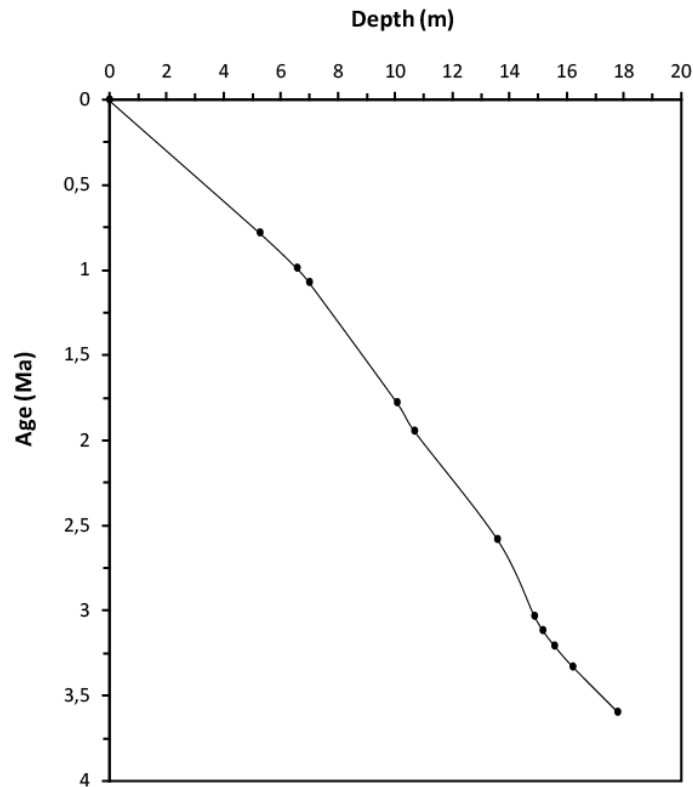
Figure 12 Linear sedimentation rate.

The abundance pattern of D. asymmetricus and D. tamalis are similar even if the number of specimens is almost doubled in *D. asymmetricus* compared with *D. tamalis*. In particular both species shows two main peaks at 2.87 Ma (at the end of the Gauss magnetic chron) and 3.30 Ma (in the middle of Mammoth sub-chronozone) for *D. tamalis*. In the curve of *D. asymmetricus* the situation is not so clear: there are two other peaks less intense at 3.39 Ma and 3.59 Ma, not shown in the *D. tamalis* curve

Discoaster brouweri seems to be minimally influenced by the same factor that involve *D. asymmetricus* and *D. tamalis* because the peaks do not coincide between them. It is possible to conclude that *D.brouweri* is influenced by other factors.

A further hypothesis can be that the peaks could be masked due to other factors.
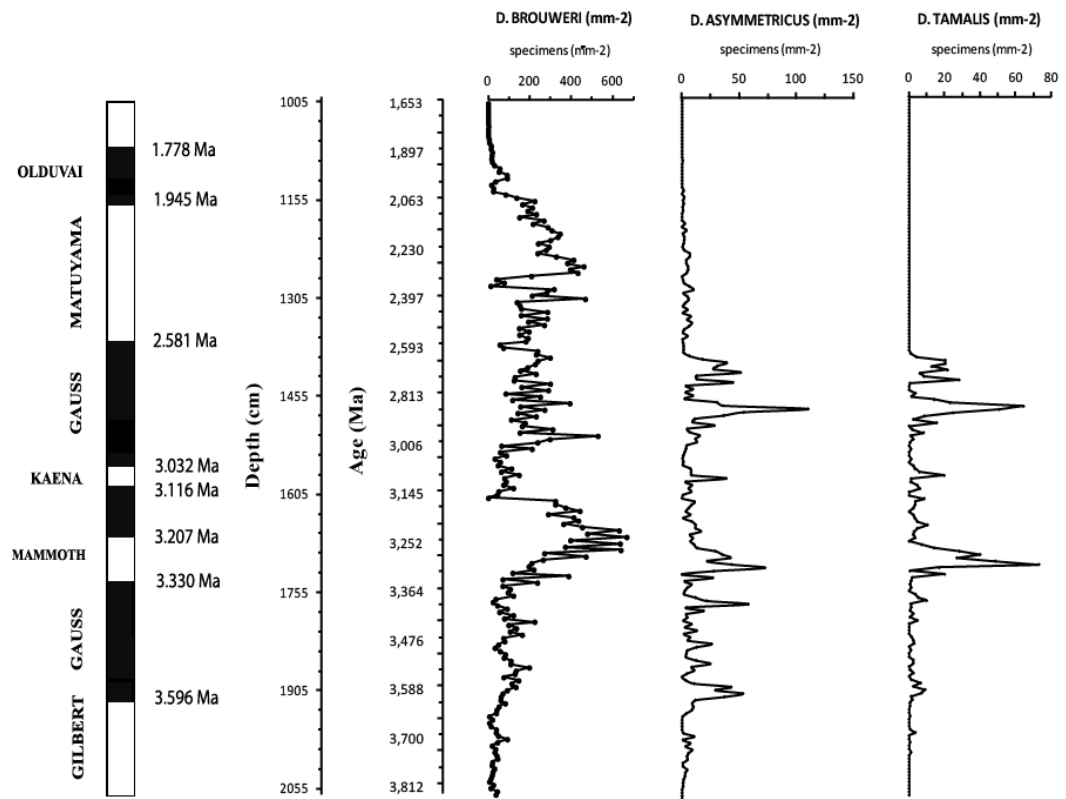
Figure 13 Comparison between the three species in core V28-179.

Irrespective of the type of species, all the three *Discoaster* meet to environmental changes during time. From the Figure 13 it is possible to note that there is an up and down trend during time. Remember that the major contribution comes from the *D. brouweri*.
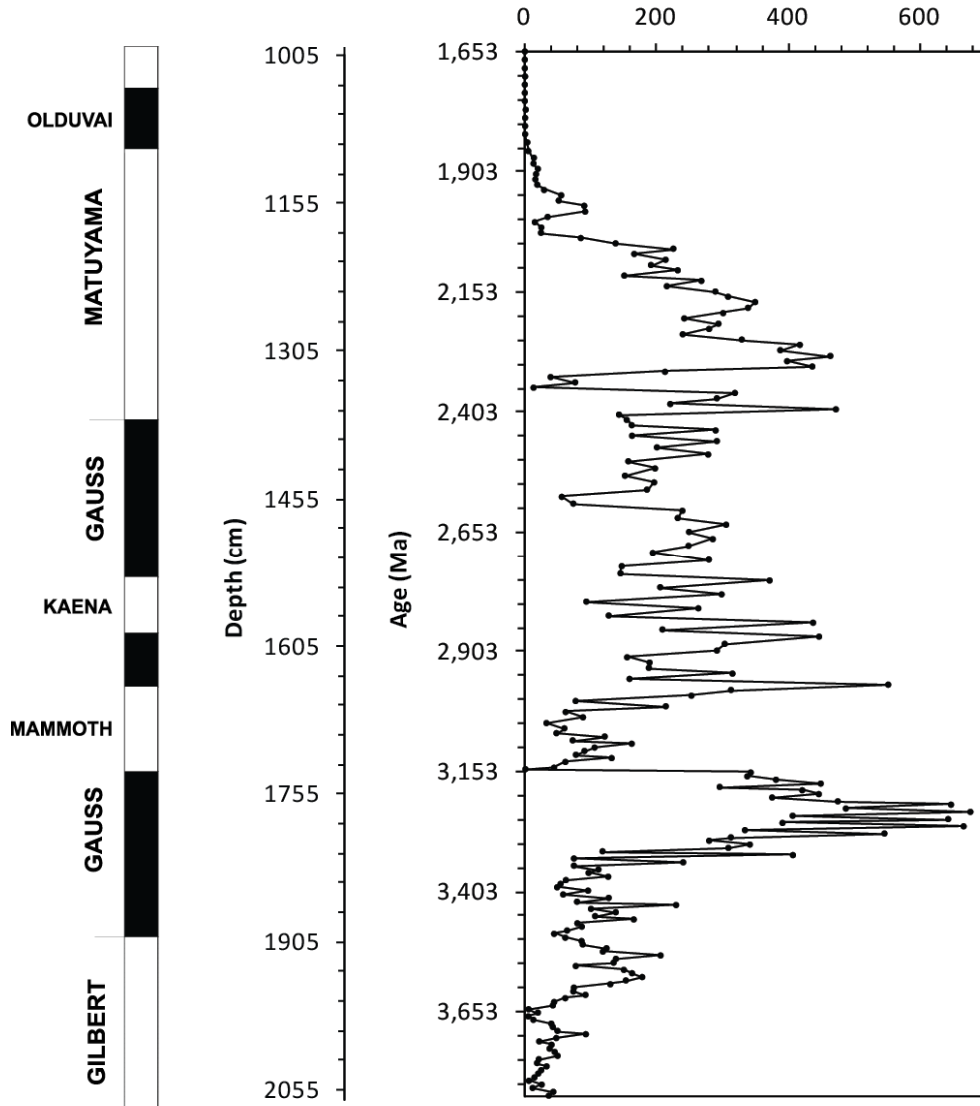
Figure 14   Total abundance of the three species.

Table 7 Comparison between *% D. brouweri*, *% D. tamalis* and *% D. asymmetricus* in depth, age, magnetostratigraphy and biostratigraphy.
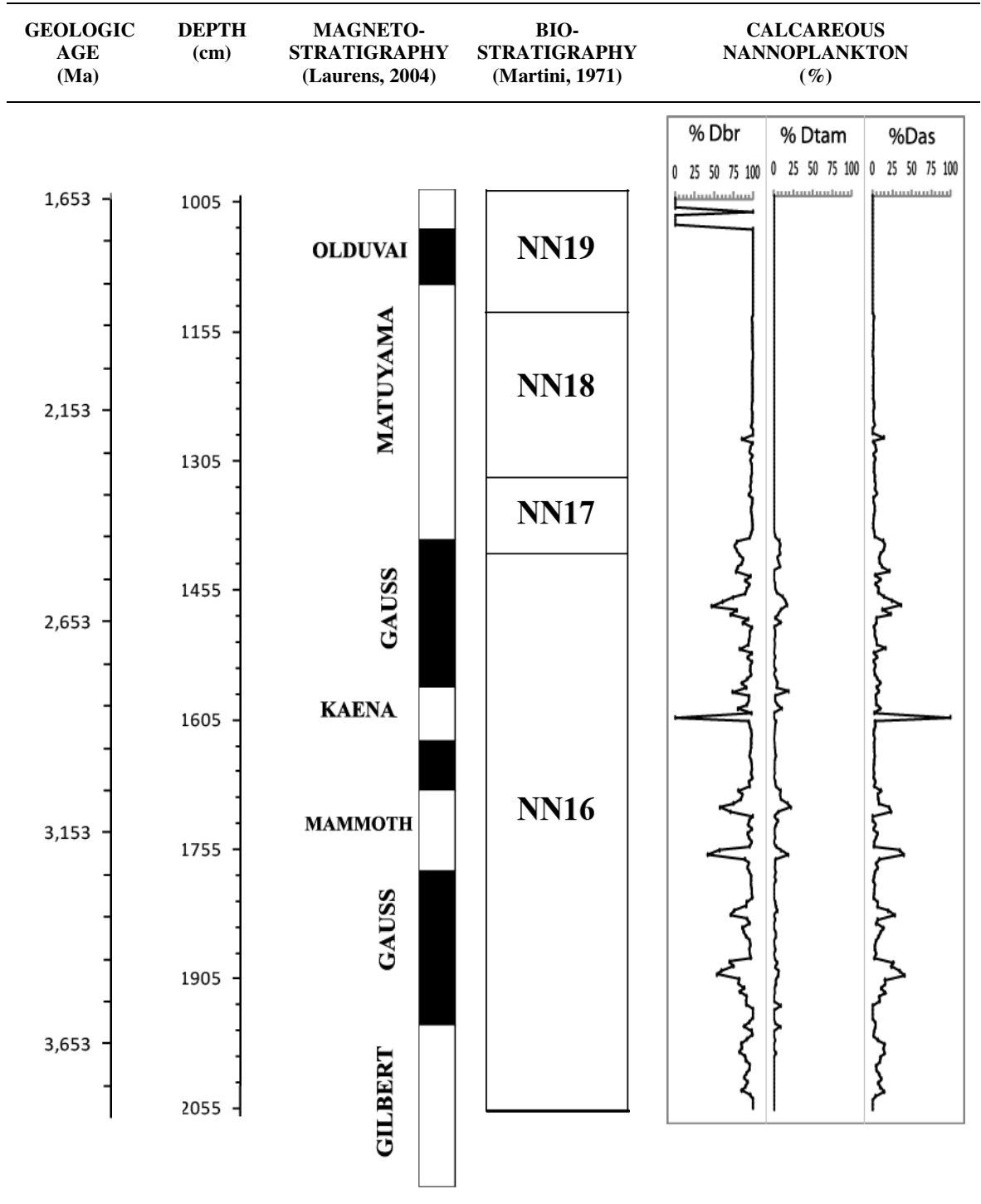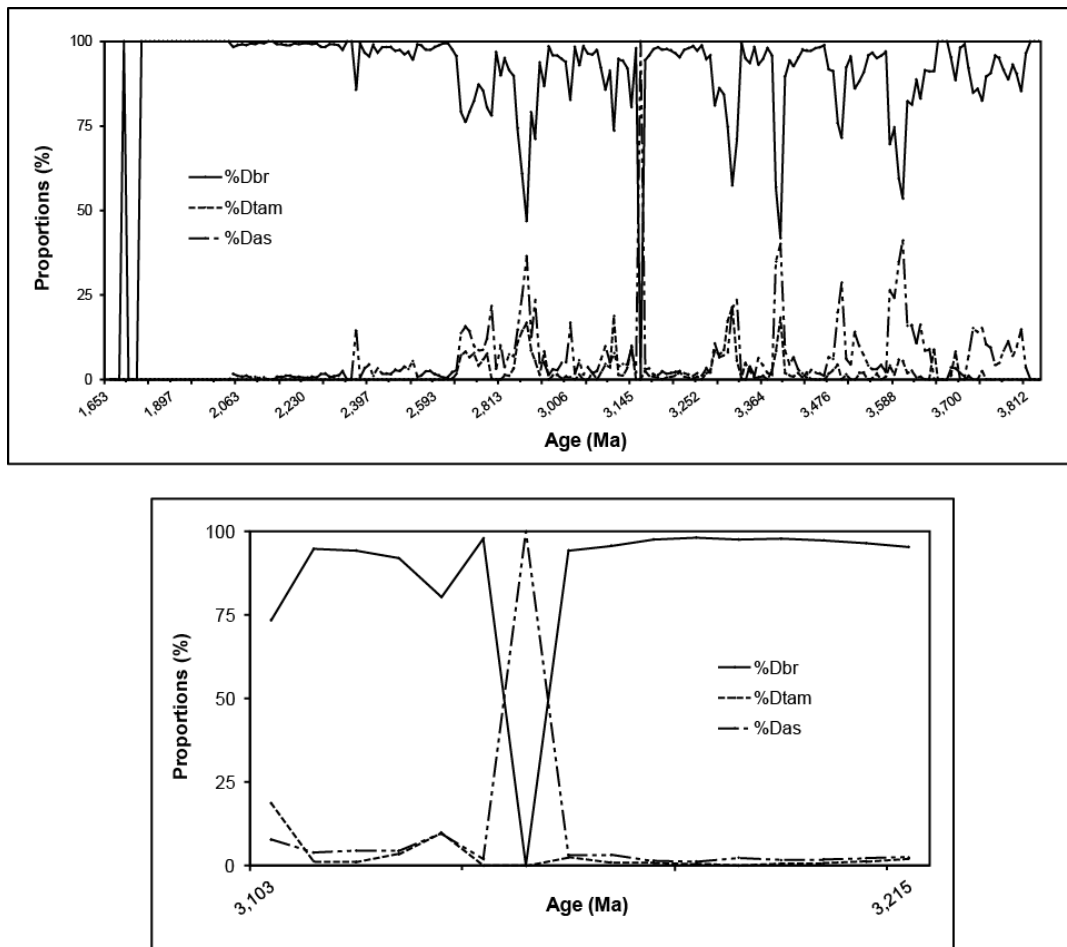
Figure 15 Proportions of *D. brouweri*, *D. asymmetricus* and *D. tamalis* and a
blow up between 3.103 Ma and 3.215 Ma (lower panel).
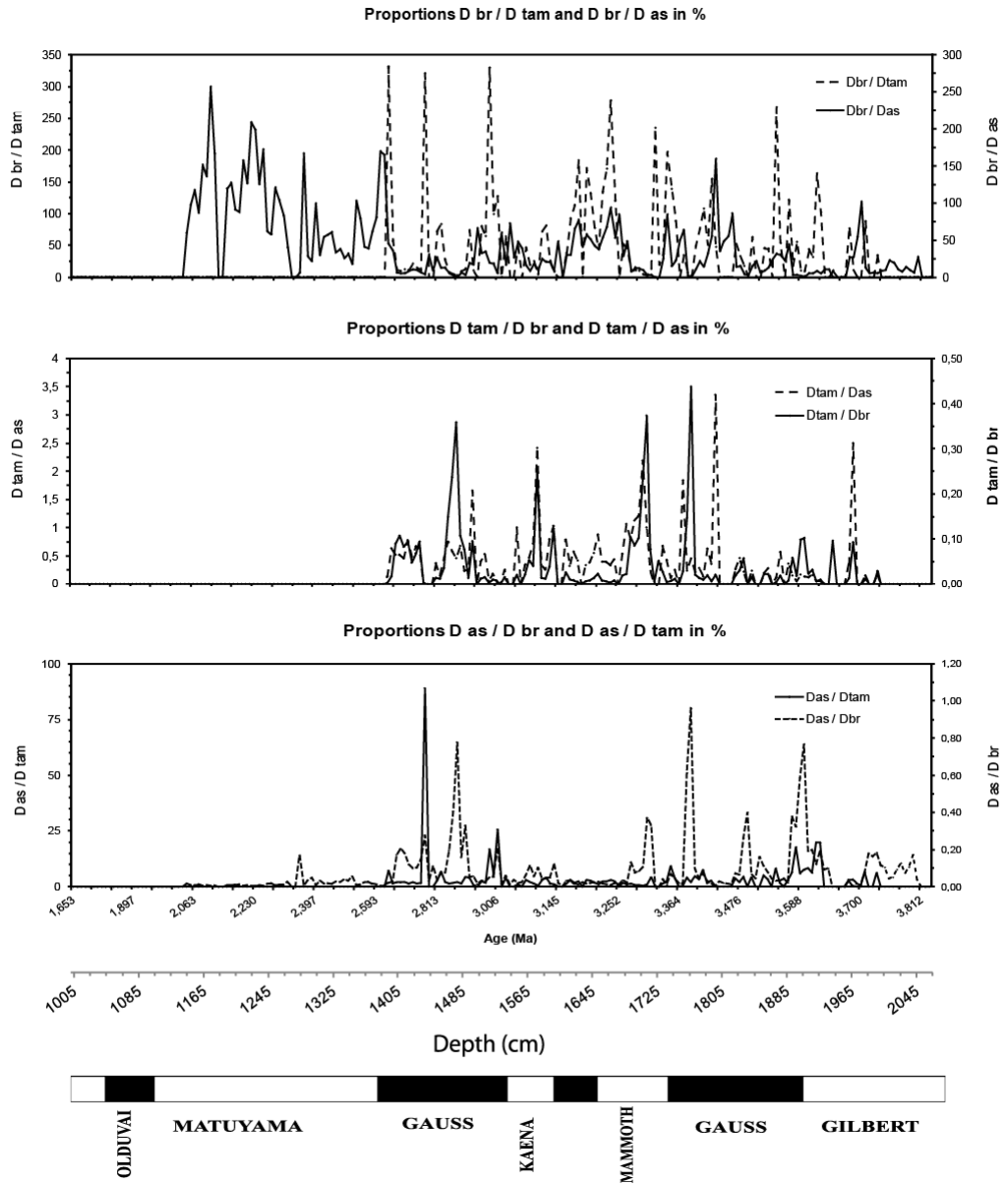
Figure 16   Corresponding proportions (%) between *D. brouweri*, *D. asymmetricus* and *D. tamalis*.

3.3 A comparison between Shackleton and Opdyke (1977) and Lourens (2004)'s magnetic scale: technological improvements during time

Different isotope studies have been performed from different cores around the world so as to understand the past climate changes and paleoenvironments.

By analyzing the magnetic properties, mineralogy and grain size it is possible to interpret the conditions in which the sediment has been deposed. Different studies were written in this regard to create a correlation method between different types of analysis; for example paleomagnetic directions of coarse and fine fraction of magnetized minerals in deep sea sediments in Pacific and Atlantic oceans (Vali et al., 1989).

Successions of an Equatorial Pacific core were correlated with sequences described by Emiliani in the Caribbean and Atlantic Ocean (Shackleton and Opdyke, 1973).

Magnetic measurements were performed by Shackleton and Opdyke (1977) on Core V28-179 at 5 cm intervals with the external alternating field method. They also analyzed carbon and oxygen isotopes on benthic foraminifers. The goal was to find glacial-interglacial fluctuations for the past 3.2 Ma and correlate the data with the standard paleomagnetic polarity time scale.

Shackleton and Opdyke's (1977) carbon and oxygen isotopes data were performed on *Globocassidulina subglobosa* in a spatial interval from 2060 cm to 1011 cm (3.8 Ma to 1.7 Ma - Lourens et al., 2004) . The $\delta^{18}O$ ‰$_o$ PDB[1] values shows a gradual increase of the ratio in aid to the heaviest isotope ^{18}O to mean the

---

[1] The original PDB sample was a sample of fossilized shells of an extinct organism called a belemnite collected decades ago from the banks of the Pee Dee River in South Carolina. The original sample was used up long ago, but other reference standards were calibrated to that original sample. We still report isotope values relative to PDB. (Source: http://wwwrcamnl.wr.usgs.gov/isoig/projects/fingernails/results/interpretdata.html)

passage from interglacial (below about 17 meters) to glacial during the first Gauss epoch.

From 1977 the International Commission of Stratigraphy (ICS) has improved the international chronostratigraphic scale; in over thirty years new technologies are evolved and consequently new interpolation techniques as extracting linear time[2] or statistical techniques. It was necessary to modify and correct uncertainties like Cenozoic stage boundaries, stage names, tuning the Neogene with 40 kyr accuracy, orbital scaling, stratigraphic integrations, data set that used Ar/Ar and U/Pb methods, evolved during time and data with statistical and mathematical techniques.

The newest Lourens et al. (2004) Geologic Time Scale (GTS 2004) present renewals in this respect and introduce the astronomical dating method for the pre-late Pleistocene. This method use the Earth's orbital cyclic parameters changes that influence the solar input and that are repeated every 413 000, 100 000, 41 000 and 21 000 years. Furthermore, also the ODP studies have greatly helped in the construction of the new time scale.

---

[2] Method to compare two spaced data set and process at least one of them in order to compare the spacing. With this method the error possibility is less than others.

Table 8 Comparison between Shackleton's and Lourens's paleomagnetic
polarity time scale. The ages for the Shackleton's time scale are
provided by depths of the core V28-179 presented in the 1977's
article.

Shackleton vs Lourens		Shackleton et al. (1977)	Lourens et al. (2004)
	Olduvai	1.66 Ma – 1.87 Ma	1.778 Ma – 1.945 Ma
	MAT-GAU	2.47 Ma	2.581 Ma
	Kaena	2.91 Ma – 2.98 Ma	3.032 Ma – 3.116 Ma
	Mammoth	3.07 Ma – 3.17 Ma	3.207 Ma – 3.330 Ma
	GAU-GIL	3.4 Ma	3.596 Ma

MATUYAMA

2.47 Ma

2.581 Ma

GAUSS

3.58 Ma

3.596 Ma

GILBERT

CHAPTER 4

CARBONATE CONTENT

4.1 Productivity and preservation

4.1.1 Origin and transport of matter and source of oceanic organic matter

The sources of carbonate on the Earth have different genetic histories involving fluvial, atmospheric and primary production carbon sources. The carbonate sediment deposited in the oceans is a important part of the global carbon cycle.

The atmospheric pathway provides long distance transport of particulate material that can reach open ocean areas. This material is called aerosols[1] and can originate from crustal weathering, volcanic emissions, seasalt generation, by chemical reaction and/or condensation. In addition to these, emissions from plants and soils, extraterrestrial particulates and, only at present, anthropogenic sources, may contribute to the carbon cycle.

Basaltic rocks that forms the sea bed are also a source adding carbon to the global carbon cycle. They interact with the ocean water through hydrothermal activity near ridges or by the weathering of these rocks or even by the extrusion of lava on the sea bed. Some elements are added in the reservoir, for the most part oxides, as Si, Al, Ca, Fe, Mn, K, Ti, Mg.

---

[1] The term Aerosol refers to all those solid and liquid particles which comes from natural or anthropogenic (from the industrial development). Primary particles that enter directly in the atmosphere and secondary particles formed through chemical reactions.

The river fluxes includes long and short term and even rare events: the long term are temporal and spatial variations during a long time, short term are fluctuations e.g. storm events and rare events are all those events which involve paroxystic events as flooding or crevasse events.

The organic matter (OM) in the oceans can have allochthonous or autochthonous origin. The first refers to an external source, mainly by river run-off, the second is produced in situ via photosynthesis of plankton (Chester, 1999).

$$6CO_2 + 6H_2O \rightarrow (C_6H_{12}O_6) + 6O_2$$
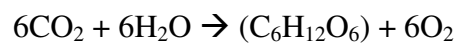
Deep-sea sediments are formed through several transport processes as gravity currents (e.g. slumps and gravity flows), geostrophic currents (transport of fine material on the bottom floor), vertical transport (from the surface to the sea-bed), surface currents (influenced by the wind and the atmospheric circulation cells, called gyres) and mid-depth currents. Depending of the transport process type, the sediments can be classified into two subdivision: pelagic and hemi-pelagic. According to Kennett (1982), hemi-pelagic sediments (muds) are classified as >25 % of the fraction >5 µm is of terrigenous, volcanogenic, or neritic origin. Pelagic deposits thus are classified as <25 % of the fraction >5 µm is of terrigenous, volcanogenic, or neritic origin. Pelagic deposits are further subdivided into pelagic clays, in which calcareous and siliceous fossils <30 %, and oozes, in which calcareous and siliceous fossils >30 %. This is commonly referred to as the "30 %" rule.

The sediment thus can have an inorganic origin, from the continent, or an organic origin, biogenous calcareous or siliceous sediment.

| Calcareous sediments | Deep-sea clay | Glacial sediments |
| Siliceous sediments | Terrigenous sediments | Ocean margin sediments |
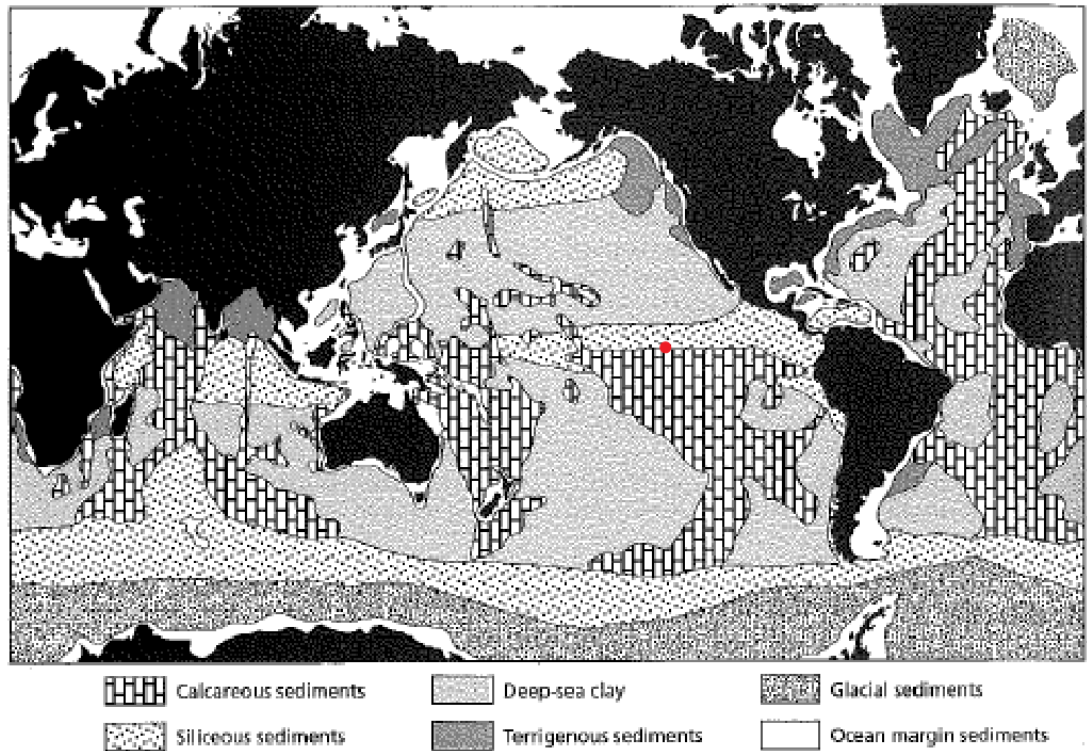
Figure 17 Distribution of the principal types of marine sediments at the present day. In the central Pacific Ocean, north of the Equator line, the westward current generate siliceous sediments. In Core V28-179 (red point), instead, prevails carbonate sediments (Figure source: Chester, 1999).

Sediments recovered from Core V28-179 are pelagic deposits from a region characterized by low sedimentation rate and input is formed by an eolian and biogenic component.

4.1.2   The carbon cycle

The carbon, together with water, is found in all living creatures and in some inorganic materials.

Carbon on Earth is stored in four main reservoir: atmosphere, biosphere, hydrosphere and lithosphere. Between these systems is present a continuous material exchange caused by physical and chemical processes that lead to particle fluxes.

An example can be the death of an organism on the continent. At the moment of the death the organic matter that composed the organism join the soil. The same path can be made from plants. A similar process occurs in the ocean and, with marine plankton forming OM that may form oil and gas deposits. These deposits may migrate due to differential pressures and return a part of the carbon cycle.

Table 9 Estimated volumes in Gt (giga tons) of CO_2 on the Earth (Source: Introduction to Climate Change United Nations Environmental Program's UNEP Global Resources Information Database (GRID) office in Arendal Norway, http://oceanworld.tamu.edu/resources/oceanography-book/carboncycle.htm).

Carbon reservoirs	
Atmosphere:	750 Gt of C, almost totally CO_2 and small quantities of CH_4, CO and chlorofluorocarbons (Sulzman, 2000).
Biosphere:	Marine organisms: 3 Gt CO_2. Terrestrial vegetation: 540-610 Gt CO_2.
Hydrosphere:	38˙000 Gt (~95 % CO_2).
Lithosphere:	Sedimentary rocks: 66 M -100 M Gt (mostly $CaCO_3$). Oil and gas deposit: 300 Gt CO_2. Coal deposit: 3˙000 Gt CO_2.
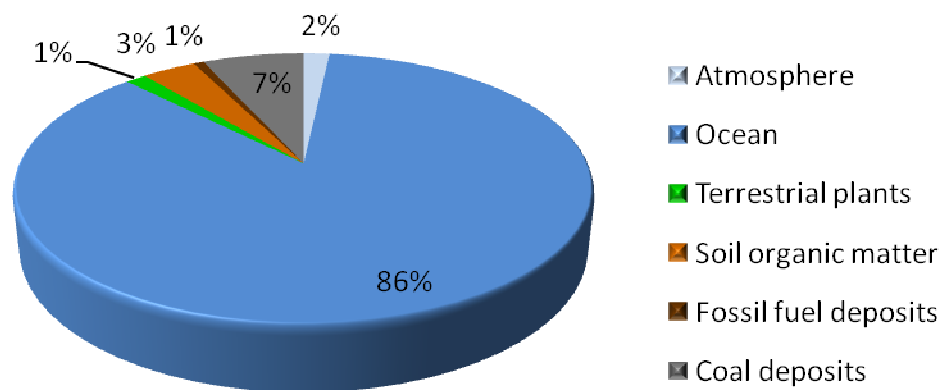
Figure 18 Percentage of C in four environmental reservoirs (atmosphere, biosphere, hydrosphere, lithosphere). The C in sedimentary rocks is not included because the quantity of C is too high. (See Table 9 for the source).
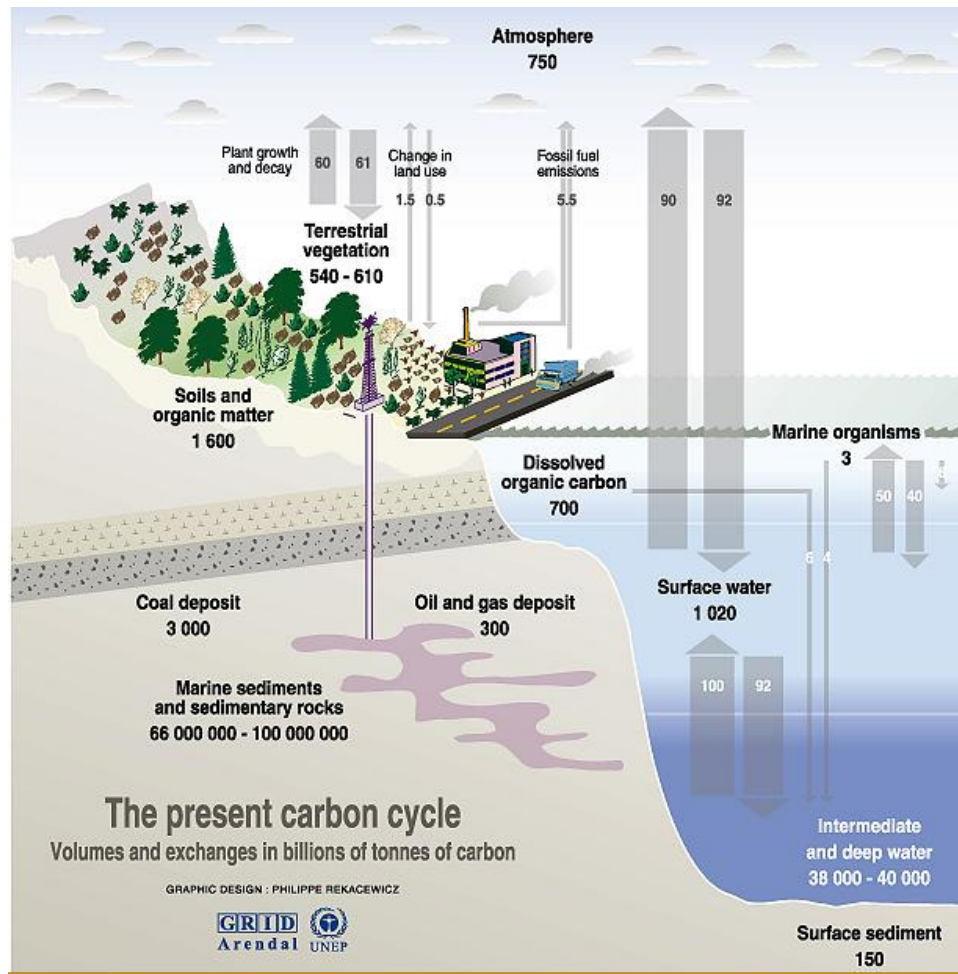
Figure 19 The Carbon Cycle (Source:

http://oceanworld.tamu.edu/resources/oceanography-book/carboncycle.htm).

The quantity of carbon is approximately the same in each of the four reservoirs, and remains in a dynamic equilibrium. However, the actual atmosphere carbon mass is less than expected. About 3 Gt are missing per year but the reason is unknown (Farquhart et al., 2011).

During the carbon cycle are involved two types of cycles: short-term and long-term.

The first one *Short-term carbon cycle* involves interactions with:

1. atmospheric CO2
2. photosynthesis (marine and terrestrial)
3. respiration (aerobic and anaerobic)
4. dissolution CO2 in aqueous systems (ocean, lakes, soil water, rivers)
5. dissolved organic carbon (in marine systems)
6. soils (organic carbon, methane, oil reservoirs)

and these processes occurs in a time scale of years.

The long-term carbon cycle involves:

Carbon inputs:

1. Volcanic and metamorphic degassing.
2. Weathering of organic carbon: $CH_2O + O_2 \rightarrow CO_2 + H_2O$

Carbon outputs:

Chemical weathering of silicate minerals

and the temporal scale is on the order of thousands to millions of years.

In the ocean the carbon exchange between organisms and "system" is important, especially with the plankton, because the carbon is used to construct shells and to grow organic matter. During the respiration the living emits carbon: CO_2 (g). A part of the remaining carbon can be stored on the sea bed in the form of dissolved inorganic carbon (DIC) or dissolved organic carbon (DOC). More than 95% of the oceanic carbon is DIC (Sulzman, 1995).

4.1.3 Surface productivity and nutrients

The sedimentation reflect 1) the surface productivity, 2) the depth of the region in which the particles flux down to the sea bed (dissolution rates during the down flux) and 3) inputs of terrigenous sediments (dilution of the biogenous sediments by terrigenous sediments). The distribution of pelagic sediments in the Pacific Ocean is a combination of biogenic (calcareous and siliceous) and eolian (terrigeneous) sources (see Chester's Figure 17 above).

The surface productivity depend upon abiotic factors as nutrients supply (N, P, Si and in minor parts CO_2, Fe, Mn, Mg, Na, Ca) and solar radiation and biotic factors as predation, and can change with temperature during seasonal or glacial-interglacial cycles and latitude.

At the present time along the Equator, in the Pacific Ocean, there is a surface high productivity zone, caused by the presence of an upwelling zone rich in nutrients. High productivity zones occur frequently at low latitudes driven by the trade winds, producing divergence along westward currents leading to upwelling of nutrient rich cold deep waters.
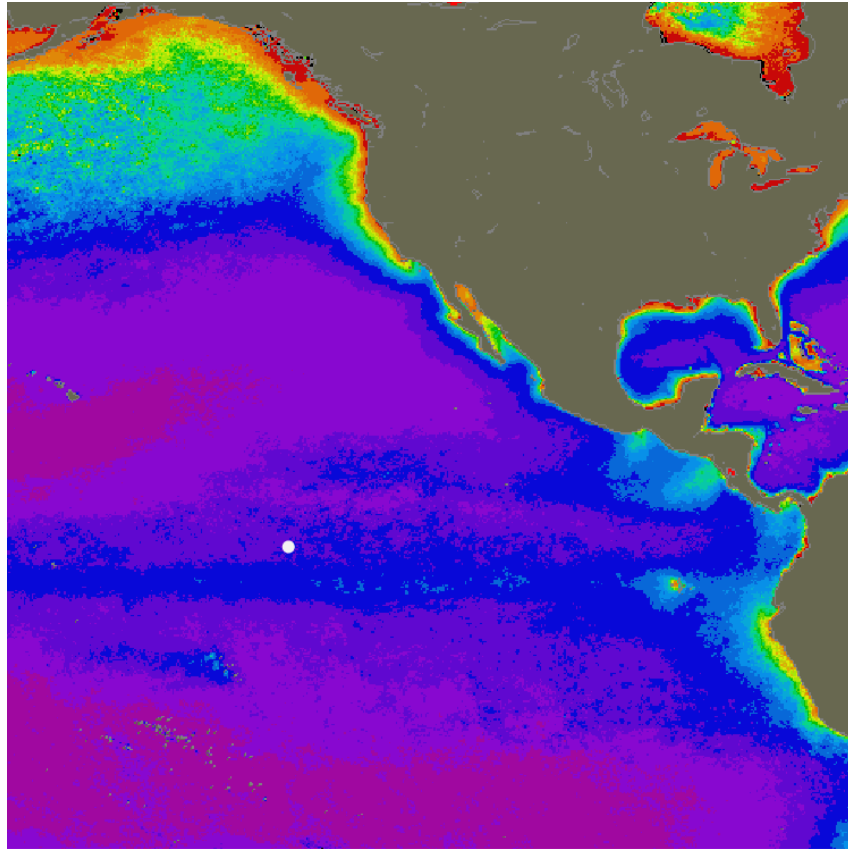
Figure 20 Actual effect of the equatorial upwelling on the productivity (Source: http://public.wsu.edu/~dybdahl/lec10.html) and location of Core V28-179 (white point).

These nutrients are essential for phytoplankton (autotrophs) organisms. In fact, in zones with high nutrients input there is a major development of living organisms.

The concentration of nutrients depends by:

- Distance: greater is the distance from the coastal upwelling zone and lower is the nutrient concentration because nutrients are used by organisms in this regions – it is called land-mass effect.
- Depth: deeper waters are richer than surface waters because nutrients are used during primary production.

- Low fertility regions are present in zones where water mixing is low
(Chester, 1999)

Concentration in the Pacific is higher than in the Atlantic, because rich-nutrients waters comes from North Atlantic Ocean and Antarctic, especially from the oxygen minimum layer and from deep water levels, where the concentration of organisms is low.

4.1.4 Transport

Transport of material in the surface water of the ocean is caused by gravity gradients, waves, pressure gradients, differences in density, wind, thermohaline anomalies, mass movement, biological processes (Figure 21).

Wind flow is in part responsible of vertical movements of upwelling and downwelling. In the upwelling movements the water is transported towards the surface from the deep ocean and it is important for living because transports of nutrients to the surface allows the plankton to reproduce. This upwelling movement occurs also along the coast where the wind carry the surface water offshore and deep water replace masses moved. Finally, there is also the Earth rotation's effect (Coriolis effect[2]) that lead to a deflection in the movement of water masses from a predetermined direction.

In addition to deep water circulation and surface water circulation is also present a mid-depth water circulation characterized mainly by differences in temperature and salinity.

---

[2] Coriolis effect is studied by the engineer Gustave-Gaspard Coriolis in 1835. He demonstrated that there was a deflection on the Newton's law if is present a rotating system. An object subjected to a rotation is deviated from its path, or even better the coordinate of the point in which is located the object undergoes to a movement of the coordinate system.

At the death of an organism, this is subjected to a vertical gravity induced transport to the sea bed. During the transfer shells are dispersed due to water mass movements and can form a Gaussian distribution under the producing area (Berger, 1970).

According to Honjo (1976), the sinking rates vary by species, physical processes (e.g. eddy diffusivity[3], latitudinal zonal distribution and descent to the sea floor which depends upon temperature and currents) and chemical processes (e.g. changes of water chemistry during the transport namely calcite saturation depth - CSD - and nutrients supply). In the central Pacific Ocean the sinking rate of coccoliths is a few micrometers / second and should be dissolved, according to the formula:

$$CaCO_3 + H_2O + CO_2 <====> Ca^{++} + 2HCO_3^-$$

(Source: http://geology.uprm.edu/Morelock/dpseabiogenic.htm)
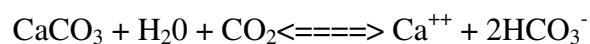
But coccoliths are well preserved because the rate of descent is high.

In 1966, Peterson developed an experiment using seventy-one calcite spheres arrayed from the sea surface to the sea bed in a vertical profile in the central Pacific, in order to demonstrate the different dissolution rates. After four months different dissolution rates could be determined through measurements of the weight loss: in the upper several meters no weight loss were observed, down to 3700 m the spheres showed a small loss of weight, and below 3700 m was present an abrupt increase in dissolution rates.

The spatial distribution of coccoliths is represented by a surface in the sea bed of about 400 km, in a water depth of 4000 m, with a sinking speed of about 130 m /day in the central Equatorial Pacific, and coccoliths should not drift horizontally more than 200 km during the descent (Honjo, 1976). This means that

---

[3] Eddy diffusivity, also called turbulent diffusion, is a process in which two or more substances are mixed in a fluid or air system thanks to eddy diffusion. It is represented by the coefficient k and is measured in m^2 / sec.

the deposition zone was not necessarily exactly identical to the production area, but can be shifted also on the water masses movements along the water column.

The type of materials transported for vast distances are fine particles from terrigenous, biogenous sources and aeolian inputs. The position of Core V28-179 reflect a low sedimentation rate, caused mainly by biogenic input with only minor terrigeneous and eolian input.
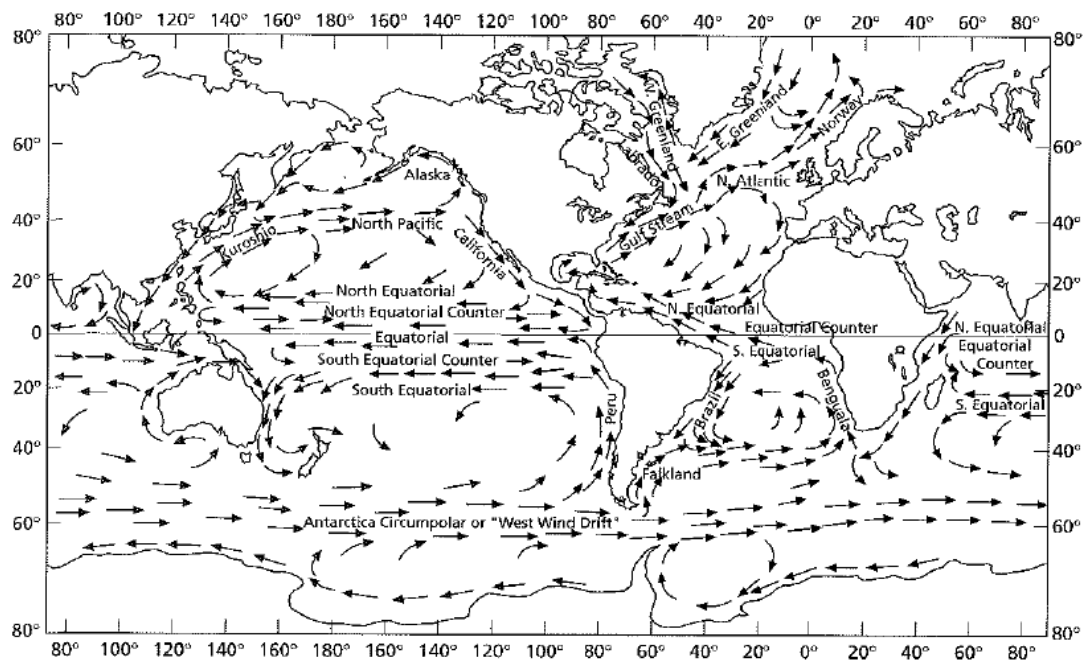
Figure 21 Surface water circulation in the World's ocean system. Note the westward circulation in the Pacific Ocean. (Source: Chester, 1999).
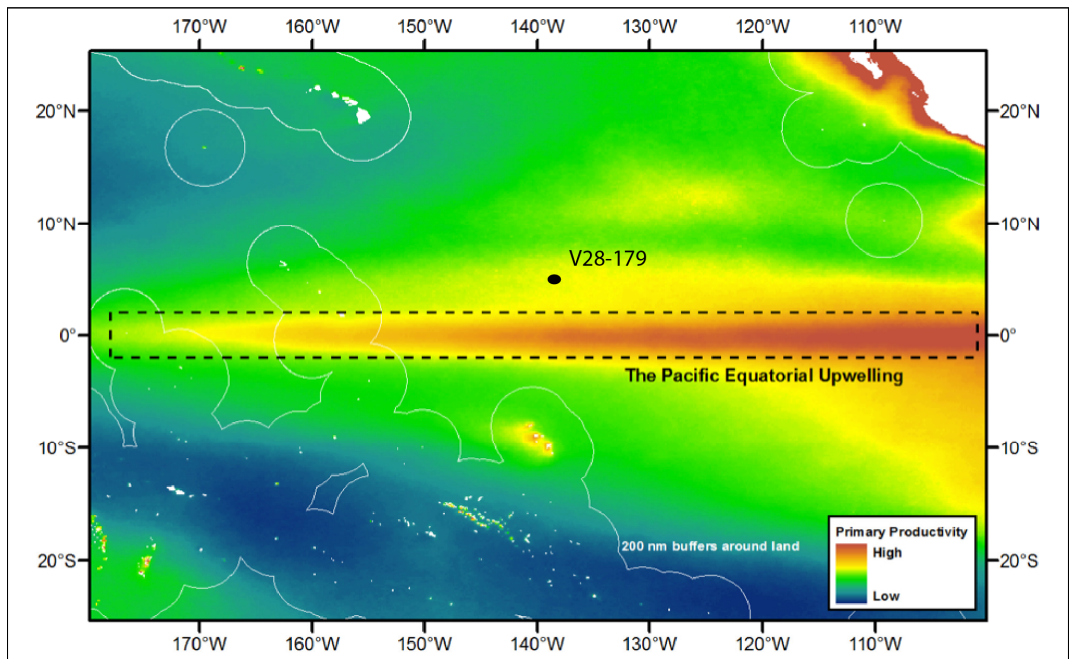
Figure 22 Primary productivity of carbonate in the east part of the Pacific.
(Source: http://www.gobi.org/Our%20Work/productive-1).
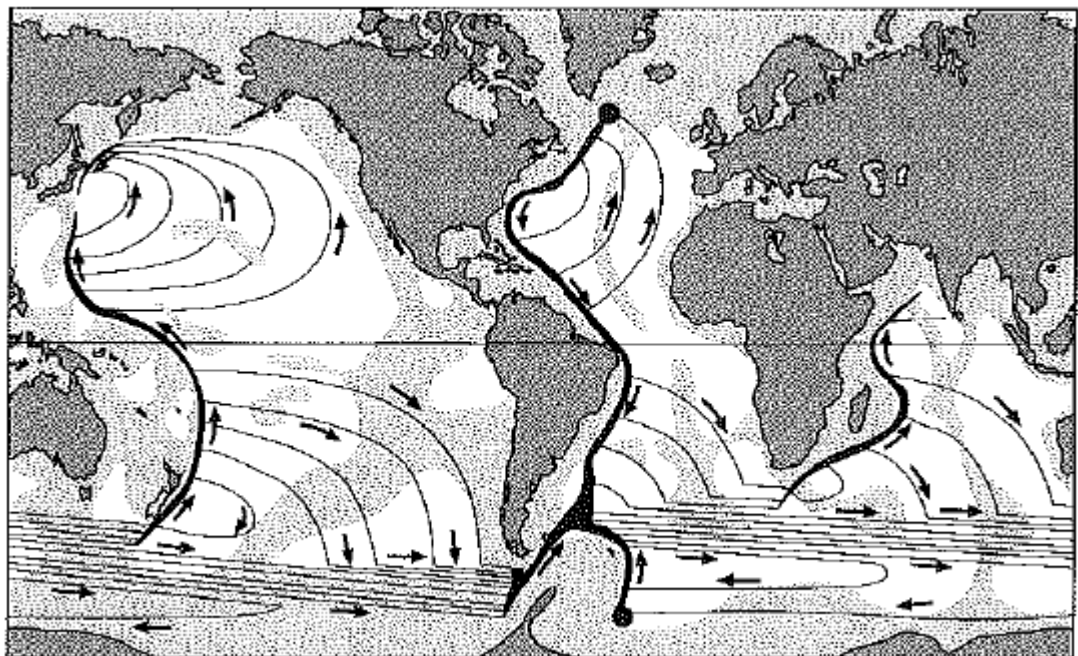
Figure 23 Horizontal deep water circulation in the World's ocean system
(Chester, 1999).
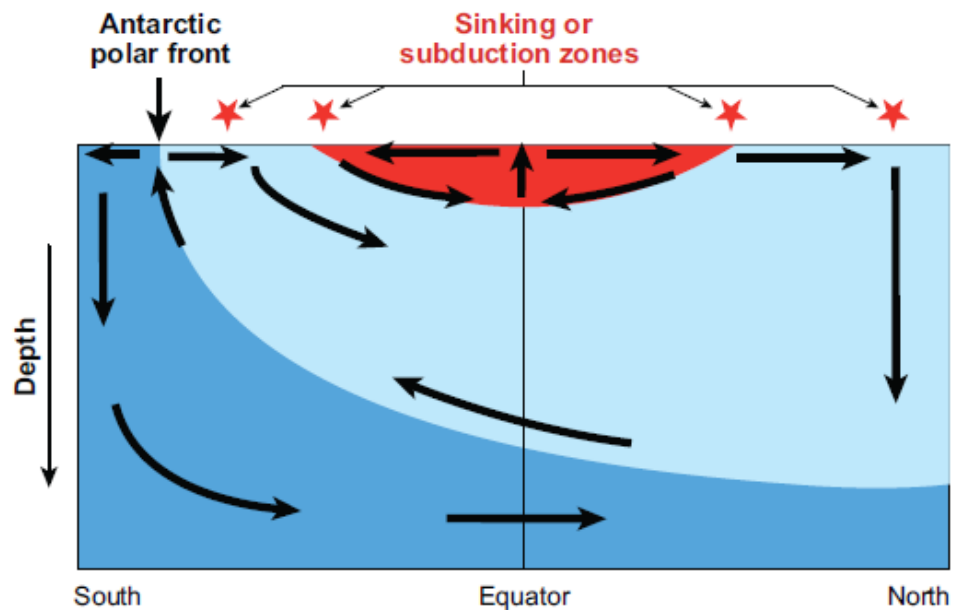
Figure 24 Vertical oceanic thermohaline circulation from the Atlantic to the Pacific Ocean. Note the upwelling on the Equator (Source: Barreiro et al., 2008).

4.1.5   Deposition

The rate of deposition depends on several factors such as water mass movements (caused by salinity, temperature and currents), depth of the sea floor (CCD) and surface production of organic matter (depends by nutrients supply). The greater the surface production rate is, the higher will the depositional rate be in an idealized system without water masses movements.

Furthermore, also the predation lead to a variations in sedimentation rate (SR). The predation can act positively or negatively on the SR; shells can be incorporated in fecal pellets, waste products of copepods (small planktonic or benthic crustaceans) and can reach the sea bed without undergoing dissolution.

It is estimated that about half of the sea floor is covered by calcareous material (Berger, 1970).
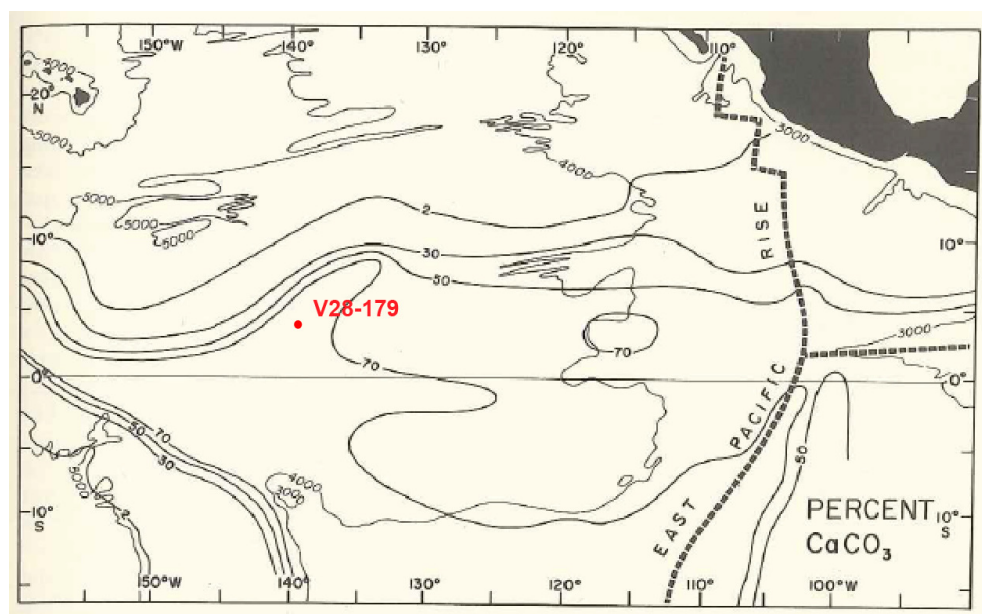
Figure 25 Surface distribution of calcareous sediments in the Pacific Ocean; isopachs are in carbonate content % (van Andel et al., 1975). Red point corresponding to position of Core V28-179.

Along the east coast of the Equator zone the productivity is emphasized by upwelling of nutrients from cold deep sea waters comes from Atlantic and Antarctic (200-500 mg C/m^2/day^{-1}; Riley and Chester, 1976) and this results in a higher carbonate sedimentation (~80 %) due to higher production of organisms (Figure 25).

The siliceous sediments tend to dissolve immediately after the death of organisms, so can accumulate only where the rate of supply is higher than the rate of dissolution. Instead, the rate of dissolution of calcareous sediments increase rapidly below about 3700 m depth in the central Equatorial Pacific (Peterson, 1966). In high productivity regions the CCD is depressed, although below 5000 m depth no carbonate is present (Riley and Chester, 1976).

With reference to van Andel et al. (1975), the CCD near the depositional area of Core V28-179 was at about 4,05 km (at ~ 4.5 Ma) to 4,5 km (at present time) to indicate a deepening, maybe due to an increase in nutrients supply and reason to variation of the level of carbonate dissolution.

Finally, it is possible to suggest that the differences in biogenic sedimentation rate at the site of Core V28-179 were caused by a combination of variable nutrient supply in the photic zone and dissolution mineralized shells at depth.

4.1.6   Post-depositional processes

After the deposition of a sediment this is subjected to cover by other sediment, if the conditions do not change. In this way conditions develop that lead to diagenesis of the sediment. Physical, chemical and biological processes may act together and transform the sediment to a rock. Chemical processes include bacterial reactions and precipitation of authigenic minerals; physical processes include physical transport, gravity-driven transport, compaction by loading of new sediment; biological processes involve benthic activity (bioturbation) by organisms, in oxic waters. This can modify chemical and physical (porosity and resistance to erosion on the sediment-water interface) conditions and can lead to increase of the transport susceptibility.

The sediments in Core V28-179 are characterized by considerable bioturbation.

As well the sediment buried is subjected to the geothermal gradient and to a progressive increase in temperature with depth. The process allow a major solubility and ductility of minerals and can cause metamorphism and state changes of minerals subjected to it. This effect, however, has not influenced the sediments in the 27 m long Core V28-179.

Depositional hiatuses can be developed in the sedimentary record for removal of layers by deep bottom currents. These changes can be caused by sea floor structural alteration that involve tectonic movements (Riley and Chester, 1976). Furthermore, the topography is a control factor for the material removal because the flux can be accelerate in connection to structural highs.

4.2 CaCO$_3$ analysis in V28-179

4.2.1 Coulometer description

We have used a Coulometer 5015 [®] to quantify the CO$_2$ component in our samples.

Figure 26 Coulometer used for the analysis, model 5015.

A coulometer can measure an accurate CO$_2$ content for example in sediment samples or in any CO$_2$-containing gas stream. A detector is used with different carbon front-end units, detecting carbon in the range of 0.01 μg to 100 mg.

The coulometer cell (graduate glass – baker with a side arm) it's filled with a monoethanolamine solution and a colorimetric pH indicator in the cathode solution. The platinum (cathode) and the silver (anode) are connected to the cell disposed between the beam of light and the detector. The cell assembly is then placed in the coulometer cell compartment between a light source and a photodetector in the coulometer.

Previously, the samples were weighted with µg precision, inserted in tubes and, before the measurement, fastened gas-tight on the acidification part of the instrument. 2M HCl are added dissolving $CaCO_3$ which releases CO_2 gas.

The gas stream is powered in the coulometer cell with the aid of a propellant gas formed by air passed through KOH solution to be free of CO_2.
Sample CO_2 is quantitatively absorbed in the solution; the cathode solution react with CO2 monoethanolamine becoming acid (hidroxietilcarbonic acid) that change the indicator color in the cathode solution.
The photodetector records the color change measured by the transmittance (%).

$$Transmittance = T = I / I_0 \cdot 100$$

I = light intensity after absorption

I_0 = light intensity befor absorption

T = 100 % when transparent cathode solution, the mediums do not absorb

T = 29-30 % in our case the titolation end point (cathode solution blue colored).
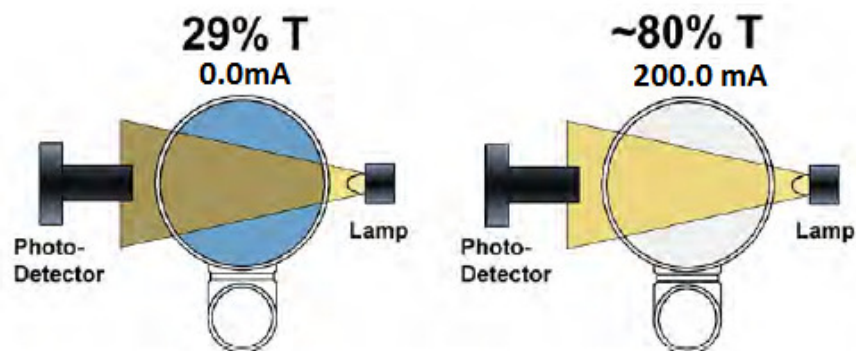
Figure 27 Transmittance through the cell (Source:
http://www.uicinc.com/SystemSheets/Principles%20of%20Operation
%20CO2.pdf).

When the transmittance increases it activates an automatic "titration-current" to neutralize the acid (approximately 1500 µg carbon/minute), basic produces at the same speed of transmission changes. When the cathode solution will return to the color output (state of the transmittance), the current stops.

The current is continuously measured and the computer program is constructed so that the difference in reading in the amount of C (µg) should not exceed 0.1% in the last 3 readings. At this point the analysis is complete and the measurement is interrupted.

Reactions are as follows:

1. Cathode reaction:

   CO_2 + $HOCH_2CH_2NH_2$ → $HOCH_2CH_2NHCOOH$
       (monoethanolamine → hydroximethilcarbon acid)
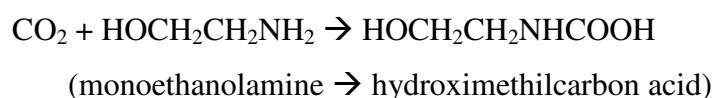
2. electrochemical production of a base:

   $2H_2O + 2e^- \rightarrow H2\ (g) + 2OH^-$
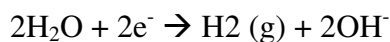
   (From anode reaction, see reaction 4)

3. Neutralization of an acid (product of absorbed CO_2 and cathode reaction solution. See reaction 1):

   $HOCH_2CH_2NHCOOH + OH^- \rightarrow HOCH_2CH_2NHCOO^- + H_2O$
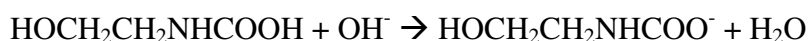
   (from reaction 1)   (from reaction 2)

4. Anode reaction:

   $Ag^+ \rightarrow Ag^+ + e^-$

         (precipitate; requested for reaction 2)

The current of the reaction (the e^- created) is measured by the coulometer. Each electron counted corresponds to one molecule of CO2 in the sample gas stream, which corresponds to one atom of carbon in the original sample. In the most basic terms, the coulometer counts carbon atoms. The amount of C is converted to $CaCO_3$ by the computer program, using a factor of 8.334.

(molecular weight $CaCO_3$ = 100.08 g/mol, molecular weight C = 12.01 g/mol; 100.08/12.01 = 8.334)

The CO_2 counted by the coulometer is, in this case, a measure of inorganic carbon content of the sample. Inorganic carbon consists of carbonate minerals. Organic carbon does not react with acid. By subtracting the inorganic carbon from the total carbon reading, the organic carbon content of the sample can be determined.

The coulometer principle is based on Faraday's rule that claim: in the electrolysis a change of 1 gr-equivalent substance gives a current of 1 Faraday. In

the coulometer 1 Faraday of electricity is 1-gr equivalent substance of CO_2 titrated, that is 1-gr equivalent of C.

1 F = 96486 coulomb

1 gr-equivalent C = 12.011 g C = 96486 coulomb

12.011 mg C = 96.486 coulomb

1 mg C = 8.033 coulomb

1 coulomb is definited like 1 ampere per second (Asec), così

1 mg C = 8.033 Asec

1 μg C = 8.033 mAsec

Coulometer circuit is constructed so that the current is converted into frequency. Instrument is calibrated to provide a particular frequency for a given current.

1 count = 0.02 mAsec

1 μg C = 8.033 mAsec

1 μg C = 8.033/0.02 = 401.65 counts

calculation can be used for an additional electronic control.

Readings correspond to the total C (μg) in the weighed amount of sample with two decimal places. Thereafter, the amount of C corrected with blank values, and then converted to $CaCO_3$ (multiplied by 8.334, see above). The amount of $CaCO_3$ is then related to the weighed amount of sample and converted into $CaCO_3$ % with a program data.

Table 10 Calibration for $CaCO_3$ for the first thirteen measurements.

	A	B	C	D	E	F	G	H	I
1	Name	Lōpnummer	Blank	Reading μg C	Corr. Reading	Sample mg	Out (y) mg	% CaCO3 Calibr.	Coulom. %
2	11-14	1	1,1	2973,03	2971,93	28,746	25,0215	87,0434	86,1618
3	21-23.5	2	1,1	3181,91	3180,81	30,640	26,7735	87,3810	86,5171
4	30-33	3	1,1	3349,28	3348,18	31,715	28,1774	88,8457	87,9827
5	40-43	4	1,1	3442,37	3441,27	31,959	28,9582	90,6106	89,7386
6	50-53	5	1,1	3034,94	3033,84	28,667	25,5408	89,0947	88,1989
7	60-63	6	1,1	3648,29	3647,19	34,039	30,6855	90,1479	89,2966
8	67-70	7	1,1	3068,07	3066,97	31,002	25,8187	83,2807	82,4466
9	77-80	8	1,1	2246,09	2244,99	30,196	18,9241	62,6707	61,9610
10	90-93	9	1,1	2073,65	2072,55	30,258	17,4777	57,7621	57,0845
11	100-103	10	1,1	2400,25	2399,15	29,127	20,2171	69,4102	68,6460
12	110-113	11	0,9	3367,70	3366,80	32,560	28,3336	87,0196	86,1760
13	120-123	12	0,9	2994,97	2994,07	31,529	25,2072	79,9492	79,1416
14	130-133	13	0,9	2847,96	2847,06	29,904	23,9741	80,1702	79,3453

Where corrected reading is D2-C2,
Out (y) mg is Corr. reading ∗ slope + intercept,
$CaCO_3$(%) calibrated is (Out (y) mg ∗ 100) / sample mg

Calibration

y = 0,008387818x + 0,093484333
R² = 0,999677346

Calibration - Microbalance

N=131

Intercept: 0,093484333

Slope: 0,008387818

R-square: 0,999677346

corrected reading = reading minus blank
y=corrected reading*slope+intercept
%CaCO3 = (y*100)/sample mg

Calibrated CaCO3 % mean values: 99.9591 %
Instruments CaCO3 % mean values: 98.5749%

Calibrated CaCO3 % std. dev.: 0.8778
Instruments CaCO3 % std. dev: 1.1053

Figure 28 Calibration curve: if the points stay on the calibration line (or very close) the calibration is correct.

4.2.2   Results

The CaCO$_3$ content principally reflect dynamics of the ocean circulation and the productivity of the ocean.

The curve of Core V28-179 can be divided into five intervals (Figure 29) corresponding to abrupt changes in composition: **(1)** from the base (4,085 Ma, corresponding to 2067.5 cm) to 3,577 Ma, **(2)** from 3,577 Ma to 3,184 Ma, **(3)** from 3,184 Ma to 1,955 Ma, **(4)** from 1,955 Ma to 0.536 Ma and **(5)** from 0,506 to 0 Ma.

The first interval **(1)** (4,085-3,577 Ma) CaCO$_3$ concentration varies between 18 % and 58 %. At 3,577 Ma **(2)** there is a fast recovery from 30 % to 70 % of carbonate content. This strong preservation could be caused by a strong increase in productivity that lead to a greater depth of CCD and the lysocline.

At 3,424 Ma, the peak, start the fall until 3,184 with an abrupt change from 3,302 to 3,254. At 3,184 Ma **(3)** start a slow recovery to 2,405 Ma (CaCO$_3$ pass from 34 % to 91 %) and is followed by a gradual fall (to ~ 40 % at 1,955 Ma).

In the fourth interval **(4)** start a very large oscillatory period with CaCO$_3$ values between 40 % and 94 % but keeping about a same media, with a light increase at the end.

From interval **(5)**, 0,536 Ma, the oscillatory trend become more stable and CaCO$_3$ content interval remains between 39 % and 87 %. At the end of the curve it seems that the trend goes up again but this could be only a momentary oscillation.

Through the entire curve it can be possible to visualize a general increase in the carbonate concentration trend and an initial cyclicity that is hidden from 2.0 Ma to the top. This cyclicity is represented by oscillations from base to ~3.9 Ma, from ~3.9 to ~3.6 Ma, from ~3.6 Ma to ~3.2 Ma and from 3.2 to 2.0 Ma. The first three cycles belong to the 405 000 kyr long eccentricity cycles, the last to the 1.2 Ma obliquity amplitude cycle.

Dunn (1982) proposed a chain model that involve first of all changes in orbital parameters. Orbital parameters are very important to the life on Earth: during the Cenozoic a change in orbital parameters had lead to stronger winds that in turn have resulted in an upwelling increase along the Equator, an increase in productivity and finally a deepening of the CCD with the result of a major accumulation rate of pelagic sediments given by a minor dissolution rate (see Chapter 4.1.5 "Deposition").

Another factor that involve a change in $CaCO_3$ concentration it should be noted in the change in oceanic circulation that may have led to variations in nutrients supply or variations in salinity and/or temperature.
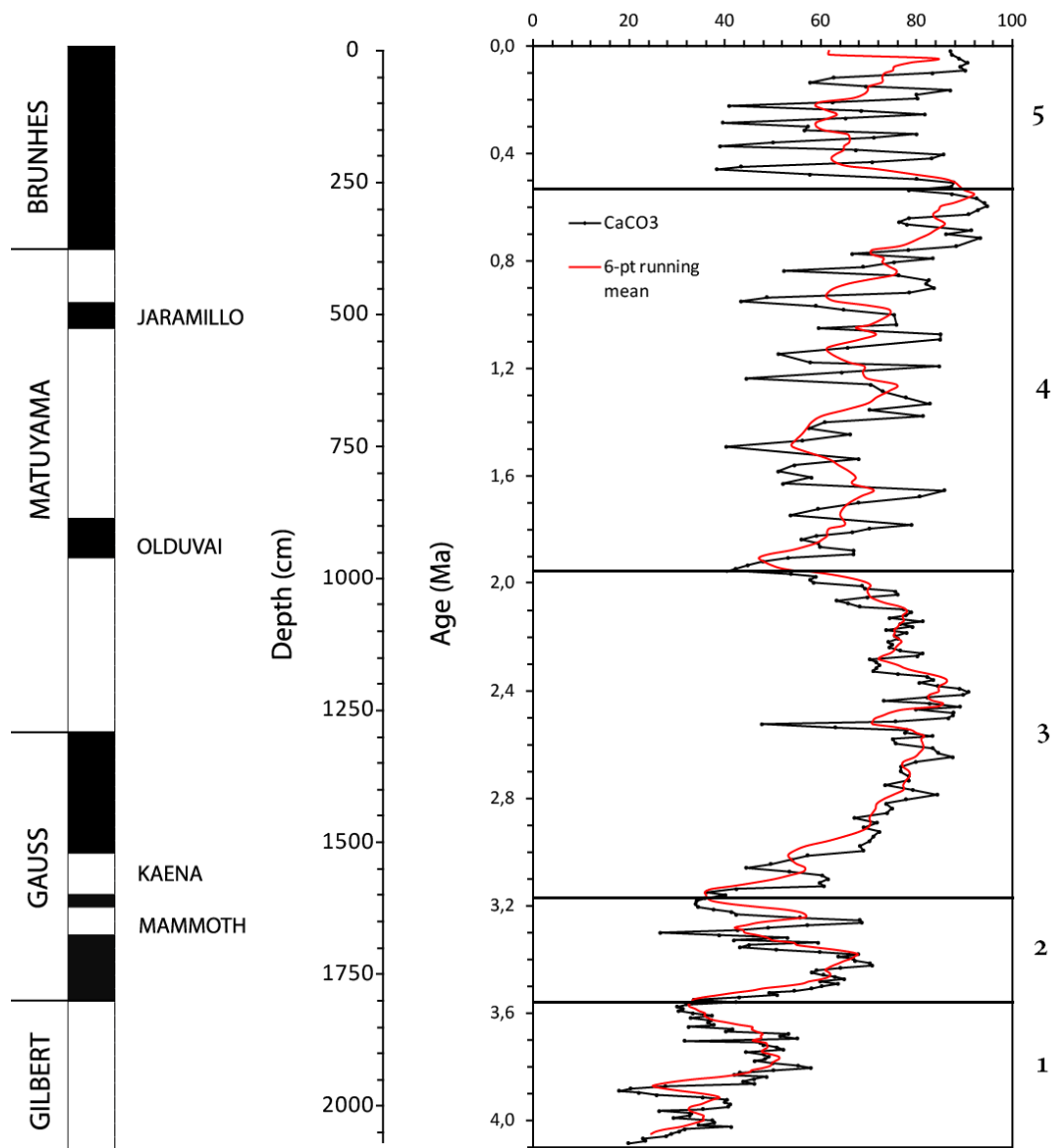
Figure 29 % CaCO₃ from 0 Ma to 4,089 Ma (core base). The age is estimated used a mean between top age and bottom age of a sample (most samples are 5 cm thick). The increase in deposition rate may have been caused by increase in nutrients supply. Numbers 1 to 5 indicates intervals described above.

CHAPTER 5

ISOTOPES IN THE OCEANIC RECORD

5.1   Introduction

Isotopes are two or more forms of an element that have the same number of protons in the nucleus of the atom (atomic number) but different number of neutrons. According to Sulzman (1995), they have similar chemical properties but they act differently in chemical reactions due to their different atomic weight (number of protons plus number of neutrons). To refer to an isotope there is a writing method to identify the types of isotopes from each other: $^{A}X_{Z}$ where X is the element, A the number of neutrons plus protons and Z the atomic number.

In a chemical element, unstable atoms or stable atoms may co-exist. The difference is based on the fact that unstable atomic nucleus continually seek the stability loosing energy and to do that they emit ionizing particles. The products are called *daughter nuclide*.

Besides to radioactive isotopes, stable isotopes can be used to understand physiological processes of plants and organisms and atmospheric temperatures to reconstruct the paleoconditions that prevailed in the past.

Core V28-179 has been analysed with respect to carbon ($^{13}C/^{12}C$) and oxygen ($^{18}O/^{16}O$) on bulk sediments. Oxygen isotopes are used as a proxy for paleotemperature, global ice volume and sea level change (Shackleton, 1967). ^{13}C isotope (also called carbon-13) is heavier than ^{12}C (carbon-12) and variations can have been used as a tracer for ocean circulation and productivity patterns (Lynch-Stieglitz, 2003).

5.2   Carbon isotopes

Carbon has 16 isotopes (from ^{8}C to ^{23}C) but only two isotopes are stable: ^{13}C and ^{12}C (Table 11).

^{13}C is heavier than ^{12}C and during physical and chemical processes the ratio δ^{13}C (^{13}C / ^{12}C) undergoes changes through time.

Table 11 Natural and artificial carbon isotopes on the Earth
(http://www.buzzle.com/articles/isotopes-of-carbon.html).

Carbon Isotope	Neutron Number	Atomic Weight (in amu)	Half Life
C^8	2	8.037675	2.0×10^{-21} sec
C^9	3	9.0310367	126.5 millisec
C^{10}	4	10.0168532	19.290 sec
C^{11}	5	11.0114336	20.334 min
C^{12}	6	12	Stable (Non-Radioactive)
C^{13}	7	13.0033548378	Stable (Non-Radioactive)
C^{14}	8	14.003241989	5.70×10^3 years
C^{15}	9	15.0105993	2.449 sec
C^{16}	10	16.014701	0.747 sec
C^{17}	11	17.022586	193 msec
C^{18}	12	18.02676	92 msec
C^{19}	13	19.03481	46.2 msec
C^{20}	14	20.04032	16 msec
C^{21}	15	21.04934	Less than 30 ns
C^{22}	16	22.05720	6.2 msec

In paleoceanography and paleoclimatology the fractionation can provide a method of analysis of the carbon cycle, based on the principle of mass conservation, using the following equation based on a standard PDB[1]

$$\delta^{13}C = \frac{(^{13}C / ^{12}C)_{\text{sampled}} - (^{13}C / ^{12}C)_{\text{standard}}}{(^{13}C / ^{12}C)_{\text{standard}}} \times 1\,000$$

The atmospheric CO_2 contains 99 % of ^{12}C and about 1 % of ^{13}C. During photosynthetic processes CO_2 is absorbed by plants, which fix CO_2 and produce glucose by the action of the enzyme ribulose bisphosphate carboxylase (O'Leary, 1988), commonly called RuBisCO[2], and the atmospheric ratio $\delta^{13}C$ increase in favour to the heavier isotope (Figure 30) during respiration.

$$6CO_2 + 6H_2O \ (+ \ \text{light energy}) \rightarrow C_6H_{12}O_6 + 6O_2$$

(Thomas, 2008. http://ethomas.web.wesleyan.edu/ees123/caiso.htm)
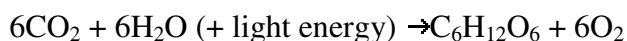
In the sea organic matter (OM) has values about -23 ‰, instead dissolved inorganic carbon (DIC) from marine organisms in the form of shells or skeletons has values about 1 ‰, closed to water values of 0 ‰ (Figure 30). The isotope fractionation of the OM depends upon the temperature of the sea water. At high temperatures the solubility of the CO_2, in form of gas, is low such as the availability for the phytoplankton and the fractionation is less (-13 ‰). At low temperatures the CO_2 solubility increases and values are around -32 ‰. The depletion of DIC in the surface water, used by phytoplankton, favour carbon-13.

---

[1] PDB (Pee Dee Belemnite), used for standard in the analysis of the carbon isotopes, derive from carbon dioxide in Pee Dee Formation (South Carolina)

[2] RuBisCO: enzyme involved in the fixation of the carbon, conversion process of CO_2 to energy (glucose) by plants.

Along the water column is present a $\delta^{13}C$ vertical gradient due to primary productivity in the surface waters ($\delta^{13}C$ value of the surface is sometimes slightly positive, up to +4 ‰ if productivity is intense - http://web.me.com/uriarte/Earths_Climate/Appendix_6.html), age of the deep waters (oldest water have a lighter isotope ratio since they have accumulated carbon from oxidized OM) and circulation patterns (Figure 31) (Thomas, 2008). Isotope analysis can be applied also in order to identify glacial-interglacial variations. Temperature, ocean chemical composition and surface pressure of CO_2 controls the solubility of the CO_2, that is more soluble in cold waters. During ice ages the concentration of CO_2 in the atmosphere is lower than interglacial periods because ^{12}C remains trapped in the ice. An opposite effect can be provided by increase in salinity at lower latitudes due to increase in ice sheets at high latitudes. (approximately 120 m depression of sea level during the last ice age, the whole ocean was about 3% saltier than it is today, according to Sigman and Boyle (2000).

Changes in quantity of carbon in reservoirs occur in time-scale of 10^5 to 10^6 years because deposition of the sediment and burial is a slow process, while during mass extinction changes can happen at a short time scale. The absence of productivity lead to enrichment in the ocean of ^{12}C and to a decrease of the $^{12}C / ^{13}C$ ratio (Thomas, 2008).
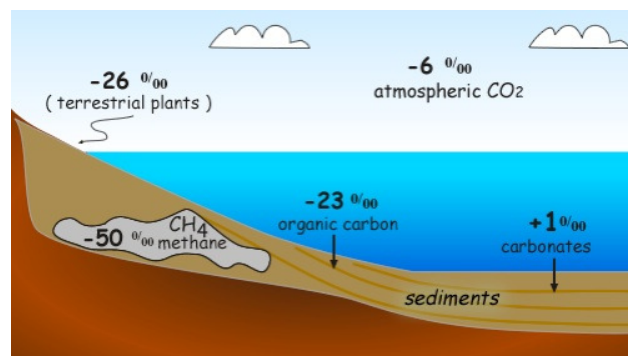
Figure 30 $\delta^{13}C$ variations in the reservoirs. Terrestrial plants absorbs more ^{12}C than ^{13}C and emits O_2, carbonates contains more ^{13}C than ^{12}C (the ratio is positive). (Source: http://web.me.com/uriarte/Earths_Climate/Appendix_6.html).
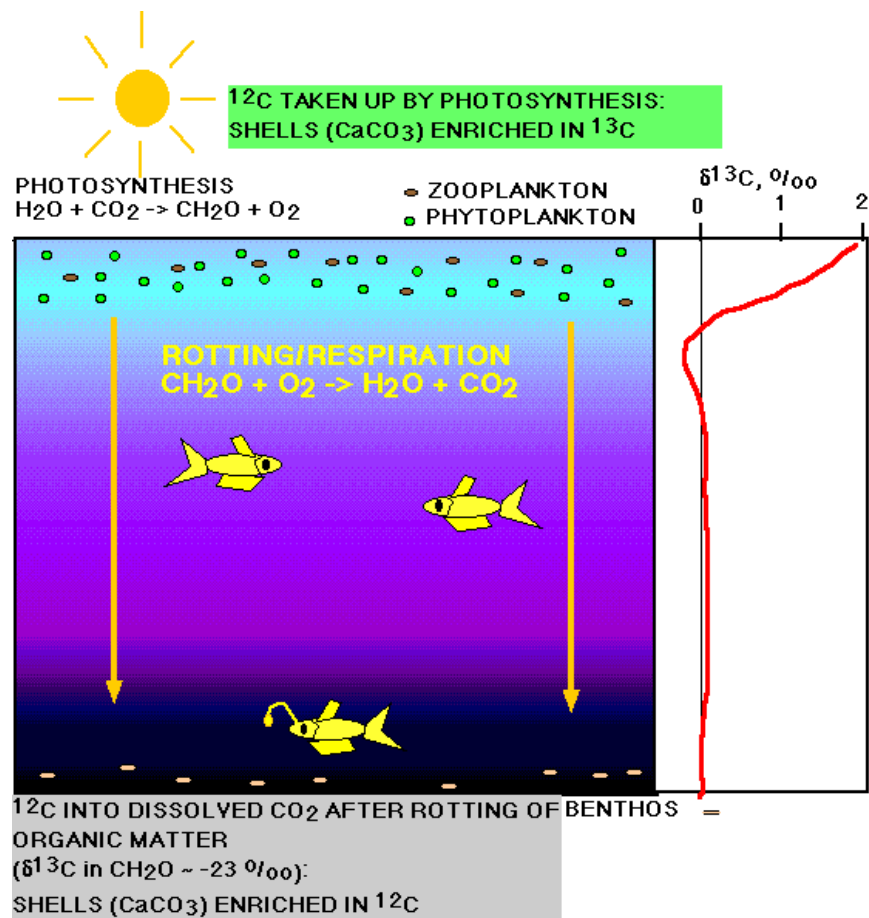
Figure 31 $\delta^{13}C$ vertical gradient. In the layer in which there is high photosynthetic activity the $\delta^{13}C$ decreases rapidly. (Source: http://ethomas.web.wesleyan.edu/ees123/caiso.htm).

5.2.1 Carbon isotope analysis

Isotopic analysis of stable carbon isotopes has been performed on bulk sediments from Core V28-179.

Carbon isotope variations range from 0,05 ‰ to 1,82 ‰ (Figure 32-a and Figure 32-b), with an average of 0,94 ‰. From the base to the top of the core significant variations are recognizable by sharp fluctuations and a wide range of values.

From the base to ~3,38 Ma there is a decreasing trend (~1.23 to 0.23 ‰ δ^{13}C), than sharp increase to ~3,2 Ma (about 1.55 ‰ δ^{13}C). From this level starts a slow decreasing till ~2,1 Ma (~0.2 ‰ δ^{13}C). A peak, centred at about 1,95 Ma (~ 1.39 ‰ δ^{13}C), begins at ~2,1 and ends at 1,78 Ma. This peak represents a large variability with oscillations from about 1.58 to 1.7 ‰ δ^{13}C and without a recognizable trend. At ~0,46 Ma a new peak is present and mark a decreasing until a value of ~0.23 ‰ δ^{13}C is reached at about 0,019 Ma. The 6-pt running mean suggests the presence of a few c. 405 000 years cycles.

The entire curve can be splitted into two parts characterized by different slope trend lines of δ^{13}C values. In the older one (from the base to ~2.1 Ma) a well-defined initial cycle becomes indefinite upward with decreasing δ^{13}C values. In the younger cycles become much more evident and at least five cycles are recognizable centered around 405 000 years.

The general decreasing trend in the older segment suggests a decrease in productivity over about two million years, which can not be attributed to periodic variations. Recalling that high δ^{13}C values express high productivity rates, since plankton use much more ^{12}C than ^{13}C, there are two possible explanations connected to the upwelling production zone rich in nutrients along the Equator line (described in chapter 4.1.3 "Surface productivity and nutrients"). The first option refers to the northward movement of the Pacific plate (van Andel, 1974; Shackleton and Opdyke, 1977) and the moving away of the coring location from

the upwelling zone. The second option takes into account the possible migration north-ward or south-ward of the upwelling high productivity zone, or its possible expansions/contractions.

In the younger part of the curve orbital parameters gain more influence on the biogenic productivity in the photic zone. As described by Milankovitch, the Earth's orbit is affected by periodical external variations involving eccentricity (the Earth rotate around the Sun following a elliptic path), axial tilt (the rotational axis of the Earth is not perpendicular to the movement direction around the Sun) and precession (change in direction of the rotation axis). The cyclicity of ~405 000 years in the δ^{13}C record can be related to eccentricity variations (according to Milankovitch is about 413 000 years; 405 000 years according to Pälike et al., 2006).

The $CaCO_3$ and δ^{13}C curves shows a strong anti-phasing: the ^{13}C / ^{12}C ratio decrease while $CaCO_3$ contents increase. This anti-phasing is clearly expressed between 0 and 2 Ma, and between 3.1 Ma and 4.1 Ma. The interval between 2 Ma and 3.1 Ma, however, does not show this strong anti-phasing. One way to explain the anti-phasing between carbonate content and carbon isotopes would be that lighter carbon isotope values implies less productivity, implying less productivity of biogenic silica and less dilution of the carbonate component, and vice versa. Why this anti-phasing system is not at work between 2 Ma and 3 Ma remains unclear. However, it is noticed that the cyclicity is less well expressed in this interval, and the high carbonate values suggest a generally low input of biogenic silica to the sediments.

Figure 32-a δ^{13}C values through middle Pliocene and Pleistocene in Core V28-179 plotted against paleomagnetic record (J = Jaramillo, O= Olduvai, K = Kaena, M = Mammoth). The dotted line at 2.1 Ma represents the separation between two different systems (Figure 32-b).
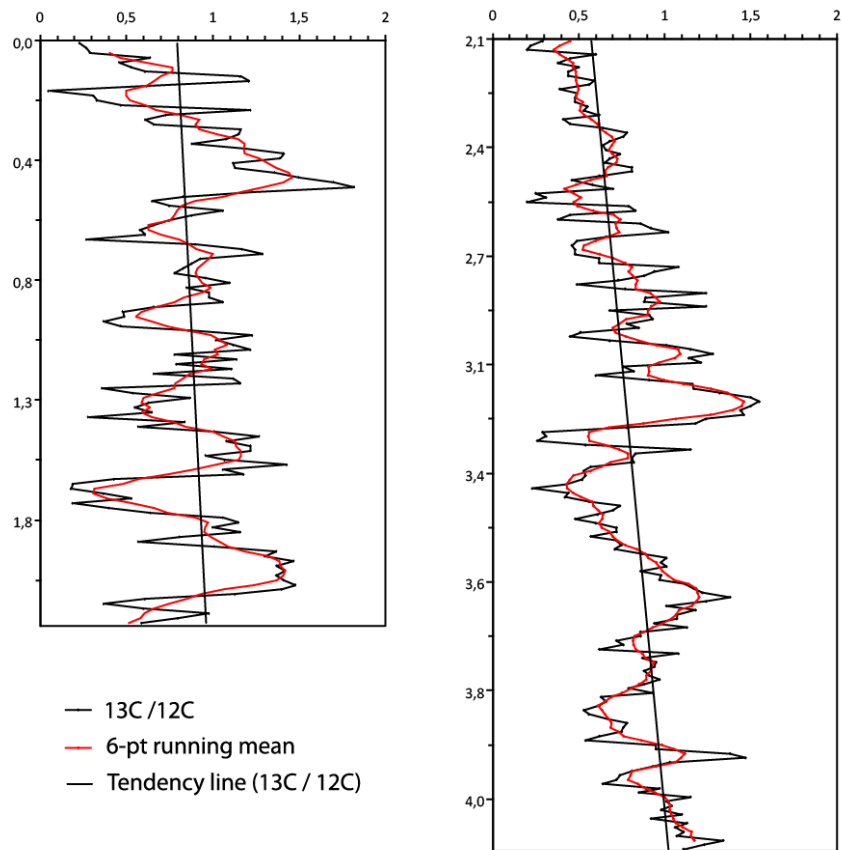
Figure 32-b Two different systems: the older one with an increase in $\delta^{13}C$ values over about 2 million years with weakly expressed c. 405 000 years long cycles, the younger one characterized by a slightly greater increase with prominent cycles of about 405 000 years.
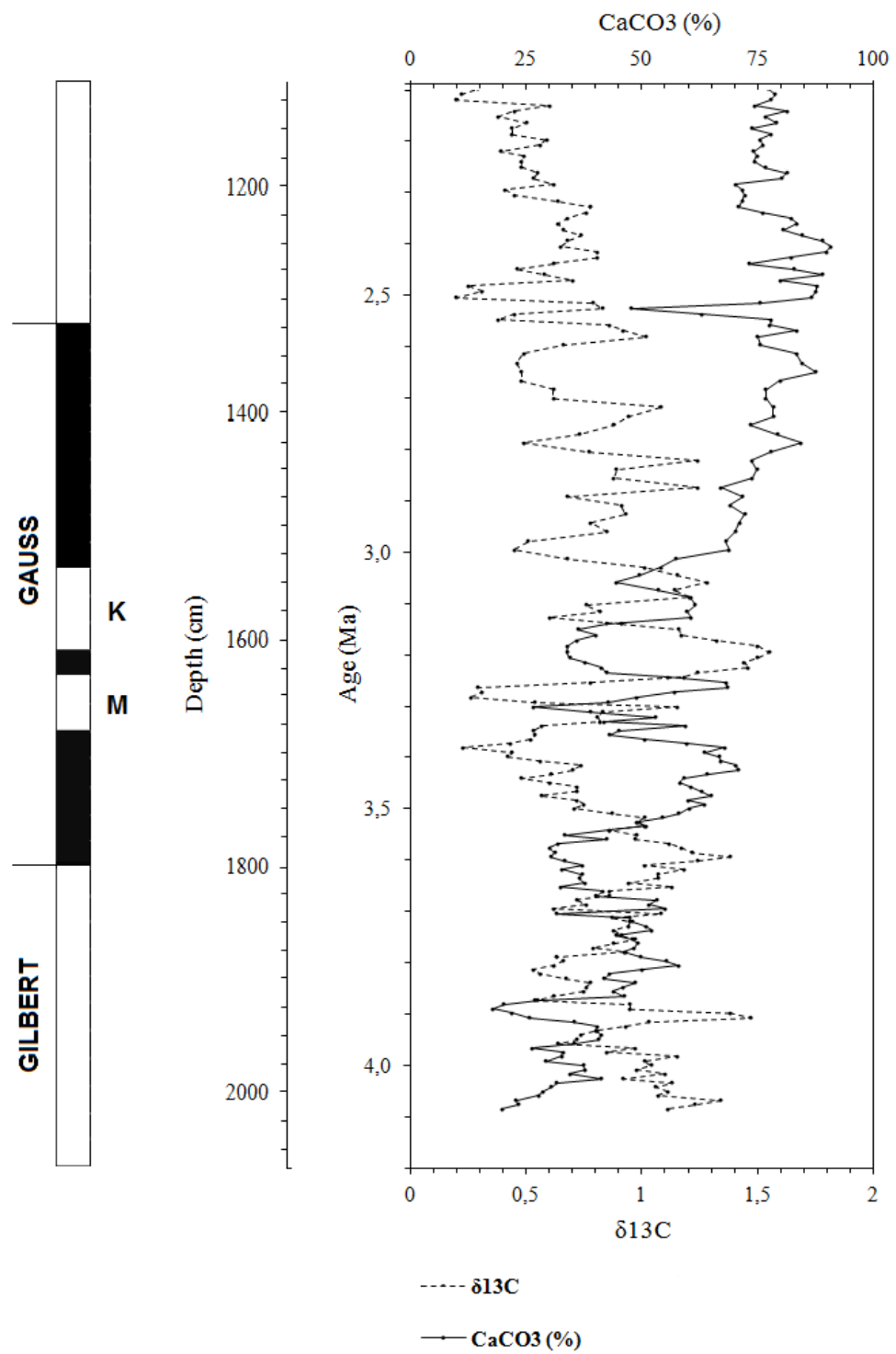
Figure 33-a Variations of carbonate (%) and $\delta^{13}C$ (‰) from the base to 2.1 Ma of Core V28-179. Magnetic events are indicated by K (Kaena) and M (Mammoth).
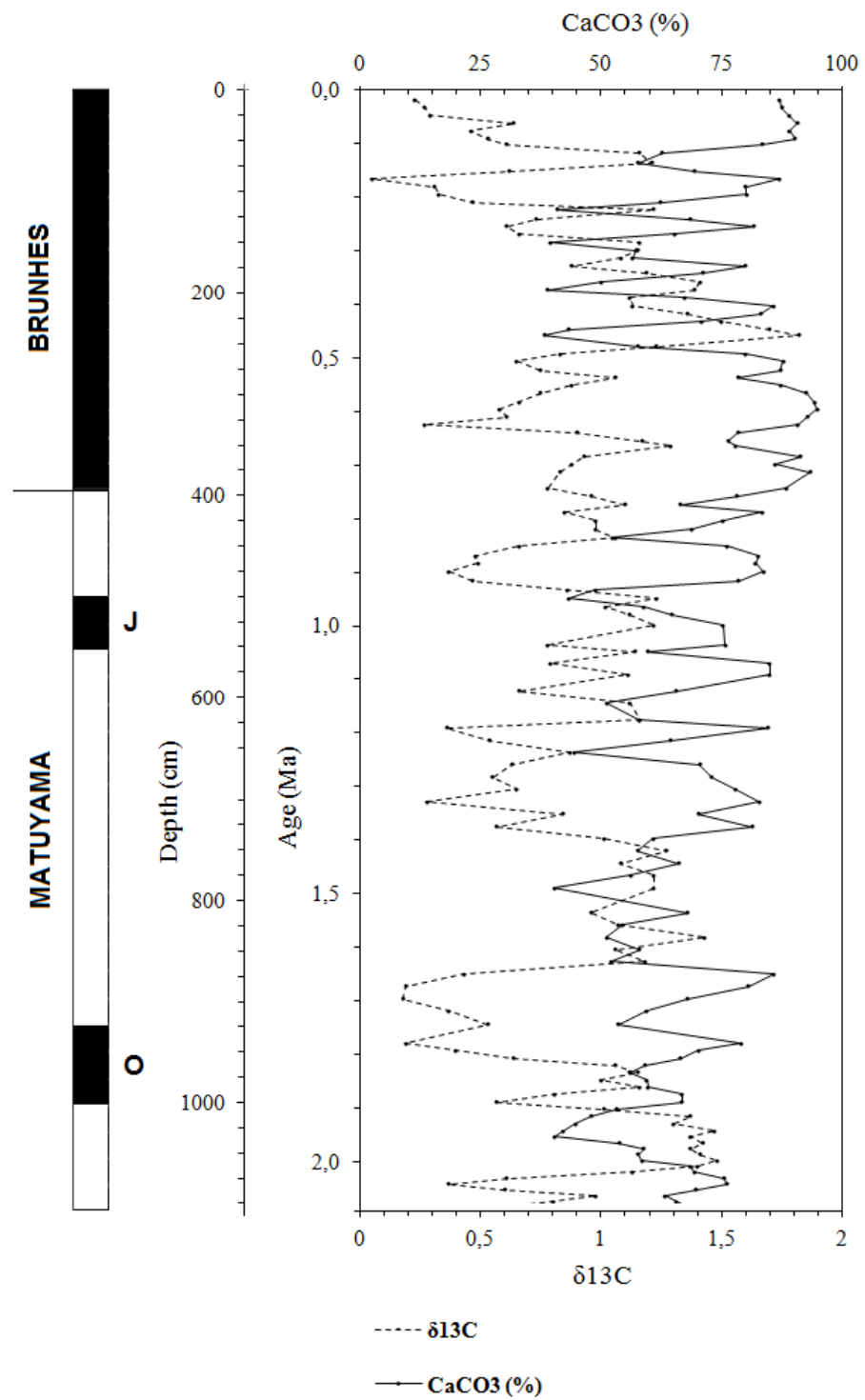
Figure 33-b Variations of carbonate (%) and $\delta^{13}C$ (‰) from 2.1 Ma to the top of Core V28-179. Magnetic events are indicated by J (Jaramillo) and O (Olduvai).

5.3   Oxygen isotopes

Oxygen has 17 radioactive isotopes with a mass number from ^{12}O to ^{28}O. Of these three are stable (^{16}O, ^{17}O and ^{18}O) and ^{16}O is the most abundant in nature (99,765%, Thomas, 2008). The ^{16}O has 8 neutrons and 8 protons while ^{18}O has 8 protons and 10 neutrons.

To perform isotopes analysis, the oxygen must to be in gas phase combined with carbon to form CO_2. The mass of the CO_2 molecule varies as a function of oxygen isotope mass.

Isotopes analysis are based on the abundance of ^{18}O on ^{16}O expressed in percentage. During physical and chemical processes this ratio is subjected to changes in mass and the molecule of CO_2 can be enriched in ^{18}O or ^{16}O. Isotopes fractionation is calculated using the expression:

$$\delta^{18}O \, (\%) = \frac{(^{18}O / {}^{16}O) \text{ sampled} - (^{18}O / {}^{16}O) \text{ standard}}{(^{18}O / {}^{16}O) \text{ standard}} \times 1\,000$$

And is expressed in "parts per thousand" (‰) and related to PDB standard (see chapter 5.2 "Carbon isotopes"). If $\delta^{18}O$ value is positive the sample is enriched in ^{18}O compared to ^{16}O.

The fractionation can be calculated also in the form of H_2O and is often used in conjunction with ^2H (Deuterium) to determine environmental processes.

Water molecules are found in three states: vapour, water and ice. The change of state need a quantity of energy that is highest to change from vapour to water or from water to ice and is lowest to change from ice to water and from water to vapour. These processes are temperature dependent and therefore allow

to estimate paleo-temperatures existing at the moment of the fractionation using sediments or planktonic species (Taylor, 2003).

During glacial periods the subtropics evaporation enriches the sea in the heaviest isotope and the lower atmosphere in the lightest isotope. The ^{16}O can return in the sea in part as rain falling and in part can be trapped in ice sheets, moving the $\delta^{18}O$ values towards the heaviest isotope (Figure 34).

In Antarctica isotopic composition can reach values about -60 ‰ respect the ocean water (Shackleton, 1967).
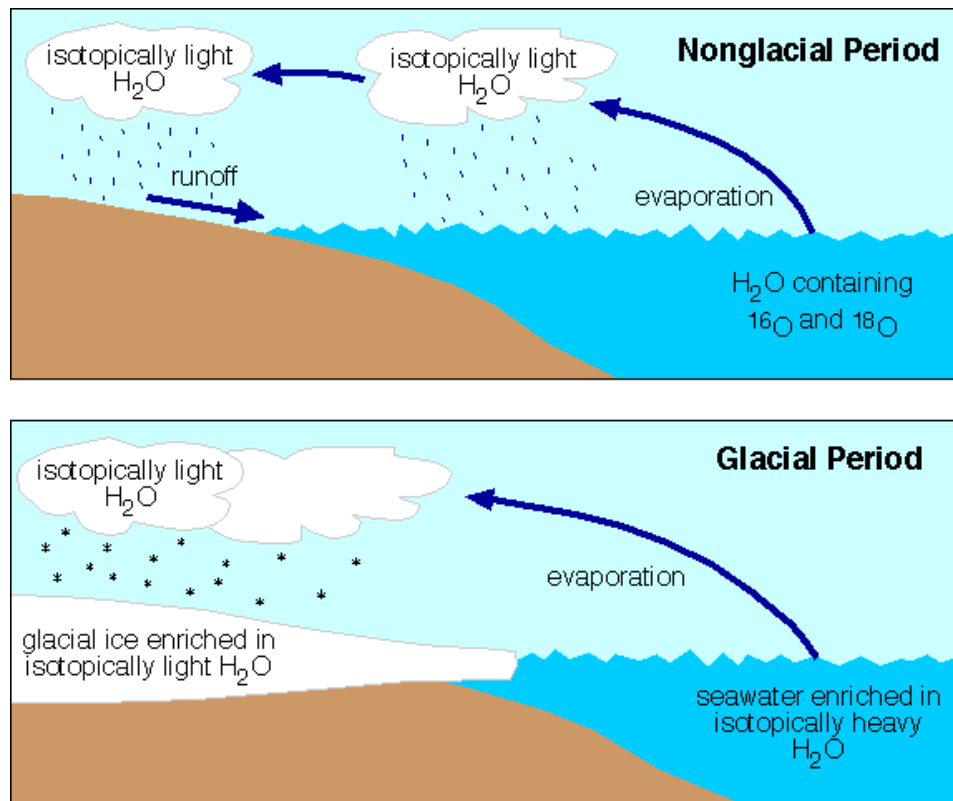
Figure 34 Oxygen isotopes variations during the formation of ice sheets
(Source: http://myweb.cwpost.liu.edu/vdivener/notes/stable_isotopes.htm)

5.3.1   Oxygen isotope analysis

An oxygen isotope record from bulk sediment is presented for Core V28-179 (Figure 35). The isotopic composition is based as deviation from Pee Dee Belemnite (PDB) standard.

Generally, an upward increase is present in $\delta^{18}O$, from about -0,5 ‰ to 0,8 ‰. At ~2.5 Ma a strong oscillation is present, coinciding approximately with the onset of northern hemisphere glaciation (Shackleton et al., 1984).

This strong variation, and therefore also increase in ^{18}O, is probably due to the increase in ice volume. Other factors, connected with global ice volume change, may be temperature, dissolution and evaporation/precipitation.

The strong decreasing from ~0.4 Ma to the top (~0,5 to -0,8 ‰ $\delta^{18}O$) indicates a warming of surface waters at the coring site of about 5°C. One way to explain this trend could be the tectonic movement of the site away from the colder upwelling zone.

Shackleton and Opdyke (1977) proposed a strong Pliocene paleoclimatic event at about 3 Ma, beginning at the base of the Mammoth. They argued that the fast increase to heavier isotope values at about 3 Ma represents the onset of Northern Hemisphere glaciations. After this event, major oscillations of glacial-interglacial cycles began. This global event has been identified by several studies in different parts of the Earth, e.g. from western Mediterranean (Combourieu and Vergnaud, 2003) and the North Atlantic (Bartoli et al., 2006).
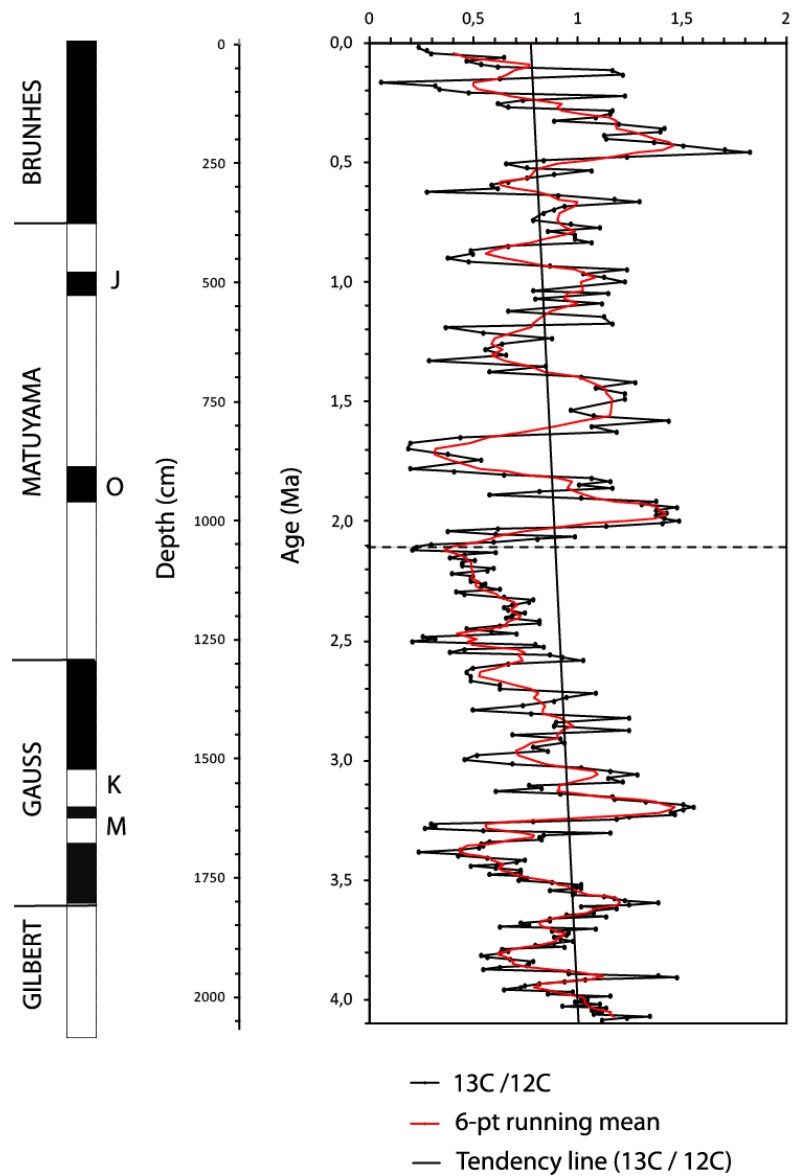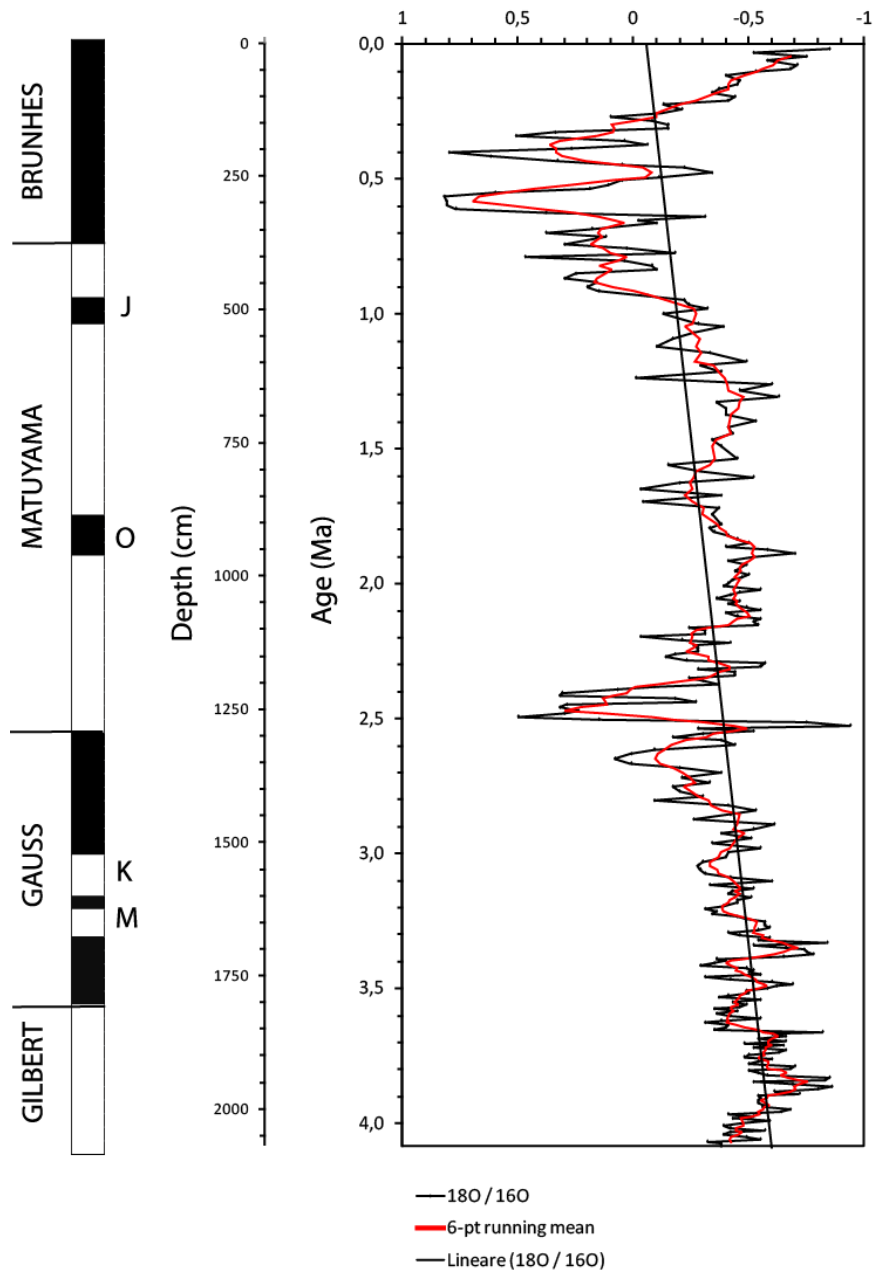
Figure 35 δ^{18}O values through middle Pliocene and Quaternary in Core V28-179 plotted against paleomagnetic record (J = Jaramillo, O= Olduvai, K = Kaena, M = Mammoth).

5.4   Comparison with the Shackleton and Opdyke (1977) isotopic record

We have compared the bulk isotope analysis, performed in this thesis, with Shackleton and Opdyke (1977) analysis made on the benthic foraminifer *Globocassidulina Subglobosa* in V28-179.

The two curves follows a remarkably similar pattern but isotopes values differs from about 1 ‰ to 2 ‰ for $\delta^{13}C$ and from about 3.50 ‰ to 4.30 ‰ $\delta^{18}O$. The difference is caused by different depth of the data acquisition (the bulk reflect the isotopic composition of the planktonic association). In fact, the oxygen isotopes values were recorded on plankton before death and remained unchanged even after the death of the organism. The samples measured by Shackleton and Opdyke, instead, were taken from benthos and have recorded in them the isotope composition of deep waters, certainly different from shallow waters. The diagenesis effect lead to oxidation of biogenic material and to release of ^{13}C accumulated in shells.

As described in chapter 4.1.4 "Transport", the oceanic thermohaline circulation carry deep cold waters from the antarctic province. Cold waters are more dense than warm waters and have isotopes values closer to ^{16}O because the water transformed in vapour near the Equator is released as rain towards high latitudes and reports in the cycle the lighter isotope. During glacial periods the water released during precipitations at high latitudes is in the form of snow and it accumulates as ice sheets, in which the lighter isotopes is trapped. So, the isotopic composition of the water from the Antarctic have an higher $\delta^{18}O$ value. The thermohaline circulation lead isotopically heavier waters to the low latitudes and for this the isotopic composition of deep waters is enriched in ^{18}O than shallow waters (Figure 37).

Conversely Shackleton (1967) explain how the temperature at the bottom of Carribean and equatorial Atlantic and others oceans can not vary more than two

or three degrees during glacial-interglacial periods, because it is already near freezering point (actually 1,5° C at 1700 meters). Changes in temperature are responsible for changes in oxygen isotopic composition and therefore the bottom isotopic variation must be caused by others factors. Shackleton proposed changes in salinity rather than temperature during Upper Pleistocene. Probably freshwaters, having less salinity, have led heaviest waters at great depths.

The $\delta^{13}C$ presents a less clear separation of only 1-2 ‰. The separation, in this case, is due to the different life cycle between benthos and plankton, which carry out photosynthesis. This process, as discussed previously, taken up ^{12}C by photosynthesis and enrich the shells in ^{13}C.
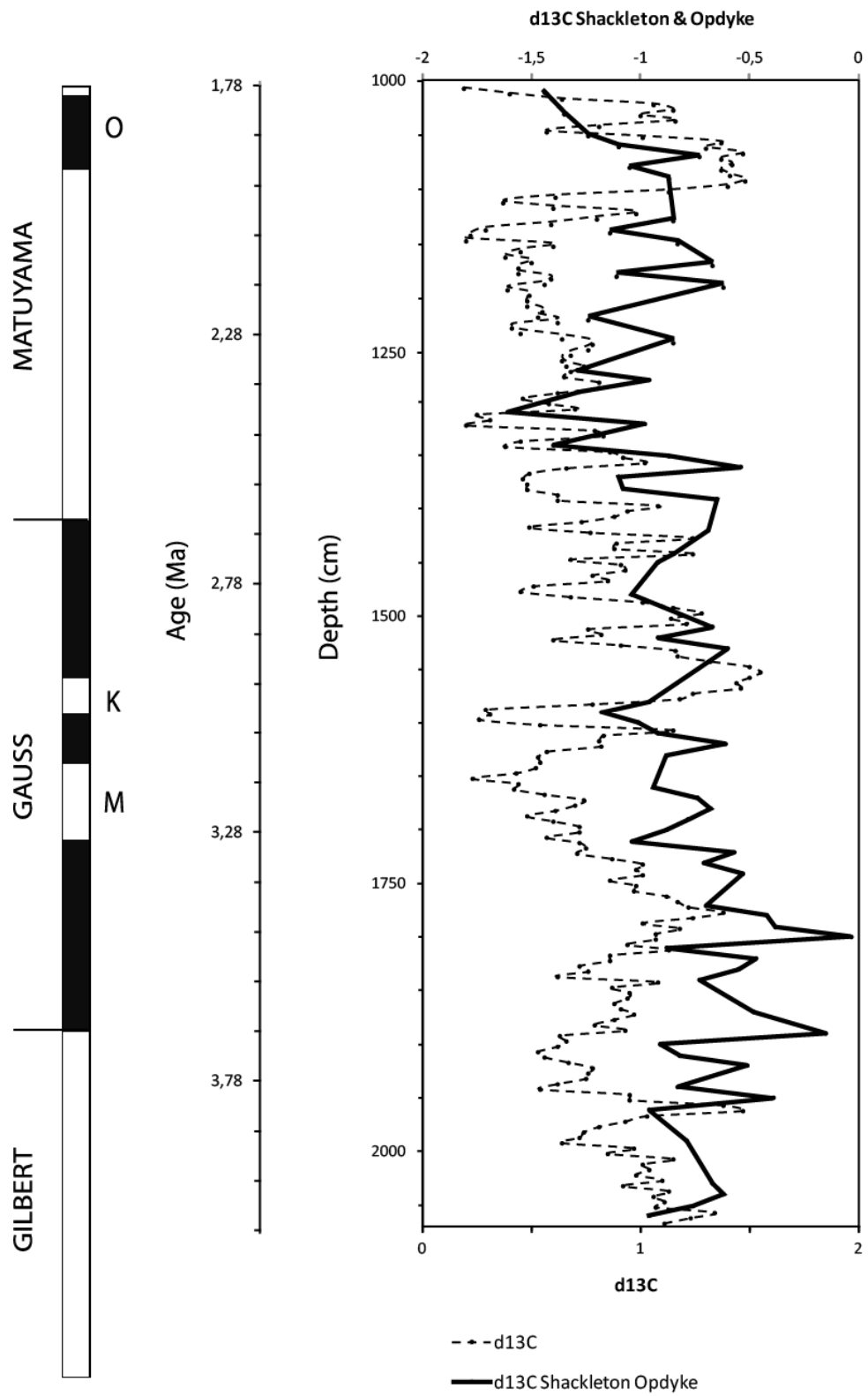
Figure 36 Comparison of benthic and bulk $\delta^{13}C$ in Core V28-179.
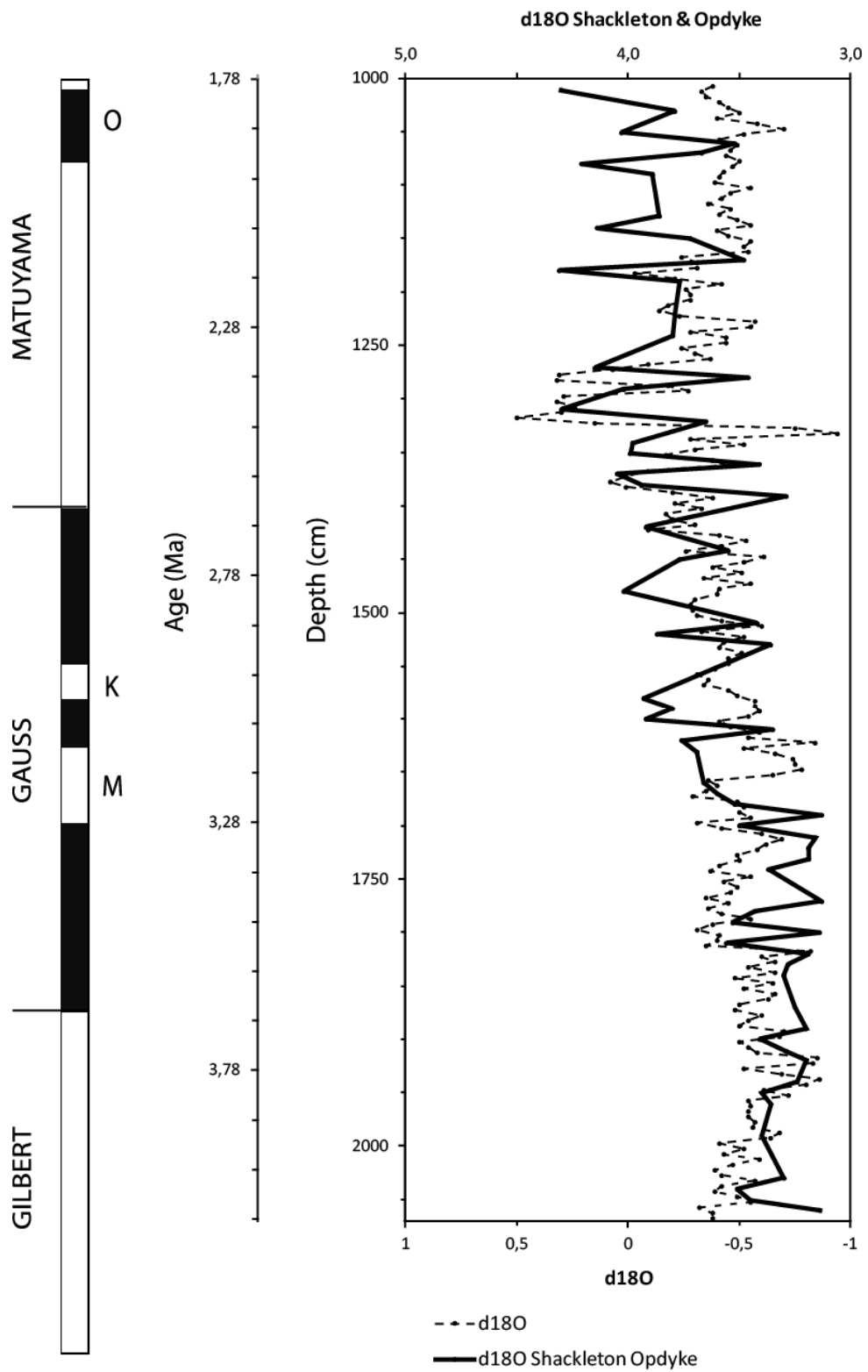
Figure 37 Comparison of benthic and bulk δ^{18}O in Core V28-179.

5.5 Comparison between Discoaster abundance, carbonate and isotopes analysis

Strong variations were detected in abundance of the three species (Table 12). Up to 666 specimens per mm^2 were counted at 3.24 Ma for *D. brouweri* and two main peaks were detected at 2.87 Ma and 3.30 Ma for *D. tamalis* and *D. asymmetricus*. The first peak is also reflected on the carbonate content and on carbon isotope values, that appear to show the end of a 405 000 years cycle. The second peak at 3.30 Ma does not coincide with any major changes in carbonate contents or carbon isotopes.

Table 12   Union of all curves analyzed
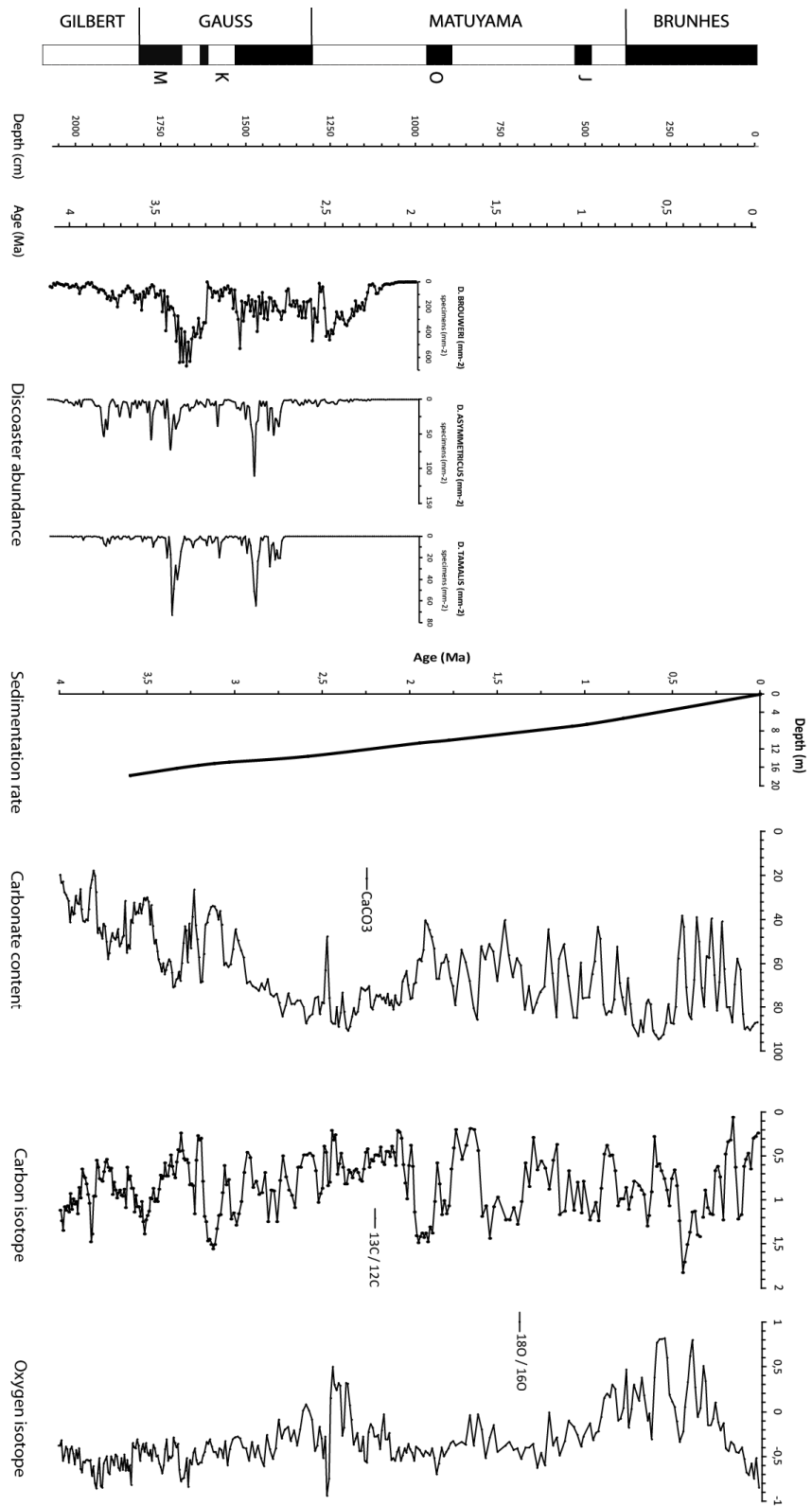
5.6 "Atlantic type" and "Pacific type" carbonate systems (Dunn, 1982)

In 1982, Dunn (1982) performed a study on the carbonate content and oxygen isotopes results between the Atlantic and Pacific oceans, based on works of Arrhenius (1952) and Emiliani (1955). Arrhenius noticed a synchronism between $CaCO_3$ fluctuation and climatic changes and proposed a strong increase in winds during glacial periods that increased upwelling along the Equator and then productivity that would lead an increase in carbonate accumulation rate. Emiliani extrapolate the oxygen isotope data from foraminifera in the North Atlantic and the Caribbean Sea and compared them with the calcium carbonate content in Equatorial Pacific cores.

They showed that during the Quaternary in the Pacific Ocean, a high-carbonate concentration was present during glacial episodes (high $\delta^{18}O$) and vice versa during interglacial episodes (low $\delta^{18}O$). In the Atlantic Ocean, instead, ruled the opposite situation (high carbonate content with low $\delta^{18}O$). These two situation were called "Pacific Type" and "Atlantic Type".

Shackleton and Opdyke (1977) used the Pliocene and Pleistocene paleomagnetic data of the Core V28-179 to create an age model and to compare oxygen isotopes results with carbonate content every ten centimetres along the core. In Figure 37 and Figure 38 it can be noted an apparent correlation upwards among increase in carbonate and increase in $\delta^{18}O$ to indicate a "Pacific Type".

Dunn (1982) suggested a reversal trend below ~1700 cm (about 3.5 Ma) indicating a shift upward from "Atlantic Type" to "Pacific Type", then from warm waters to cold waters.

A further subdivision is given by the Pliocene carbonate cyclicity of 100-ka that would have masked the higher cyclicity of 400-ka (eccentricity of the Earth's orbit) pre North Hemisphere Glaciation (NHG). In the Quaternary, post-

NHG the cyclicity of 100-ka it seems to be much more evident. This indicates a strong influence of the orbital parameters.
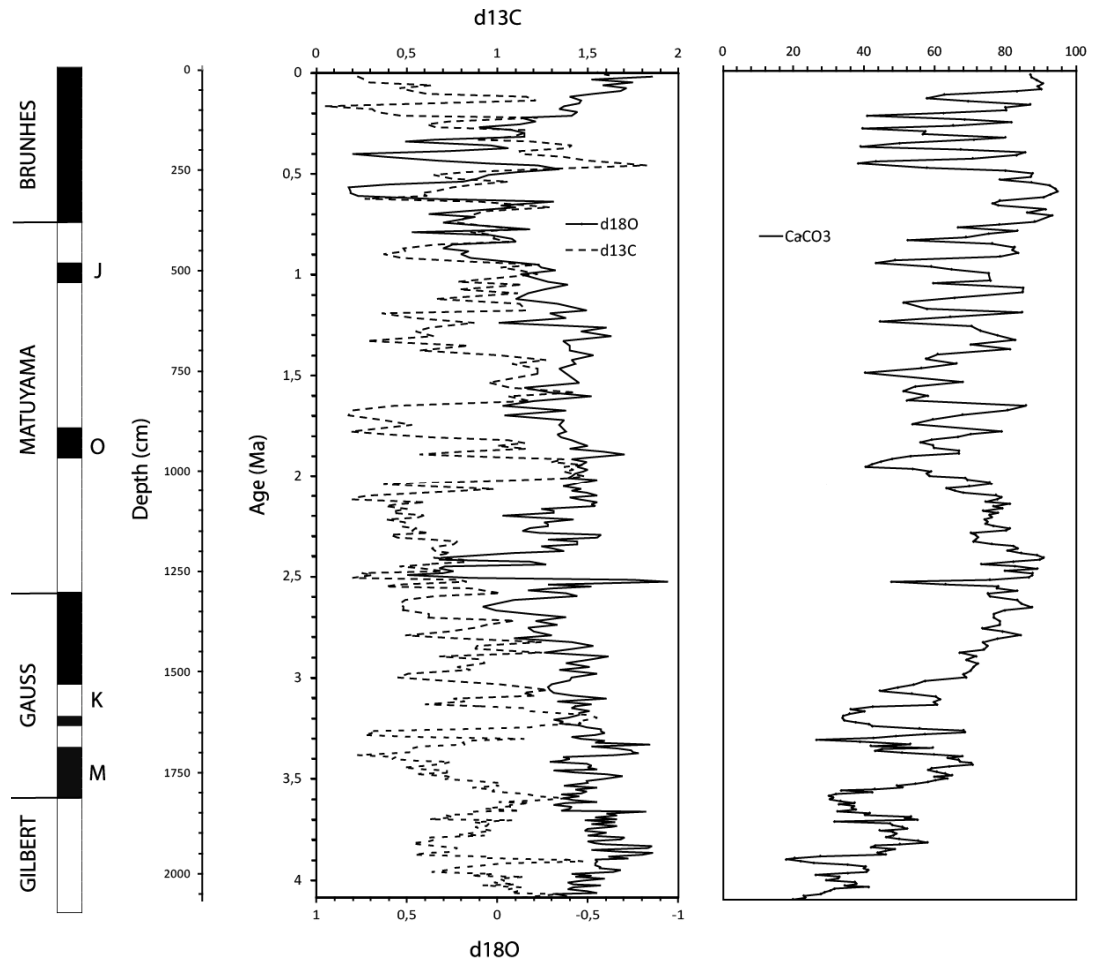
Figure 38 Carbon isotopes plotted against oxygen isotopes (‰) and carbonate content (%) of Core V28-179.

CHAPTER 6

PLIO-PLEISTOCENE CLIMATE DYNAMICS

6.1 Introduction

During the last five million years, global temperatures have changed continuously due to changes in external forces (Milankovitch forces) which obliquity, eccentricity and axial precession. Thus, these variations have affected global temperatures through seasonal variations in the carbon dioxide concentration in the atmosphere, sea surface and deep water temperatures, winds, albedo[1], monsoons, upwelling areas, global ice volume, sea level fluctuations, geographic position of the continents and therefore also the influence of biogeochemical cycles. All these factors are strongly connected and change each other.

During the early Pliocene (~5 Ma) the CO_2 concentration in the atmosphere and sea surface temperatures (SST) around tropics and the Equator were similar to the present but the climate is in a state of disequilibrium. Around 3 Ma, the sea level was 30-40 m higher than today (Sarnthein et al., 2009). What were the reasons and what were the consequences of this warm-to-cold climate transition?

---

[1] From the Latin *Album* "white", is the incident light fraction on a surface that is reflected. Is the reflectivity power of a surface. The value depends on the material that is struck by light and on the wave length of the light. The light can be in part absorbed or reflected, depends on the type of material.

6.2 Methods to identify temperature variations in the ocean system

In the early Pliocene ocean temperatures were higher than today. Evidence of periodic temperature oscillations has been obtained from oxygen isotopic analysis of Atlantic, Pacific Oceans and Caribbean Sea deep-sea cores. Benthic foraminifers showed that bottom waters in the Pacific were at the same temperature of today but in the Atlantic were 2.1 °C lower during glacial ages (Emiliani, 1955).

In order to reconstruct temperatures in paleo-ocean waters it is necessary to know the isotopic composition of the water during the formation of the foraminifer shell. In fact the isotopic composition depends by the vapour pressure on the water-atmosphere surface, that is higher if more H_2O^{18} is present and lower vice versa (Emiliani, 1955).

$$T = 16.5 - 4.3\,(\delta\text{-}A) + 0.14\,(\delta\text{-}A)^2$$

$$\text{Where } \delta = 10^3\ \frac{{}^{18}O/{}^{16}O(sample) - {}^{18}O/16O\ (standard)}{{}^{18}O/{}^{16}O\ (standard)}$$

$$\text{And } A = \frac{{}^{18}O/{}^{16}O\ (W') - {}^{18}O/{}^{16}O\ (W)}{{}^{18}O/{}^{16}O\ (W)}$$

The vapour moves towards poles, releasing ^{18}O on the way (see Chapter 5 "Isotopes in the oceanic record"). The isotopic composition on polar the ice sheet and waters is enriched in ^{16}O and this is reflected on the bottom water that

receives colder waters through circulation from polar regions (Emiliani, 1955). A further variation can be induced by dissolution of carbonates and silica after the death of an organism that release ^{18}O.

The relationship between oxygen isotopic composition and temperature is given by the type of plankton/benthos that is analyzed, because there is a vertical stratification of the living forms, dependent on the living conditions of the organism (temperature of the water relative to the density/salinity, thickness of the photic zone relative to the transparency of the water). If these parameters change during time the plankton adapts to these conditions.

Shackleton (1967) identified oscillations of about 1°C to 6 °C sea surface temperatures, with 1.65 ‰ $\delta^{18}O$ variation in the Atlantic Ocean and the Caribbean Sea every 40 000 years. Both deep and surface waters registered changes of about 1.5 ‰ $\delta^{18}O$ during glacial-interglacial cycles.

Another test can be performed using dissolved inorganic carbon isotope ($\delta^{13}C_{DIC}$). The oceanic circulation is a means of transport of nutrients. The waters from the Antarctic ocean are depleted in nutrients but get enriched reaching the Pacific. Especially, the North Pacific is the most nutrient-enriched water (Ravelo, 2007). The $\delta^{13}C_{DIC}$ in the Antarctic and North Atlantic mixing zone is heavier than in the past. This means a better ventilation in the past because high $\delta^{13}C_{DIC}$ means lower nutrients and higher $\delta^{18}O$, maybe caused by the final closure of the Panama seaway during the early-middle Pliocene (at least 4 Ma) (Figure 39). This would lead to a series of feedbacks and perhaps to the onset of the North Hemisphere glaciation (NHG), which started at about 3 Ma. The depletion of the $\delta^{13}C_{DIC}$ expanded to Central and South Atlantic and is emphasized in the Pacific during the onset of the NHG (Ravelo et al., 2007).

Another analysis which can be made on shells is the Mg/Ca method. After the death of an organism, a dissolution process begins, dependent on the water parameters, and loss of Mg-rich calcite (Skinner et al., 2007).
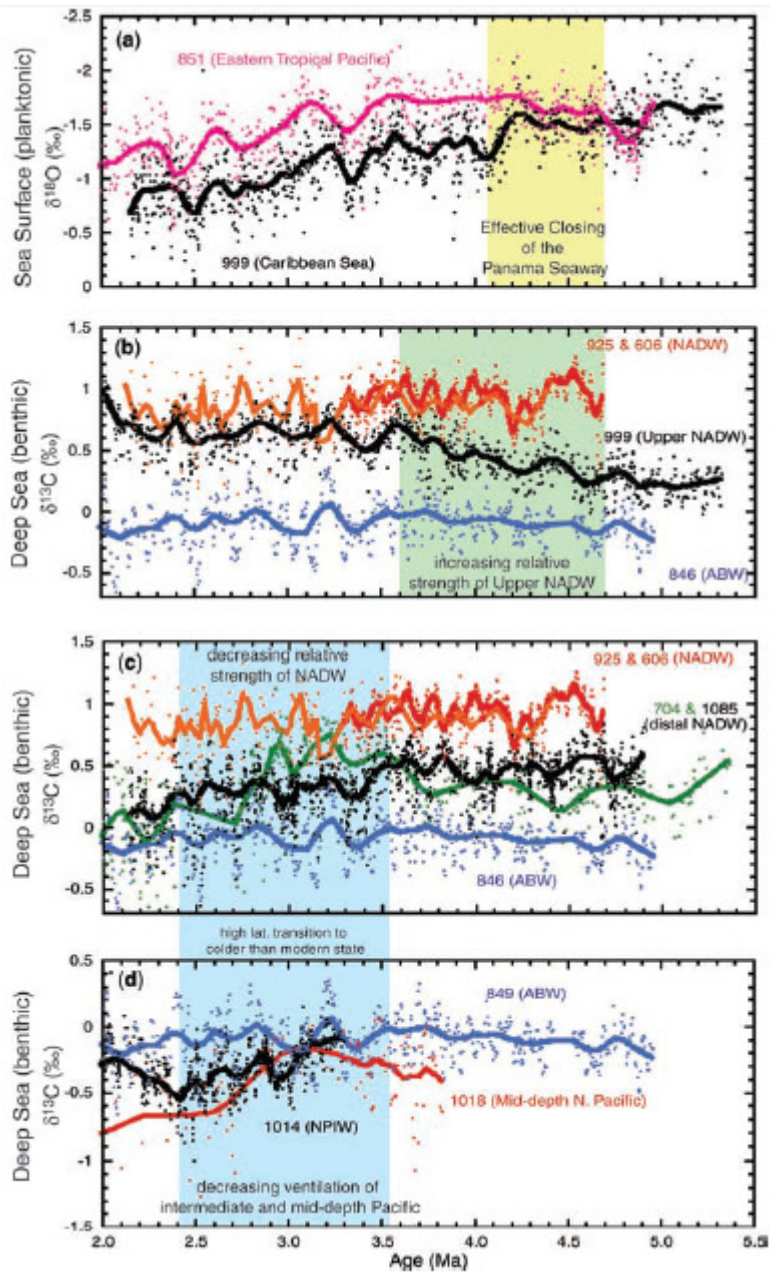
Figure 39 Carbon and oxygen isotope values for the past 5.5 Ma to 2.0 Ma from Atlantic and Pacific sites and principal changes in the water circulation (from Ravelo et al., 2007).. The closing of the Panama Seaway led to decrease in ventilation (decrease in $\delta^{18}O$) of the North Atlantic mid water and the onset of the North Hemisphere Glaciation (Ravelo et al., 2007).

Another used method to reconstruct paleotemperatures is the alkenone paleothermometry (Placencia et al., 2010), that employs organic biomarkers produced by some species of coccoliths. This method use U_{37} to identify the growth temperature, the productivity and the pCO_2 of waters (Lawrence et al., 2006).

6.3 Initiation of the Northern Hemisphere Glaciation: temperature variations in space and time

Temperature variations are present both vertically and horizontally in oceans and ranging from -2 °C at the poles to 28 °C along the equatorial area.
The vertical stratification along the water column is underlined by the thermocline level, that separates the surface ocean from the deep ocean.

The surface ocean has a higher temperature due to solar heating, and depends on latitude. Actually the thermocline is located from 100-200 m and even down to 1000 m. The presence of the thermocline is inhibited at high latitudes and at middle latitudes during seasonal variations. The deep ocean, under the thermocline, is characterized by low temperatures, about 5 °C to 1 °C. The range of temperature variation as a function of latitude is shown in Figure 40.

Since about 50 million years ago, a global cooling began caused by a complex of factors involving changes in Milankovitch forces and plate tectonics (Zachos et al., 2001). A series of feedbacks were developed as changes in basin geometry, sunlight distribution, greenhouse gases, sea surface temperatures, monsoons, and coastal upwelling (Fedorov et al., 2006).
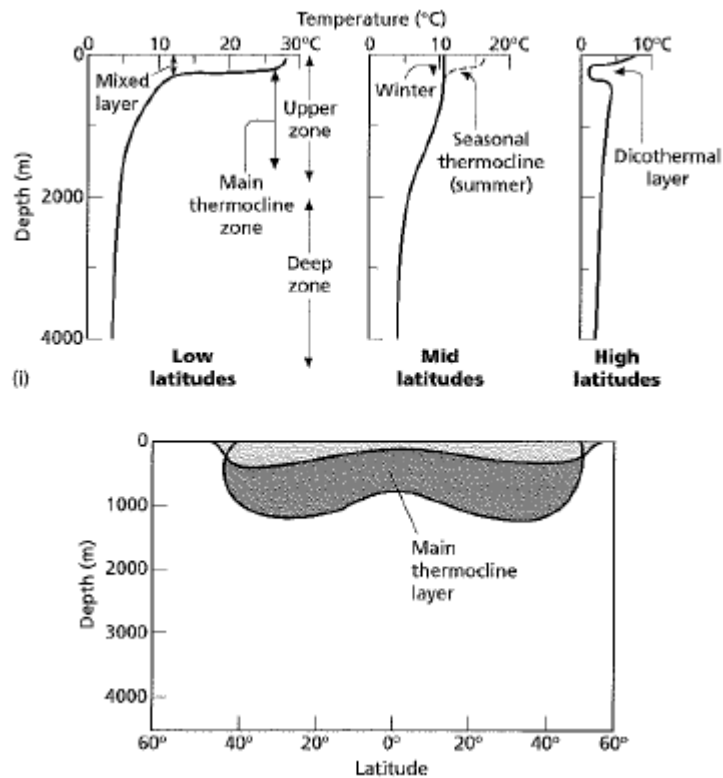
Figure 40 Vertical and horizontal temperature variations (Chester, 1999).

Around 35 million years ago the presence of these phenomena is manifested in a development of large ice sheets in Antarctica and around 3 Ma in northern continents. About 2.7 Ma there is evidence from Pacific cores about glaciations in the Northern Hemisphere (Fedorov et al., 2006). During the Pliocene in the Pacific Ocean, cold surface temperatures were absent at lower latitudes. The temperatures were 3 °C higher than today and the CO_2 atmospheric concentrations was about 30 % higher than pre-industrial Holocene values (Filippelli and Flores, 2009).

The transition between the early Pliocene warm period and the mid-Pleistocene cold period is supported by the onset of the NHG. This change is accompanied by changes in amplitude and frequency of Milankovitch cycles and then distribution of solar heating on Earth's surface. Other causes that may have been involved is the closure of the Isthmus of Panama, the Tibetan uplift and the

restriction of the Indonesian seaway (Lisiecki and Raymo, 2007). These changes in tectonic gateways and topography has influenced all the entire Earth's water and atmospheric circulation and the concentration of gases in atmosphere (such as water vapour) (Ravelo et al., 2007).

Specially the deep thermohaline circulation changed and intensified the heat transport from tropics to North Atlantic, increasing temperatures. In the Pacific Ocean appeared upwelling areas, especially in the east equatorial zone, and decreased sea surface temperatures, leading to a decrease in vapour content over these upwelling areas resulting to increasing of high-latitude albedo. During the Pleistocene, then, along upwelling areas the primary productivity increase (Filippelli and Flores, 2009).

The wind-system changed due to difference in pCO_2 (sea surface temperature due to the thermocline gradient) from west to east Pacific and passed from El Niño[2] (Figure 41) permanent condition to intermittent condition at ~3 Ma (Fedorov et al., 2006; Ravelo et al., 2007).

---

[2] Climatic phenomena that occurs in the Equatorial Pacific Ocean between 3 and 7 years actually. Is caused by the difference between east and west sea surface temperature. During "normal" conditions equatorial currents travelling from east to west and the thermocline deepens from ~50 m to ~200-400 m resulting in a difference of about 5 °C. High precipitation level persist on the west side of the Pacific Ocean. During El Niño conditions are set high precipitation rates on the east coast and dry conditions to the west (Ravelo et al., 2006).
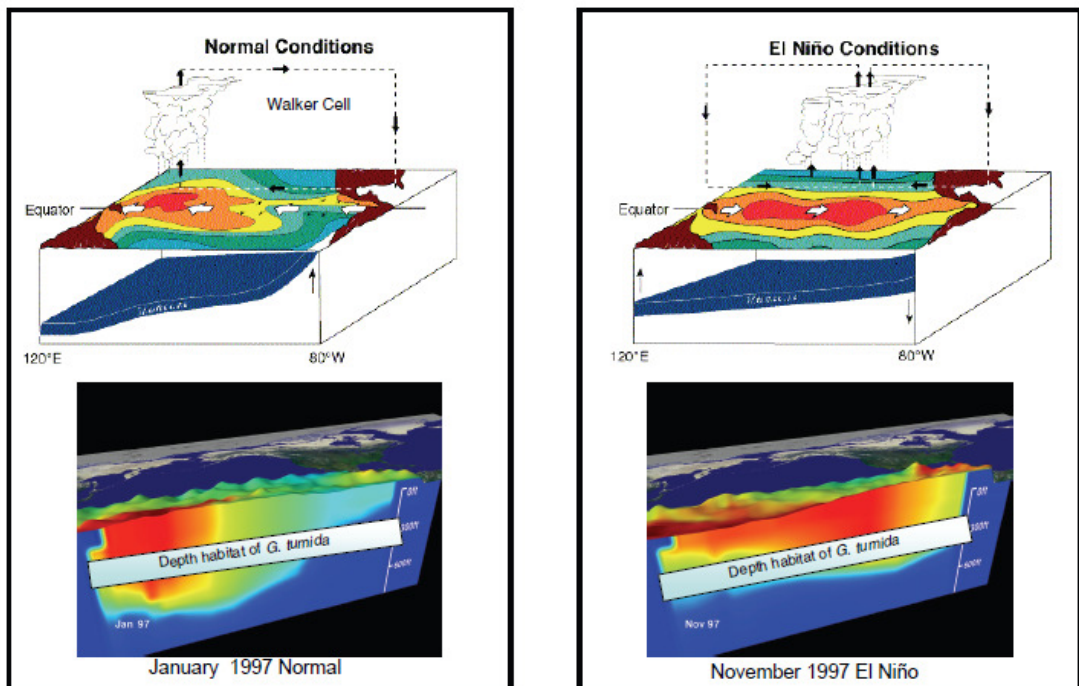
Figure 41 El Niño phenomena in the Equatorial Pacific Ocean. Intermitted conditions are shown during seasonal variation. The habitat of foraminifer *G. tumida* change whit temperature (Ravelo et al., 2006).

6.3.1   Changes in orbital parameters

Around 3 Ma obliquity cycles changes from a period of 40 000 years to multiples (80 000 and 120 000 years) masked in 100 000 years cyclicity (Fedorov et al., 2006) closing to δ^{18}O variations from benthic and variations in $CaCO_3$ preservation (Farrell and Prell, 1991; Shackleton, 1967; Sarnthein et al., 2009).

Lisiecki and Raymo (2007) created a model to define orbital changes using amplitude modulation. They measured the ratio of amplitude response using a given frequency and correlate power of forcing and response. For the obliquity the

41-kyr modulation match well with $\delta^{18}O$ values (Figure 42 and Figure 43). Furthermore, from 4 to 2 Ma obliquity sensitivity increased, but from 1.8 Ma to 0 decreased. At 1.4 Ma there is the passage from a obliquity-dependent to a non obliquity-dependent climate and a strong decrease in 41-kyr response and decline in the interglacial periods duration with a superimposing in the mid-Pleistocene of the 100-kyr system (Lisieki and Raymo, 2007).
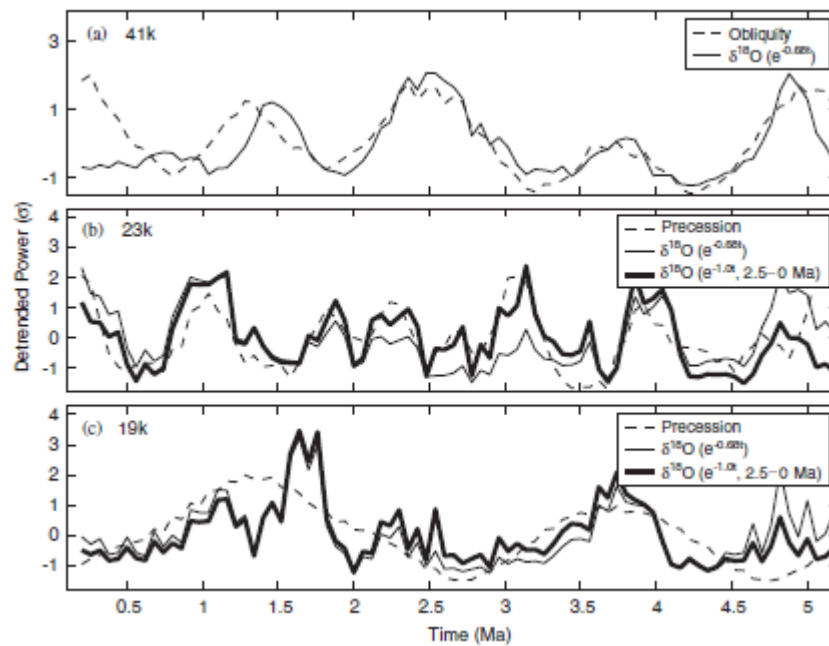
Figure 42 $\delta^{18}O$ values at (a) 41-kyr obliquity, (b) 23-kyr precession and (c) 19-kyr precession parameters (Lisiecki and Raymo, 2007).
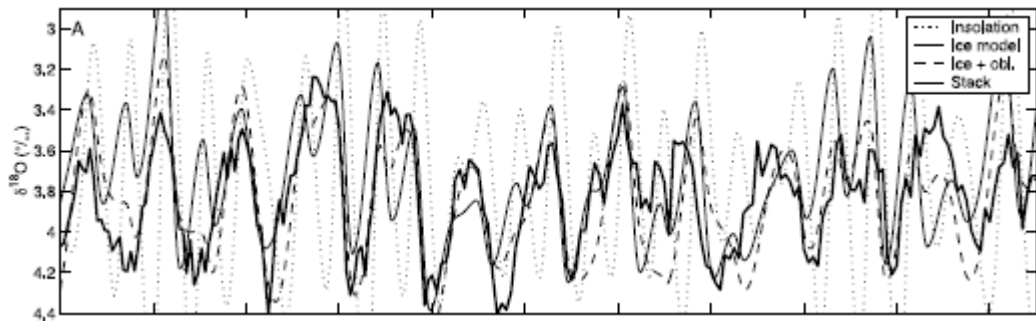
Figure 43 $\delta^{18}O$ values with insolation and obliquity at 65° N (Lisiecki and Raymo, 2005) to demonstrate matches between oxygen isotopes, ice sheets, insolation and obliquity.

This, together with plate tectonics changes, results in a variation of the solar heating on the Earth's surface that caused changes on the thermocline depth, change in the ocean circulation system and distribution of warm and cold waters. The development of upwelling cold waters in some regions has led to arid conditions in Africa and cooler conditions in North America and the development of the NHG (Ravelo et al., 2007).

6.4   How climate changes has affected the ways of life of plankton

Living forms are a useful method to identify climate changes because they adapt to environmental conditions that vary over time as the calcite compensation depth and mass movements of waters as well as temperature, salinity, nutrients supply and thickness of the photic zone (chemical, physical and biological conditions), not counting the natural selection as predation. All these factors can

influence each other but the most important environmental changes occurred due to external forces.

Actually, during El Niño condition, the warm phase of water lead to reduce in plankton production (because reduce in upwelling zone and then nutrient input). Also along Benguela and California coasts are reproduced dramatic changes in mesozooplankton abundance due to long-term climate changes (Hays et al., 2005). Weather changes also influences the ocean stratification through thickness of the photic zone, surface temperatures and nutrient recycling from deep layers (Hays et al., 2005)

Since oceans cover most of the Earth's surface, processes that occurs in oceans have repercussions also on the land, given that the life cycle and the whole climate system are destabilized.

Was performed a correlation between isotopes values, carbonate content of Core V28-179 and eccentricity, obliquity and axial precession cycles described by Maslin and Ridgwell (2005) during the mid-Pleistocene transition. Carbon isotopes show a good correspondence with eccentricity during the last 500 000 years (Figure 44), emphasizing the importance of 100 000 years cycles. At about 300 000 years seems to start an anti-phasing period. The oxygen isotopes show a good correspondence along almost the entire curve (Figure 45), except in the interval from about 350 000 years to 450 000 years. The carbonate content show the best correspondence (Figure 46): the 100 000 years cyclicity it seems to be clear. The curves are in phase until about 250 000 years, with a slight separation from 450 000 years to 350 000 years, and from 250 000 years to 0 years are in anti-phase.

All three curves (δ^{18}O, δ^{13}C and $CaCO_3$) do not present a perfect correspondence among peaks in the same time level. This is can be caused by different sedimentation rates.

It is evident the influence of changing in orbital parameters, and hence the climate, in the $CaCO_3$ content and in oxygen and carbon isotopic composition.
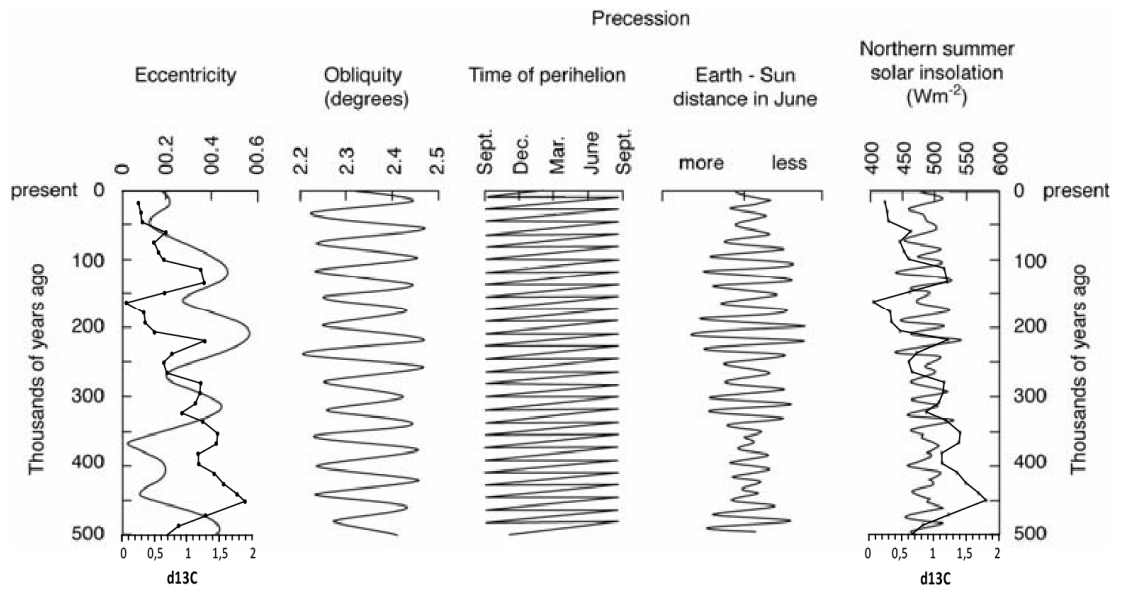
Figure 44 Overlapping of δ¹³C curve with eccentricity and solar insolation during the last 500 000 years. The dotted curve belongs to Core V28-179. (Maslin and Ridgwell, 2005).
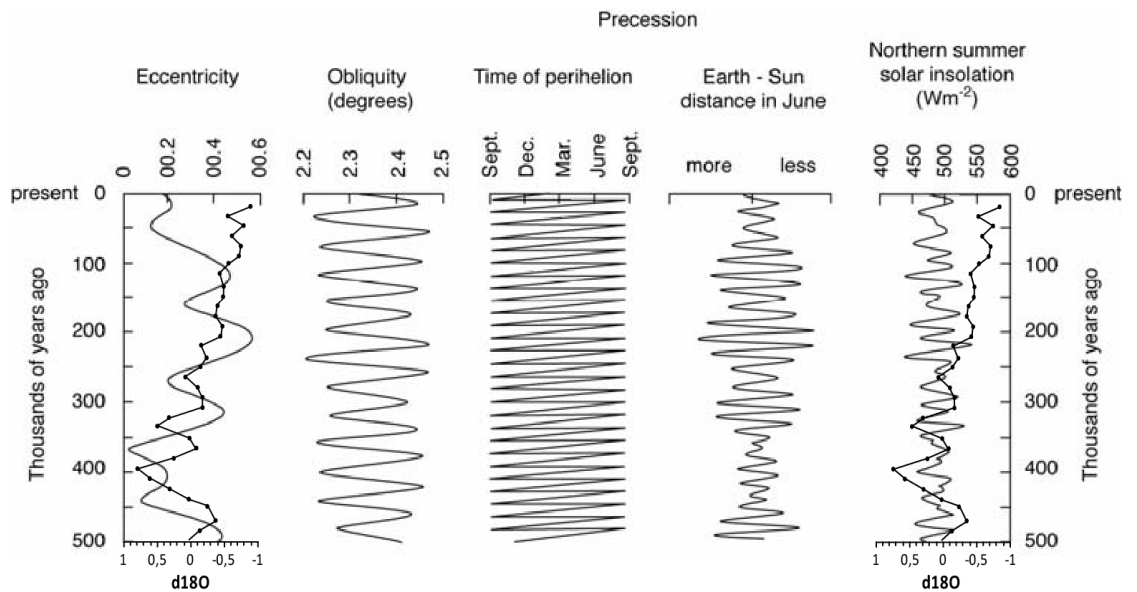
Figure 45 Overlapping of δ¹⁸O curve with eccentricity and solar insolation during the last 500 000 years. The dotted curve belongs to Core V28-179. (Maslin and Ridgwell, 2005).
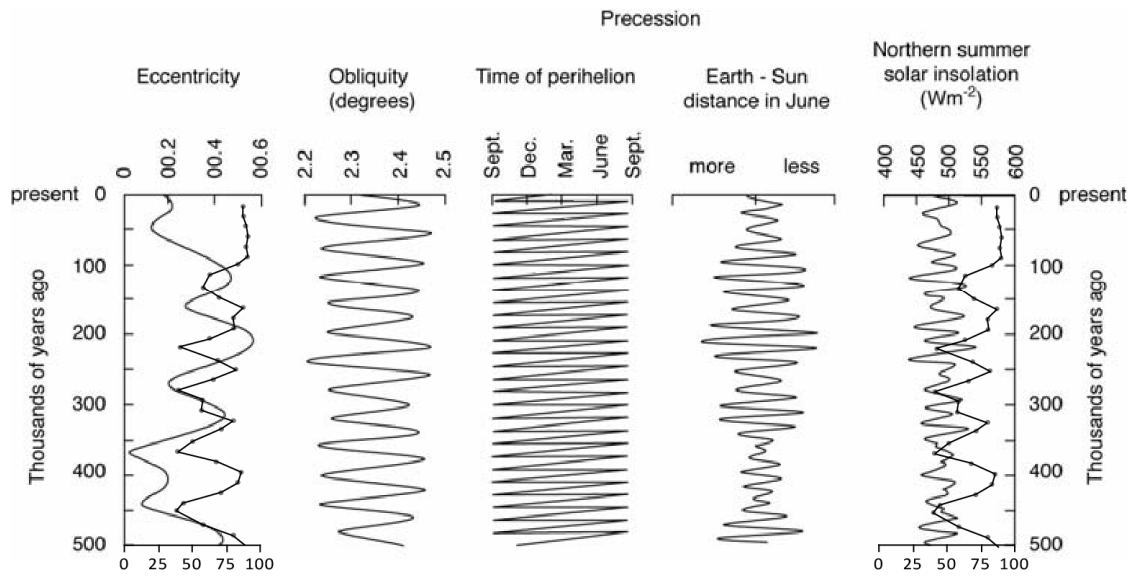
Figure 46 Overlapping of carbon content curve with eccentricity and solar insolation during the last 500 000 years. The dotted curve belongs to Core V28-179. (Maslin and Ridgwell, 2005).

CONCLUSIONS

In this study analysis has been performed on:

- Fossil content, particularly *Discoaster brouweri*, *Discoaster tamalis* and *Discoaster asymmetricus*. More accurate studies on abundance, number of specimens per mm^2, proportions between species, eventual first appearance / last appearance and common presences.

- Sedimentation rates

- Magnetic stratigraphy

- Carbonate content

- Oxygen and carbon isotopes. Comparison with carbonate content and Shackelton and Opdyke's isotopic record.

- Climate dynamics during Plio-Pleistocene

The aim was to identify possible climate changes occurring at the time of deposition of Core V28-179 from the Pacific Ocean, from 4,08 million years to the present time.

A clear change in the deposition mode occurs between 2.5 Ma and 2.1 Ma: the cyclicity becomes more indistinct. The carbonate content, initially tends to increase to values of 90 % and is thereafter reflected in large fluctuations in short periods of time. The same happens with the carbon isotopes. The change is also evident in the oxygen isotopes, but the trend is much more linear, with strong oscillations only at ~2.5 Ma and from about 1.5 Ma to the present time.

Therefore, these changes can be interpreted as variations in orbital parameters and due to plate tectonic modifications with the development of feedback such as changes in oceanic circulation, changes in nutrients supply in oceans, changes in the pressure of CO_2 at the water-atmosphere interface, change in climate and development of the Northern Hemisphere Glaciation. Previous studies, carried out in different parts of the Earth, confirm that the onset of glaciation affected global climates and ocean circulation patterns.

Key data are provided by oxygen and carbon isotopes, in support to this thesis. However, also the abundance data of calcareous nannofossils seem to reflect the onset of the NHG. A more detailed and accurate comparison with core samples at high latitudes may be a valuable help to understand better and interpret the initiation of the ice age period. Future studies about volcanic activity may be compared with the paleoceanographic and paleoclimatic trends observed in the stable isotopic and carbonate data sets.

The coexistence of many different factors has contributed to the onset of Plio-Pleistocene glaciations.

How many glaciations like this will happen again in the future? Technologies will evolve so much that it will be possible not only predict but even to stop these natural events? Will there be a great glacial age that can end societal life on the Earth as we know it today?

The appendices are available only by request

APPENDIX A CORE V28-179 – AGE AND DEPTH DATA.

APPENDIX B DISCOASTER ABUNDANCE DATA

APPENDIX C COULOMETER RESULTS

APPENDIX D CARBON ISOTOPES RESULTS

E-mail: miriam.paccagnella@gmail.com

REFERENCES

ANDERSON R. N., (1986), *Marine Geology A planet Earth Prospective,* Lamont-Doherty Geological Observatory, Columbia University, John Wiley & Sons, pp. 328.

ARRHENIUS G., (1952), *Sediment cores from the East Pacific*, Rep. Swed. Deep-Sea Exped., Vol. 5, pp. 1-227.

BACKMAN J., RAFFI I., RIO D., FORNACIARI E., PÄLIKE H., (submitted), *Biozonation and biochronology of Miocene through Pleistocene calcareous nannofossils from low and middle latitudes*.

BACKMAN J., SHACKLETON N.J., (1983), *Quantitative biochronology of Pliocene and early Pleistocene calcareous nannofossils from the Atlantic, Indian and Pacific Oceans*, in 'Marine Micropaleonotlogy', 8, Elsevier Scienze Publishers, pp. 141-170.

BANDY O., CASEY R. E., WRIGHT R.C., (1971), *Late Neogene planktonic* zonation, magnetic reversals, and radiometric dates, Antarctic to the tropics, Antarctic Research Series, VOL. 15, pp. 1-26.

BARREIRO M., FEDEROV A., PACANOWSKI R., PHILANDER S.G., (2008), *Abrupt Climate Changes: How Freshening of the Northern Atlantic Affects the Thermohaline and Wind-Driven Oceanic Circulations,* Annu. Rev. Earth Planet. Sci., 36, pp. 33-58.

BARTOLI G., SARNTHEIN M., WEINELT M., (2006), *Late Pliocene millennial-scale climate variability in the northern North Atlantic prior to and after the onset of Northern Hemisphere glaciations*, Paleoceanography Vol. 21, Issue: 4, Publisher: Amer Geophysical Union, pp. 1-15.

BERGER, W.H., (1970), *Biogenous deep-sea sediments: fractionation by deep-sea circulation*, Bull. Geol. Soc. Am., 81, pp. 1385-1402.

BERGGREN W.A., VAN COUVERING J.A., (1974), *The late Neogene: biostratigraphy, geochronology and paleoclimatology of the last 15 million years in marine and continental sequences,* Developments in paleontology and stratigraphy, Vol 2, Elsevier Scientific Publishing Company, pp. 216.

BILLUPS K., (2002), *Late Miocene through erasly Pliocene deep water circulation and climate change viewed from the sub-Antarctic South Atlantic,* Paleogeography, Paleoclimatology, Paleoecology 185, pp. 287-307.

BILLUPS K., RAVELO A.C., ZACHOS J.C., (1997), *Early Pliocene deep water circulation: stable isotope evidence for enhanced northern component deep water*, N. Shackleton, et al. (Eds.), Proc. ODP, Sci. Results, 154: College Station, TX (Ocean Drilling Program), pp. 319-330.

BROECKER W. S., (2003), *The oceanic CaCO3 cycle* , In: The Oceans and Marine Geochemistry (ed. H. Elderfield), Treatise on Geochemistry (eds. Holland, H.D. and Turekian, K.K.), Elsevier- Pergamon, Oxford, 6, pp. 529-549.

BUKRY D., (1971), *Cenozoic calcareous nannofossils from the Pacific Ocean,* Trans. San Diego Soc. Nat. Hist., VOL. 16, pp. 307-327.

BUKRY, D., OKADA, H., (1980), *Supplementary modification and introduction of code numbers to the low latitude coccolith biostratigraphic zonation* (Bukry, 1973; 1975). Mar. Micropalentol., VOL.5, pp. 321-325.

BURDRIGE D. J., (2006), *Geochemistry of Marine Sediments,* Princeton Univ. Press., pp. 609.

BURKLE L. H., TRAINER J., (1979), *Middle and late Pliocene datum levels from the central Pacific*, Micropaleontology Vol. 25, pp. 281-293.

BUTZIN M., LOHMANN G., BICKERT T., GROSFELD K., (2003), *Evolution of ocean circulation and climate during Miocene: results from GCM simulations,* EGS-AGU-EUG Joint Assembly 06, Nice, France, pp. 1.

CANDE S.C., KENT D.V., (1995), *Revised calibration of the Geomagnetic Polarity Time Scale for* the Late Cretaceous and Cenozoic, Journal of Geophysical Research, Vol. 100, NO. B4, pp. 6093-6095.

CHESTER R., (1999), *Marine Geochemistry*, Department of Earth Science, University of Liverpool, 2nd edition, Blackwell science, pp. 506.

COLIN DÈ VERDIERE A., TEE RAA L., (2009), *Weak oceanic heat transport as a cause of the instability of glacial climates,* in "Climate Dynamics, Vol. 35, Number 7-8, pp. 1237-1256.

COMBOURIEU NEBOUT N., VERGNAUD GRAZZINI C., (2003), *Late Pliocene Northern Hemisphere glaciations: The continental and marine responses in the central Mediterranean*, Quaternary Science Reviews, Volume 10, Issue 4, 1991, pp. 319-334.

CROWLEY J.T., HYDE W.T., (2008), *Transient nature of late Pleistocene climate variability*, Nature, Vol. 456, Issue: 7219, pp. 226-230.

CRUCIFIX M., (2011), *Oscillators and relaxation phenomena in Pleistocene climate theory,* Phil. Trans. R. Soc. A 2012 370, pp. 1140-1165.

CURRY, W.B., SHACKLETON, N.J., RICHTER, C., ET AL., (1995), *Proc. ODP*, Init. Repts., 154: College Station, TX (Ocean Drilling Program), pp. 1-1111.

DEAN A.D., (1982), *Change from "Atlantic-type" to "Pacific-type" carbonate stratigraphy in the middle Pliocene Equatorial Pacific Ocean*, in 'Marine Geology, 50', Elsevier Scientific Publishing Company, Amsterdam, pp. 41-60.

DEAN A.D., MOORE T.C., JR, (2011), *Late Miocene—Pliocene (Magnetic Epoch 9—Gilbert Magnetic Epoch) calcium-carbonate stratigraphy of the equatorial Pacific Ocean: Summary*, in 'Geological Society of American Bulletin', Part II of the Bulletin, v. 92, no. 3, pp. 408–451.

EMILIANI C., (1955), *Pleistocene temperatures*, J. Geol, Vol. 63, pp. 534-578.

FARNETI R., DELWORTH T.L., (2010), *The role of mesoscale eddies in the remote oceanic response to altered Southern Hemisphere winds,* J. Phys. Oceanogr., Vol. 40, 10, pp. 2348-2354.

FARQUHAR G.D., FASHAM M.J.R., GOULDEN M.L., HEIMANN M., JARAMILLO V.J., KHESHGI H.S., LE QUÉRÉ C., SCHOLES R.J., WALLACE D.W.R., ARCHER D., ASHMORE M.R., AUMONT O., BAKER D., BATTLE M., BENDER M., BOPP L.P., BOUSQUET P., CALDEIRA K., CIAIS P., COX P.M., CRAMER W., DENTENER F., ENTING I.G., FIELD C.B., FRIEDLINGSTEIN P., HOLLAND E.A., HOUGHTON R.A., HOUSE J.I., ISHIDA A., JAIN A.K., JANSSENS I.A., JOOS F., KAMINSKI T., KEELING R.F., KICKLIGHTER D.W., KOHFELD K.E., KNORR W., LAW R., LENTON T., LINDSAY K., MAIER-REIMER E., MANNIN A.C., MATEAR R.J., McGUIRE A.D., MELILLO J.M., MEYER R., MUND M., ORR J.C., PIPER S., PLATTNER K., RAYNER P.J., SITCH S., SLATER R., TAGUCHI S., TANS P.P., TIAN H.Q., WEIRIG M.F., WHORF T., YOOL A., PITELKA L., RAMIREZ ROJAS, (2001), Executive Summary, In (book chapter): 3, *The Carbon Cycle and Atmospheric Carbon Dioxide,* In: Climate Change 2001: The Scientific Basis. Contribution of Working Group I to the Third Assessment Report of the Intergovernmental Panel on Climate Change (J.T. Houghton, Y. Ding, D.J. Griggs, M. Noguer, P.J. van der Linden, X. Dai, K. Maskell, C.A. Johnson (eds)), Print version: Cambridge University Press. This version: GRID-Arendal website, pp. 183-238.

FARRELL J.W., PRELL W.L., (1991), *Pacific CaCO3 preservation and δ18O since 4 Ma: paleoceanic and paleoclimatic implications,* in 'Paleoceanography, Vol. 6, NO. 4', pp. 485-498.

FARRELL J.W., RAFFI I., JANECEK T.C., MURRAY D.W., LEVITAN M., DADEY K.A., EMEIS K.C., LYLE M., FLORES J.A., HOVAN S., (1995), *Late Neogene Sedimentation Patterns in the Eastern Equatorial Pacific Ocean,* In 'Pisias', N.G., Mayer, L.A., Janecek, T.R., Palmer-Julson, A., and van Andel, T.H. (Eds.), *Proc. ODP, Sci. Results,* 138: College Station, TX (Ocean Drilling Program), pp. 717–756.

FEDOROV A.V., BRIERLEY C., EMANUEL K., (2010), *Tropical cyclones and permanent El Niño in the Early Pliocene,* Nature 463, pp. 1066-1070.

FEDOROV A.V., RAVELO A.C., DEKENS P.S., DeMENOCAL P., BARREIRO M., PACANOWSKI R., PHILANDER S.G., (2006), The Pliocene paradox (Mechanisms for a permanent El Niño), Science 2006, pp. 1485-1489.

FILIPPELLI G.M., FLORES J.A., (2009), *From the warm Pliocene to the cold Pleistocene: a tale of two oceans*, *Geology* Vol. 37, pp. 959-960

FORNACIARI, E., AGNINI, C., CATANZARITI, R., RIO, D., BOLLA, E.M., VALVASONI, E., (2010), *Midlatitude calcareous nannofossil biostratigraphy, biochronology and evolution across the middle to late Eocene transition*, Stratigraphy VOL. 7 (4), pp. 229–264.

GARTNER S., (1969), Correlation of Neogene planktonic foraminifer and calcareous nannofossils zones. Trans. Gulf Coast Assoc. Geol. Soc., 19: 585-599
GRADSTEIN F., OGG J.G, SMITH A.G., et al. (2004), A geologic time scale, Cambridge University Press, pp. 589.

GIBBS S., SHACKLETON N.J., YOUNG J.R., (2004), *Orbitally-forced climate signals in mid Pliocene nannofossil assemblages*, Mar. Micropaleontol. Vol. 51, pp. 39–56.

GRADSTEIN F., OGG J.G, SMITH A.G., BLEECKER W., LAURENS L.J., (2004), A new geologic time scale , with special reference to Precambrian and Neogene, Geological Society of the Philippines, Episodes, 27(2): 83-100, pp.18.

GRANT K.M., DICKENS G.R., (2002), Coupled productivity and carbon isotope records in the southwest Pacific Ocean during the late Miocene-early Pleistocene *biogenic bloom*, in 'Palaeogeography, Palaeoclimatology, Palaeoecology 187', pp. 61-82.

GUSSONE N., EISENHAUER A., TIEDEMANN R., HAUG G.H., HEUSER A., BOCK B., NÄGLER T.F., MÜLLER A., (2004), *Reconstruction of Caribbean sea surface temperature and salinity fluctuations in response to the pliocene closure of the Central American Gateway and radiative forcing, using delta Ca-44/40, delta O-18 and Mg/Ca ratios*, Earth and Planetary Science Letters (2004) Volume: 227, Issue: 3-4, pp. 201-214.

GUYODO Y., CHANNELL J.E.T., (2002), *Effects of variable sedimentation rates and age errors on the resolution of sedimentary paleointensity record*, Geochemistry Geophysics Geosystems, Vol. 3, 1048, pp.18.

HAYS G.C., RICHARDSON A.J., ROBINSON C., (2005), *Climate change and marine plankton*, Trends in Ecology & Evolution, Vol. 20, Issue 6, pp. 337-344.

HAYWOOD A.M., DEKENS P., RAVELO C., WILLIAMS M., (2005), *Warmer tropics during the mid-Pliocene? Evidence from alkenone paleothermometry and a fully coupled ocean-atmosphere GCM*, in 'Geochemistry, Geophysics, Geosystems', Vol. 6, Number 3, pp. 20.

HEEZEN B. C., (1977), *Influence of Abyssal circulation on Sedimentary Accumulations in Space and Time,* Developments in Sedimentology 23, pp. 215.

HONJO S., (1976), *Coccoliths: production, transportation and sedimentation*, Marine Micropaleontology, 1, pp. 65-79

JIANG S., (2007), *Applications of calcareous nannofossils and stable isotopes to Cenozoic paleoceanography: Examples from the eastern equatorial Pacific, western equatorial Atlantic and southern Indian Oceans*, The Florida State University, pp. 189.

JANIN M.C., (1987), *The Imprints of Cenozoic Calcareous Nannofossils from Polymetallic Concretions: Biostratigraphic Significance for two Crusts from the Central Pacific (Line Islands Ridge and Mid-Pacific Mountains),* Volume 115, Issues 3–4, December 1993, pp. 289–306.

JIANG Z., LIU Q., (2012), *Magnetic characterization and paleoclimatic significances of the late Pliocene-early Pleistocene sediments at site 882A, northwestern Pacific Ocean*, in 'Science China, Earth Sciences', Vol. 55, February 2012, pp. 323-331.

JUMARS P.A., WHEATCROFT R.A., (1989), *Responses of benthos to changing food quality and quantity, with a focus on deposit feeding and bioturbation.* In: Berger WH, Smetacek FS, Wefer G (eds) *Productivity of the ocean: present and past.* John Wiley & Sons, Dahlem, pp. 235–253.

KAMPTNER E., (1967), *Kalkflagellaten-Skelett treste aus Tiefseeschlamm des Südatlantischen Ozeans*, Ann. Naturhist. Mus. Wien, 71, pp. 117-198.

KARAS C., NÜRNBERG D., GUPTA A.K., TIEDEMANN R., MOHAN K., BICKERT T., (2009), *Mid-Pliocene climate change amplified by a switch in Indonesian subsurface throughflow*, Nature Geoscience Vol. 2, pp. 434 – 438.

KATZ M.E., WRIGHT J.D., MILLER K.G., CRAMER S.B., FENNEL K., FALKOWSKI P.G., (2005), *Biological overprint of the geological carbon cycle*, Mar. Geol., Vol. 21, pp. 323-338.

KENNETT J. P., (1982), *Marine Geology:* Prentice-Hall, Englewood Cliffs New Jersey, pp. 813.

KENNET J.P., VON DER BORCH C.C., (1986), *Southwest Pacific Cenozoic paleoceanography*, in KENNETT J.P., VON DER BORCH C.C., et al., Init. Repts. DSDP, 90 (Pt. 2): Washington (U.S. Govt. Printing Office), pp. 1943-1517.

LAWRENCE K.T., LIU Z., HERBERT T.D., (2006), *Evolution of the Eastern Tropical Pacific Through Plio-Pleistocene Glaciation*, Science 7 April 2006: Vol. 312, no. 5770, pp. 79-83.

LEE S., POULSEN C.J., (2006), Sea ice control of Plio–Pleistocene tropical Pacific climate evolution, Earth and Planetary Science Letters, Volume 248, Issue 1-2, pp. 253-262.

LISIECKI L.E., RAYMO M.E., (2007), *Plio–Pleistocene climate evolution: trends and transitions in glacial cycle dynamics*, Quaternary Science Reviews, Vol. 26, pp. 56-69.

LYLE M., (2003), *Neogene carbonate burial in the Pacific Ocean,* in Paleoceanography, Vol. 18, No. 3, pp. 4.

LYNCH-STIEGLITZ J., (2003), *Tracers of the Past Oceanic Circulation*, Treatise on Geochemistry, Vol. 6, pp. 433-451.

MARSH M. E., (2003), *Regulation of $CaCO_3$ formation in coccolithophores*, Comp. Biochem. Physiol, B Biochem, Mol. Biol., Vol. 136, pp. 743-754.

MARTINI, E., (1971), *Standard Tertiary and Quaternary calcareous nannoplankton zonation*, In Farinacci, A. (Ed.), Proc. Second Planktonic Conf.: Rome (E. Tecnoscienza), pp. 739-785.

MASLIN M.A., RIDGEWELL A., (2005), Mid-Pleistocene Revolution and the "eccentricity myth", Special Publication of the Geological Society of London, Vol. 247, pp. 19-34.

McMANUS D. A., CHAMLEY H., (1991), Marine Geology Vol. 99 – NO. 3 / 4, Special issue Deep Ocean Sediment Transport, International Journal of Marine Geology, Geochemistry and Geophisics.

MENARD H. W., (1964), *Marine Geology of the Pacific,* International series in the Earth Sciences, McGraw Hill Book Company, pp. 271.

MOLINEAUX L., (1971), *A complete result magnetometer for measuring the remanent magnetization of rocks,* Geophys. J.R. astr. Soc. 24, pp. 429-434.

O'LEARY M. H., (1988), *Carbon isotopes in photosynthesis*, Bio Science, Vol. 38, No. 5, pp. 328-336.

PETERSON, M. N. A., (1966), *Calcite: rates of dissolution in a vertical profile in the Central Pacific*: Science, Vol. 154, pp. 1542-1544.

PLACENCIA J.A., GARCÉS-VARGAS J., LANGE C.B., HEBBELN D., (2010), *Alkenone-based temperature patterns along the eastern South Pacific Coastal Ocean: the effect of upwelling and advection on the sedimentary alkenone unsaturation-index ($U^{K'}_{37}$)*, Biogeosciences Discuss., 7, pp. 545–564.

PÄLIKE H., NORRIS R.D., HERRLE J.O., WILSON P.A., COXALL H.K., LEAR C.H., SHACKLETON N.J., TRIPATI A.K., WADE B.S., (2006), The Heartbeat of the Oligocene Climate System, *Science* 22, Vol. 314 no. 5807, pp. 1894-1898.

RAFFI I., BACKMAN J., RIO D., SHACKLETON N.J., (1993), *Plio-Pleistocene nannofossil biostratigraphy and calibration to oxygen isotope stratigraphies from Deep Sea Drilling Project Site 607 and Ocean Drilling Program Site 677*. Paleoceanography, Vol.8, pp.387-408.

RAYMO M.E., RUDDIMAN W.F., SHACKLETON N.J., OPPO D.W., (1990), *Evolution of Atlantic.-Pacific $\delta^{13}C$ gradients over the last 2.5 m.y.,* Earth and Planetary Science Letters 97 (3-4), pp. 353-368.

RAFFI I., FLORES J.-A., (1995), *Pleistocene through Miocene calcareous nannofossils from eastern equatorial Pacific Ocean (Leg 138)*, In Pisias, N.G., Mayer, L.A., Janecek, T.R., Palmer-Julson, A., and van Andel, T.H. (Eds.), Proc. ODP, Sci. Results, 138: College Station, TX (Ocean Drilling Program), pp. 233-286.

RAVELO A.C., BILLUPS K., DEKENS P.S., HERBERT T.D., LAWRENCE K.T., (2007), *Onto the ice ages: proxy evidence for the onset of Northern Hemisphere glaciation*, in Haywood, Gregory and Schmidt (eds) Deep-time Perspectives on Climate Change: Marrying the Signal from Computer Models and Biological Proxies, The Geolgoical Society, London, pp. 563-573.

RAVELO A.C., DEKENS P.S., McCARTHY M., (2006), Evidence for El Niño-like conditions during the Pliocene, GSA Today, 16, pp. 4-11.

REY J., GALEOTTI S., (2008), *Stratigraphy. Terminology and Practice*, Technip Édit. - B.R.G.M. - TOTAL, pp. 176.

RILEY J. P., CHESTER R., (1976), *Chemical Oceanography,* Department of Oceanography, The University of Liverpool, England, Vol 5, 2nd edition, Academic press, pp. 401.

RIO, D., SPROVIERI, R., RAFFI, I., (1984), *Calcareous plankton biostratigraphy and biochronology of the Pliocene-Lower Pleistocene succession of the Capo Rossello area, Sicil*, Marine Micropaleontology, Vol. 9, pp. 135-180.

SARNTHEIN M., BARTOLI G., PRANGE M., SCHMITTNER A., SCHNEIDER B., WEINELT M., ANDERSEN N., GARBE-SCHÖNBERG D., (2009), *Mid-Pliocene shifts in ocean overturning circulation and the onset of Quaternary-style climates,* Clim. Past, 5, pp. 269-283.

SHACKLETON N.J., (1967), *Oxygen Isotope Analyses and Pleistocene Temperatures Re-assessed*, Nature, Vol. 215, pp. 15-17.

SHACKLETON N.J., BACKMAN J., ZIMMERMAN H., KENT D.V., HALL M.A., ROBERTS D.G., SCHNITKER D., BALDAUF J.G., DESPRAIRIES A., HOMRIGHAUSEN R., HUDDLESTUN P., KEENE L.B., KALTENBACK A.J., KRUMSIEK K.A.O., MORTON A.C., MURRAY J.W., WESTBERG-SMITH J., (1984), *Oxygen isotope calibration of the onset of ice-rafting and history of glaciation in the North Atlantic region*, *Nature* Nr. **307**, pp. 620 – 623.

SHACKLETON N. J., HALL M. A., PATE D., (1995), *Pliocene stable isotope stratigraphy of site 846*, Pisias, N.G., Mayer, L.A., Janecek, T.R., Palmer-Julson, A., and van Andel, T.H. (Eds.), Proceedings of the Ocean Drilling Program, Scientific Results, Vol. 138, pp. 337- 355.

SHACKLETON N.J., OPDYKE N.D., (1973), *Oxygen isotope and palaeomagnetic stratigraphy of Equatorial Pacific core V28-238: Oxygen isotope temperatures and ice volumes on a 10^5 year and 10^6 year scale*, Quaternary Research (1973), Vol. 3, Issue: 1, Publisher: Elsevier, pp. 39-55.

SHACKLETON N.J., OPDYKE N.D., (1977), *Oxygen isotope and paleomagnetic evidence for early Northern Emisphere glaciations*, in 'Nature Vol. 270', 17 November 1977, pp. 216-219.

SIDDALL M., HÖNISCH B., WAELBROECK C., HUYBERS P., (2010), Changes in deep Pacific temperature during the mid-Pleistocene transition and Quaternary, Vol. 29, Issues 1–2, pp. 170–181.

SIGMAN D. M., BOYLE E. A., (2000), *Glacial/interglacial variations in atmospheric carbon dioxide*, Nature, Vol. 407, Issue 6806, pp. 859-869.

SKINNER L.C., ELDERFIELD H., HALL M., (2007), *Phasing of millennial climate events and northeast Atlantic deep-water temperature change since 50 ka BP,* Geophysical Monograph Series, Vol. 173, pp. 197-208.

SPROVIERI R. ET AL., (1998), *Integrated calcareous plankton biostratigraphy and cyclostratigraphy at site 964*, Robertson, A.H.F., Emeis, K.-C., Richter, C., and Camerlenghi, A. (Eds.), Proceedings of the Ocean Drilling Program, Scientific Results, Vol. 160, pp. 155-165.

STEINMETZ J. C., (1991), *Calcareous Nannoplankton Biocoenosis: Sediment Trap in the* Equatorial Atlantic, Central Pacific, and Panama Basin, in: Woods Hole Oceanographic Institution. Ocean Biocoenosis Series, Vol. 1, pp. 85.

SULZMAN E.W., (1995), *The Carbon Cycle*, Global Change Instruction Program, University Corporation for Atmospheric Research, Boulder, CO. (In press), pp. 28.

TAN SIN HOK, (1927), *Discoasteridae incertae sedis.* Proc. Sect. Sc. K. Acad. Wet. Amsterdam,Vol. 30, pp. 411-419.

VALI H., VON DOBENECK T., AMARANTIDIS G., FÖRSTER O., MORTEANI G., BACHMANN L., PETERSEN N., (1989), *Biogenic and lithogenic magnetic minerals in Atlantic and Pacific deep sea sediments and their paleomagnetic significance,* Geologische Rundschau, Vol. 78, Number 3, pp. 753-764.

VAN ANDEL T. H., HEATH G. R., MOORE JR. T. C., (1975), Cenozoic History and Paloeceanography of the Central Equatorial Pacific Ocean, a Regional Synthesis of Deep Sea Drilling Project Data, The Geological Society of America Memoir, Vol. 143, pp. 134.

VAN ANDEL T.H., TJEERD H., (1974), *Cenozoic Migration of the Pacific Plate, Northward Shift of the Axis of Deposition, and Paleobathymetry of the Central Equatorial Pacific*, Geology, Vol. 2, Issue 10, pp. 507

VINCENT E., (1981), *Neogene carbonate stratigraphy of Hess Rise (central North Pacific) and paleoceanographic implications*, In Thiede, J., Vallier, T.L., et al., Init. Repts. DSDP, Vol. 62, Washington (U.S. Govt. Printing Office), pp.571-606.

WADE B.S., PÄLIKE H., (2004), *Oligocene climate dynamics*, Paleoceanography, Vol. 19, pp. 16.

WESTERHOLD T., RÖHL U., DONNER B., McCARREN H. K., ZACHOS J. C., (2011), *A complete high-resolution Paleocene benthic stable isotope record for the central Pacific (ODP Site 1209)*, Paleoceanography, Vol. 26, pp. 13.

WINTERER E.L., EWING J.I., DOUGLAS R.G., JARRAD R.D., LANCELOT Y., MOBERLY R.M., MOORE T.C., ROTH P.H., SCHLANGER S.O., (1971), *Deep Sea Drilling Project Initial Reports Vol. 17*, pp. 922.

XANTHAKIS J., LIRITZIS I., TZANIS E., (1995), *Periodic variation of $\delta^{18}O$ values from V28-239 Pacific Ocean deep-sea core,* Moon, Planets Vol. 66, pp. 253-278.

ON-LINE MATERIALS

BUTZIN M., LOHMANN G., BICKERT T., GROSFELD K., *Evolution of ocean circulation and climate during the Miocene: Results from GCM simulations*, University of Bremen, Department of Geosciences

COHEN K. M., GIBBARD P. L., (2008), *Global chronostratigraphical table for the last 2.7 million years*, Episodes, 31, No. 2, pp. 243-247.

OSBORNE A., (2012), *Neodymium isotopes as a tracer for past ocean circulation – the Pliocene closure of the Central American Seaway*, pp. 1.

TAYLOR R., (2003), *Oxygen isotopes* (website: http://www.geography.ukzn.ac.za/seminars/oxygen_isotopes.pdf).

THOMAS E., (2008), *Stable Carbon Isotopes in Paleoceanography*. (website: http://ethomas.web.wesleyan.edu/ees123/caiso.htm).

THOMAS E., *Oxygen isotopes: The thermometer of the Earth.* (website: http://ethomas.web.wesleyan.edu/ees123/paleoxiso.htm).

http://geology.uprm.edu/Morelock/dpseabiogenic.htm - Biogenic sediments

http://geophysics.ou.edu/solid_earth/notes/mag_earth/earth.htm - Paleopole position from 16th century

http://globecarboncycle.unh.edu/CarbonCycleBackground.pdf - Global carbon cycle

http://ie.lbl.gov/education/info.htm - Isotopes

http://myweb.cwpost.liu.edu/vdivener/notes/stable_isotopes.htm - Oxygen isotopes variations and formation of ice sheets

http://nannotax.org/category/nanno-taxonomy/nannoliths/discoasteraceae/discoaster/d-brouweri-group/discoaster-triradiatu - Discoaster triradiatus description

http://nannotax.org/category/nanno-taxonomy/nannoliths/discoasteraceae/discoaster/d-brouweri-group/discoaster-asymmetric - Discoaster asymmetricus description

http://nannotax.org/category/nanno-taxonomy/nannoliths/discoasteraceae/discoaster/d-brouweri-group/discoaster-brouweri - Discoaster brouweri description

http://oceanworld.tamu.edu/resources/oceanography-book/carboncycle.htm - carbon cycle

http://personalpages.manchester.ac.uk/staff/neil.mitchell/eqpac/eqpac.html - Equatorial Pacific Sediments and Paleoceanography

http://public.wsu.edu/~dybdahl/lec10.html - Equatorial upwelling and productivity

http://web.me.com/uriarte/Earths_Climate/Appendix_6.html - Carbon isotopes in paleoclimatic research.

http://wwwrcamnl.wr.usgs.gov/isoig/projects/fingernails/results/interpretdata.html - PDB meaning

http://www.answers.com/topic/geomagnetism-1 - Declination and Inclination description

http://www.buzzle.com/articles/isotopes-of-carbon.html - Carbon isotopes

http://www.deepseadrilling.org/85/dsdp_toc.htm - Deep Sea Drilling Project Reports and Pubblications

http://www.deepseadrilling.org/33/dsdp_toc.htm - Deep Sea Drilling Project Reports and Pubblications.
Introduction: Background and Explanatory Notes, Deep Sea Drilling Project Leg 85, Central Equatorial Pacific, Shipboard Scientific Party, DSDP Volume LXXXV.

http://www.gobi.org/Our%20Work/productive-1 - production of phytoplankton worldwide from satellite observations

http://www.grida.no - Introduction to Climate Change United Nations Environmental Program's UNEP Global Resources Information Database (GRID) office in Arendal Norway

http://www.ngdc.noaa.gov/ngdc.html - National Geophysical Data Center (National Oceanic and Atmospheric Administration)

http://www.odplegacy.org/default.html - ODP Legacy

http://www-odp.tamu.edu/publications/202_IR/chap_02/c2_f12.htm - Time scale of the past 16 Myr

http://www.ucl.ac.uk/GeolSci/micropal/calcnanno.html - Calcareous nannofossils

http://www.uicinc.com/SystemSheets/Principles%20of%20Operation%20CO2.pdf – Coulometer principles of operation

http://www.whoi.edu/oceanus/viewArticle.do?id=2508 – Oceanus (Woods Hole Oceanographic Institution)

http://www2.brevard.edu/reynoljh/vita/magnetostratigraphy.html - Correlation Method

http://www2.ocean.washington.edu/oc540/lec01-16/ - Oceanography 540 -Marine Geological Processes--Winter Quarter 2001